TREBALL FI DE CARRERA

Títol

Holocene lahar history of Villarrica Volcano

Autor/a

Mateu Llurba Ruiz

Tutor/a

Marc De Batist

Isabel Cacho Lascorz

Departament

Renard Centre of Marine Geology (UGent)

Dept. Estratigrafia, Paleontologia i Geociències Marines,

Facultat de Geologia (UB)

Intensificació

Data

Juny de 2014

Acknownledgements

Thanks to Prof. Dr. Marc De Batist and the University of Ghent, for giving me the opportunity to develop this research project and learn and work with the best.

Gracias a Isabel Cacho, mi tutora. Por apoyarme desde la distancia, por ayudarme siempre que la he necesitado y por el interés que me ha mostrado.

Thanks to my mentor, Dr. Maarten Van Daele. Thank you for all your dedication, your support and for all the knowledge you have shared with me. Thanks for your involvement since the first day to the last and for making lahars, Chilean volcanoes and lakes part of my life always and forever!

Thanks to Dr. Sebastien Bertrand. Seb, my office mate, thanks for your patience, for your teaching, for all the knowledge you have shared with me, for your daily English lessons and for creating such a good atmosphere both inside and outside the office!

I also want to say thank you to all the members of RCMG for welcoming me like one of them since the first day and help me whenever I need.

A Roberto, ¡gracias por estar siempre ahí!

Als meus “amX”. Gràcies per deixar-me compartir durant aquests anys tants bons moments al vostre costat i per ajudar-me a arribar fins aquí. Sense vosaltres no ho hauria aconseguit.

Finalment, gràcies a la meva família. Especialment al Mateu i la Lourdes, els meus pares, i a la Virginia i la Maria, les meves germanes. Us ho dec tot, os lo debo todo.

Abstract

Villarrica Volcano is one of the most active volcanoes in south-central Chile. There are many hazards related to the volcano, but its main hazard for humans through Villarrica's history have been the lahars. Since the arrival of the Spanish colonists (1550) to the towns beside the volcano, it have been reported hundreds to thousands of casualties and the towns were repeatedly destroyed by lahars.

From the necessity to understand its behaviour for future events and reconstruct its past. Short and long sediment cores were taken from the lakes beside the volcano –Villarrica and Calafquén–. For studying them, pictures were taken from the original cores and a histogram equalization was applied for having more visual information. CT-scans of the cores were obtained to analyse in high detail. Also the magnetic susceptibility curve was obtain and compared to the other information.

It has been concluded that the distribution of the clay caps of recent well-known lahar events (during 20th century) show that they are deposited by a combination of under- and interflows. After measuring the thickness of the lahars of Holocene age in the long cores in both lakes show that the general trend in both lakes is similar that is to increase progressively. They are linked to rainfall (climate), but also for example the Pucón eruption (which changed the morphology of the volcano) changed the frequency of the events in the centuries after the eruption in both lakes, with first a quiescence of approximately 700 years to Lake Calafquén.

Resum

El Volcà Villarrica és un dels volcans més actius en el centre-sud de Xile. Al llarg de la història eruptiva del volcà se li coneixen molts perills relacionats, però el principal perill per als éssers humans han estat els lahars. Des de l'arribada dels colonitzadors espanyols (1550) a les ciutats més properes al volcà, es té constància de centenars de milers de víctimes i danys materials deguts a l'acció d'aquest fluxos de material volcànic i aigua.

Des de la necessitat de comprendre el seu comportament per futurs esdeveniments és important reconstruir el passat. Testimonis de sediment curts i llargs van ser presos dels llacs al costat del volcà –Villarrica i Calafquén–. Per estudiar-los es van obtenir imatges dels testimonis originals i es va aplicar una equalització de histograma per obtenir més informació. També se'ls hi va aplicar ressonàncies magnètiques (CT-scans) per analitzar-ho detalladament i es va obtenir la corba de susceptibilitat magnètica per comparar els resultats visuals amb informació complementària.

Després d'estudiar els resultats, s'ha arribat a la conclusió que la distribució de les capes d'argila de gra fi dels esdeveniments més recents (durant segle XX) mostren que van ser dipositades mitjançant una combinació de fluxos baixos i intermitjos. El gruix dels lahars d'edat Holocena en els testimonis llargs, mostren que la tendència general en tots dos llacs és similar, i que no només estan directament relacionats amb les precipitacions (clima), sinó també, per exemple, l'erupció Pucón (3700 anys) va canviar la morfologia del volcà i conseqüentment la freqüència dels esdeveniments en els posteriors segles a l'erupció.

Table of contents

Acknownledgements.....I
Abstract.....III
Resum.....IV
Table of contents.....VI
List of figures.....VII
List of tables.....XI
Chapter 1: Introduction.....1
1.1 Motivations.....1
1.2 Objectives.....1
Chapter 2: General Settings.....3
2.1 Chile.....3
2.2 Volcanism in Chile.....5
2.2.1 Tectonics.....5
2.2.2 Eruption types.....5
2.2.3 Chilean volcanic zones.....6
2.3 Products of volcanoes.....7
2.3.1 General products of volcanoes.....7
2.3.2 Lahars.....8
2.4 Lakes in southern Chile.....11
2.5 Lacustrine sedimentation.....13
2.5.1 Lake stratification.....13
2.5.2 Lake sedimentation.....14
Chapter 3: Regional Setting.....17
3.1 Study area.....17
3.1.1 Lake origin.....17
3.1.2 Limnology.....18
3.1.3 Bathymetry and catchment area.....18
3.2 Villarrica Volcano: Geology and eruptive history.....19
Chapter 4: Material and methods.....23
4.1 Material.....23
4.2 Methods.....25

4.2.1 Image acquisition and image analysis 25
4.2.2 High-resolution magnetic-susceptibility (MS) 28
4.2.3 X-ray computed tomography (CT) 29
4.2.4 Lahars pathway length measuring method 30
Chapter 5: Results 31
5.1 Short cores 31
5.1.1 Counting of the last century lahar events 31
5.1.2 Thickness of the lahars clay cap during the 20th century. 34
5.1.3 Depth and distance measurements 35
5.1.4 Comparison of clay cap thickness with depth and inflow distance 39
5.2 Long cores 47
5.2.1 Description of the lahars in the sedimentary record of Lake Villarrica. 49
5.2.2 Description of the lahars in the sedimentary record of Lake Calafquén. 52
Chapter 6: Discussion 55
6.1 Short cores 55
6.1.1 Lake Calafquén 55
6.1.2 Lake Villarrica 59
6.2 Long cores 62
6.2.1 Application of the different age models to the correlation of the lahars 62
6.2.2 Relation between the precipitation model and the evolution of the lahars during the Holocene 65
Chapter 7: Conclusions and future research 67
7.1 Conclusions 67
7.2 Future research 68
References 69
Appendix i
Appendix A: ii
A.1 20th EDs description in short cores from Lakes Villarrica and Calafquén ii
A.2 Measurements of the thickness of the clay cap of the lahars of the 20th century and its depths in Lakes Villarrica and Calafquén xxi
Appendix B: xxiii
B.1 Description of the long core records xxiii
B.2 Correlation of the lahars based on VIL1 and CAL2 in Lake Villarrica and Calafquén, respectively xxxvi

List of figures

Figure 2.1 Sketch map of Chile, showing the main topographical zones.....3

Figure 2.2 Schematic map of the Andes range divided in the four volcanically active zones.....4

Figure 2.3 Classification of subaerial explosive volcanic eruptions based on explosiveness and the height of eruption column.....5

Figure 2.4 Types of magmatic eruptions.....6

Figure 2.5 Conceptual model showing the changes in water/sediment ratio, and the sequence of deposicional and erosional processes observed in modern lahars.....9

Figure 2.6 Picture placed at one of the historical lahar pathways of Villarrica Volano illustrating an ideal cross section of a sub-aerial lahar.....10

Figure 2.7 Geomorphological map of the study area in the northern Chilean Lake District: 1:250,000.....12

Figure 2.8 Vertical profile of solar radiation and temperature in the water column of a temperate lake.....13

Figure 2.9 Types of density flow.....15

Figure 2.10 Distribution mechanisms and resulting types of proposed for clastic sedimentation in oligotrophic lakes with annual thermal stratification.....15

Figure 2.11 Schematic illustration of the formation of lahar deposits in lacustrine environaments.....16

Figure 3.1 Location of the study area in South-Central Chile.....17

Figure 3.2 Chronological distribution of the isotherms in Lake Villarrica from the winter of the year 1978 until the same season in 1979.....18

Figure 3.3 Granit blocks with a volume up to 40 m^3, dragged some kilometres by the power of a lahar during 1971 Villarrica Volcano eruption.....20

Figure 4.1 Location of the sediment cores used in this thesis in lakes Villarrica and Calafquén..23

Figure 4.2 Calibration models based on 14C ages using the calibration curve SHCAL13 from Lake Villarrica and Lake Calafquén.....25

Figure 4.3 Example of a processed core image before and after applying a histogram equalization.....26

Figure 4.4 Screenshot of the program ImageJ during the digitization process of the lahars clay cap.....27

Figure 4.5 Screenshot of the program Corelyzer during the processing of the long cores.....28

Figure 4.6 Pictures of the Siemens SOMATON Definition Flash medical X-ray CT scanner (a) and the control room……29

Figure 5.1 Picture (N), Histogram Equalization processed image (HE), X-ray CT-scan image (CT) and Magnetic Susceptibility (MS) graph of core VI11; before and after being analysed……33

Figure 5.2 Historical lahar pathways compared with the thickness of the linked lahar's clay cap deposits……35

Figure 5.3 Bathymetry of Lake Villarrica and Lake Calafquén……36

Figure 5.4 Relation between the thickness of the lahar clay cap and the depths of the cores in Lake Villarrica in the eruptive event of 1904……40

Figure 5.5 Relation between the thickness of the lahar clay cap and the depths of the cores in Lake Villarrica in the eruptive event of 1908……40

Figure 5.6 Relation between the thickness of the lahar clay cap and the depths of the cores in Lake Villarrica in the eruptive event of 1909……40

Figure 5.7 Relation between the thickness of the lahar clay cap and the depths of the cores in Lake Villarrica in the eruptive event of 1920……41

Figure 5.8 Relation between the thickness of the lahar clay cap and the depths of the cores in Lake Villarrica in the eruptive event of 1948-1949……41

Figure 5.9 Relation between the thickness of the lahar clay cap and the depths of the cores in Lake Villarrica in the eruptive event of 1963-1964……41

Figure 5.10 Relation between the thickness of the lahar clay cap and the depths of the cores in Lake Villarrica in the eruptive event of 1971……42

Figure 5.11 Relation between the thickness of the lahar clay cap and the depths of the cores in Lake Villarrica in the eruptive event of 1991……42

Figure 5.12 Relation between the thickness of the lahar clay cap and the depths of the cores in Lake Calafquén in the eruptive event of 1948-1949……43

Figure 5.13 Relation between the thickness of the lahar clay cap and the depths of the cores in Lake Calafquén in the eruptive event of 1963-1964……43

Figure 5.14 Relation between the thickness of the lahar clay cap and the depths of the cores in Lake Calafquén in the eruptive event of 1971……43

Figure 5.15 Relation between the thickness of the lahar clay cap and the straight distance from the lahar inflow points to the cores in Lake Villarrica during the 20th century……44

Figure 5.16 Relation between the thickness of the lahar clay cap and the straight distance from the lahar inflow points to the cores in Lake Calafquén during the 20th century……45

Figure 5.17 Relation between the thickness of the lahar clay cap and the pathways from the lahar inflow points to the cores in Lake Villarrica during the 20th century……46

Figure 5.18 Relation between the thickness of the lahar clay cap and the pathways from the lahar inflow points to the cores in Lake Calafquén during the 20th century……46

Figure 5.19 Pictuare and processed image applying a HE of the cores CAL2 and CAL1……..47

Figure 5.20 Pictuare and processed image applying a HE of the cores VIL1, VIL3 and VIL4……48

Figure 5.21 Thickness of the correlated lahars of all cores projected on the depth of the master core (VIL1) in Lake Villarrica……..50

Figure 5.22a Relationship between the cumulative thicknesses of the correlated lahars and depth based on the master core (VIL1) in Lake Villarrica……..51

Figure 5.22b Relation between the number of lahars each 50 cm, the depth based on the master core (VIL1), and the cumulate thickness of the lahars each 50 cm……51

Figure 5.23 Thickness of the correlated lahars of all cores projected on the depth of the master core (CAL2) in Lake Calafquén……53

Figure 5.24a Relationship between the cumulative thicknesses of the correlated lahars and depth based on the master core (CAL2) in Lake Calafquén……..54

Figure 5.24b Relation between the number of lahars each 50 cm, the depth based on the master core (CAL2), and the cumulate thickness of the lahars each 50 cm……54

Figure 6.1 Interpretation of the sedimentation process based on the relation between the thickness of the lahar clay cap and the depth of the short cores in the event of 1963-1964 in Lake Calafquén……..56

Figure 6.2 Interpretation sedimentation process based on the relation between the thickness of the lahar clay cap and the depth of the short cores in the event of 1971 in Lake Calafquén……57

Figure 6.3 Relation between the thickness of the lahar clay cap and the straight distance from the lahar inflow points to the cores in Lake Calafquén during the 20th century……57

Figure 6.4 Relation between the thickness of the lahar clay cap and the pathways from the lahar inflow points to the cores in Lake Calafquén during the 20th century……58

Figure 6.5 Interpretation of the relation between the thickness of the lahar clay cap and the depths of the cores in the eruptive events of 1971 and 1908 in Lake Villarrica.....59

Figure 6.6 Relation between the thickness of the lahar clay cap and the straight distance from the lahar inflow point V1 to the cores in Lake Villarrica during the events of 1908 and 1971……60

Figure 6.7 Evolution of the number of the lahars during the Holocene in the lakes Villarrica and Calafquén……..63

Figure 6.8 Relationship between the cumulative thicknesses, represented by the size of the colored circles, the number of the correlated lahars each 50 cm, and the age in Cal yr BP based on the master core (VIL1) in Lake Villarrica……64

Figure 6.9 Relationship between the cumulative thicknesses, represented by the size of the colored circles, the number of the correlated lahars each 50 cm, and the age in Cal yr BP based on the master core (CAL2) and the age model in Lake Calafquén.....65

Figure 6.10 Evolution of the lahars during the Holocene in the lakes Villarrica and Calafquén sumarized.....66

Figure 6.11 Holocene precipitation estimates based on a water balance model for Laguna Aculeo in south-central Chile (33°50'S).....66

List of tables

Table 2.1 Grain-sized based nomenclature for common types of volcaniclastic rocks.....7

Table 3.1 Morphometric parameters of Lake Villarrica and Lake Calafquén.....19

Table 3.2 historically reported eruptions of Villarrica Volcano including reported VEI (volcanic eruption induced) and lahars (bold), and the volcanic event diposits (EDs, in light grey) attributed to Villarrica Volcano with varve year and inferred calendar year.....21

Table 4.1 Locations, length, sampling year and depths of sediment cores discussed in this study.....24

Table 5.1 Main features of the most important sedimentary deposits present in the short core record.....32

Table 5.2a Straight distance between the lahar inflow points and each of the cores in Lake Villarrica.....37

Table 5.2b Straight distance between the lahar inflow points and each of the cores in Lake Calafquén.....37

Table 5.3a Lahar pathways from the lahar inflow points to the deepest cores measured on the bathymetry map of the Lake Villarrica.....38

Table 5.3b Lahar pathways from the lahar inflow points to the deepest cores measured on the bathymetry map of the Lake Calafquén.....38

Table 6.1 Estimated age of the samples from the master cores of lakes Villarrica and Calafquén of two historical eruptive events.....62

Chapter 1: Introduction

1.1 Motivations

Pleistocene and Holocene volcanoes of the Chilean Andes are a natural laboratory for the study of volcanism, magma genesis and volcanic hazards in the context of oceanic-continental plate collision (Stern et al., 2007). Lahars are one of the main natural hazards derived from the volcanic activity. These rapidly flowing mixtures of rock debris and water from a volcano have already been studied by many authors (Maizels, 1989; Rodolfo and Arguden, 1991; Smith and Lowe, 1991; Pierson, Janda *et al*., 1992; Orton, 1996; etc.) and after their work can be concluded that some aspects of these events are unique to volcanic areas considering that it is essential to have volcanic material, a great amount of water and enough slope to run.
In many regions, such as "La Región de los Ríos" and "Región de la Araucania" in South-Central Chile (where the study area of this thesis is; Fig. 3.1), these features are accomplished and lahars have caused hundreds to thousands of casualties, as well as a tremendous amount of structural and economic damage in all the towns located beside the lakes at the foot of the Andean Chain (González-Ferrán, 1994; Petit-Breuilh, 2004).

Lakes are one of the most useful ecosystems for palaeoenvironmental investigations since they provide a continuous record of the lake depositional history, with high temporal resolution and records of volcanic and seismic activity. Considering this, to better understand the lahar evolution of Villarrica Volcano it is important to look at the record of the past lahars in Lakes Villarrica and Calafquén. The first Spanish colonist, led by Pedro de Valdivia (1540), only started settling in Chile in 1540. The town of Villarrica (The main town in the study area and next to Villarrica Volcano; see Chapter 3) was first founded in 1551, but then was destroyed by the Mapuches, the Chilean natives, and founded again in 1882 (Petit-Breuilh, 2004; Fig. 3.1). Since the arrival of the Spanish colonist, lahars have been reported, describing its casualties, pathways, magnitude and where they reached the lakes Villarrica and Calafquén (Fig. 4.1). But before 1550 there are no records of lahar occurrence, and between 1551 and 1900 the records are scarce and incomplete.

This Thesis is based on the work already done by Van Daele (2013) and Van Daele et al. (2014) who studied and described the characteristics of the sedimentary event deposits related to volcanic activity of Villarrica Volcano in the last 500 years.

The study area of this thesis are two lakes (Calafquén and Villarrica) bordering the Villarrica Volcano, and it tries to improve the understanding of the deposits (turbidites) of lahars in both lakes.

1.2 Objectives

The objectives of this thesis can be grouped into two different clusters.

1- Detailed study of historical lahar deposits from the last 100 yrs. For the last century, the lahar pathways that were used during eruptions are well known, as well as the magnitude of the

lahars. Sediment cores allowed to study the fining-upwards clay cap of the lahar deposits related to all these lahar events in high detail (i.e. thickness, depth and distance from the lahar inflow point using magnetic susceptibility analysis, visual identification from the pictures of the cores, processed images applying a histogram equalization and X-ray CT-scan images). This was done in order to understand:

(i) how lahars were deposited in Lakes Villarrica and Calafquén (density flow, turbidity current, underflow, interflow, and overflow);
(ii) how they relate to the magnitude of the lahars, depth, and distance from the point that the lahar reaches the lake and the bathymetry of the lake;
(iii) What is the influence of the season (influence of lake stratification).

2- Correlation of the lahar deposits for the past ~10,000 yrs based on the study of the thickness and depth using magnetic susceptibility analysis, visual identification from the pictures of the cores and processed images applying a histogram equalization of long distal sediment cores from both lakes. The main objective of this second part is to reconstruct the Holocene lahar history of Villarrica Volcano. This lahar history could not only give information on the activity of Villarrica Volcano (few or a lot of lahars compared to its general activity?), but also on its morphology (more lahars to a certain lake?), or on the influence of climate on lahar formation, as snow that can easily melt is needed for lahar formation in this region.

Chapter 2: General Settings

2.1 Chile

Chile occupies a narrow but extremely elongated strip of land in the southeastern corner of the South-American continent. Its length is up to 4270 km, making it one of the longest north-south countries in the world. It lays squeezed between the vast Southern Pacific ocean to the West and the towering Andes Mountains to the East. Covering such a huge latitudinal length and altitudinal differences, it should pose no surprise that the country encompasses a lot of different climatologic zones. These include the driest place on Earth, the Atacama Desert in the North, and one of the wettest places on earth with almost 325 days of rain, Bahia Feliz in the South of the country. The Chilean Margin is thought to be an area of active subduction since Middle Jurassic times when Gondwana began to move again and the Indian and South Atlantic oceans started opening up (Kay et al., 1989). Plate tectonics have shaped the country for the last millions of years and the most obvious expression of this force is the Andes mountain chain. The country itself generally gets subdivided into three distinct N-S geological regions according to their geomorphological appearance, and all are the result of the subduction of oceanic plates under the South American continent. These distinct regions include from West to East: the coastal range, the Central depression and the main Andes range (Fig. 2.1). Only the last two regions will be introduced here because the study area covers these two geological regions in South-central Chile (72°30'W – 71°30'W).

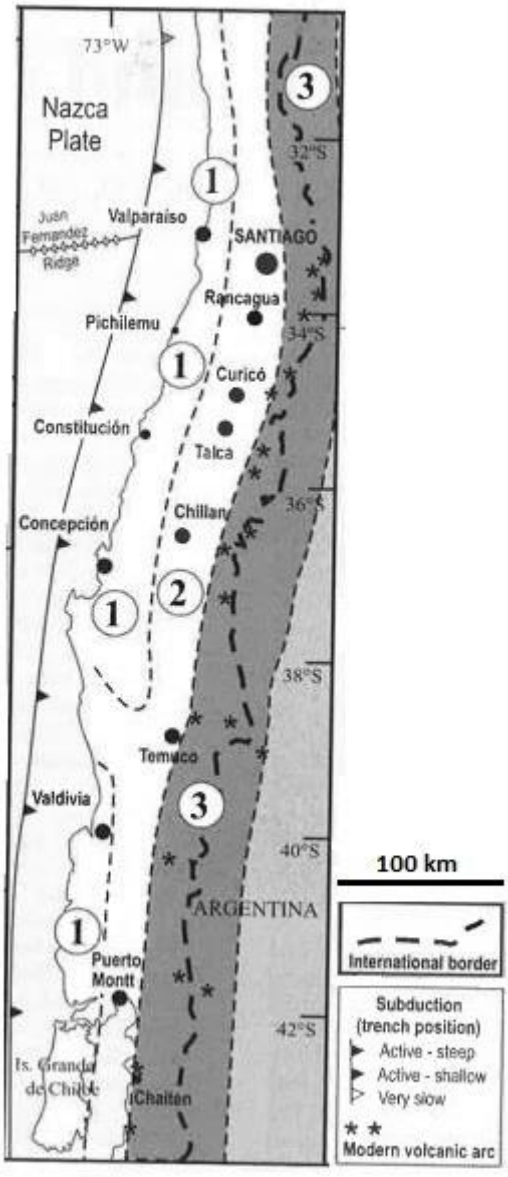

Figure 2.1 Sketch map of Chile, showing the main topographical zones: 1, Coastal zone (Coastal Cordillera); 2, Central Depression, or Central Valley; 3, Main Cordillera (Andes Range). Active and dormant volcanoes, and the generalized location of eastward-dipping subduction zones are schematically illustrated (figure modified from Pankhurst and Hervé, 2007).

The Central Valley is a low-lying area of about 60 km in width, located between the Coastal Range and the Andes range (Fig. 2.1). It represents a graben that progressively collapsed from North to South during the formation of the Andes. During the Quaternary, this depression accumulated large amounts of materials eroded from the nearby Coastal and Andean ranges by the action of glaciers, rivers and other earth weathering processes. Due to the flat topography of the Intermediate Depression, the presence of fertile soils, mild climate conditions and abundant water resources, it constitutes one of the most suitable areas for human occupation in Chile (Pankhurst and Hervé, 2007).

The Andes range is the longest continental mountain chain in the world extending for about 8000 km along the western margin of the South-American continent. The range extends through seven countries, including Chile. It is the result of subduction of the Nazca plate and the northern part of the Antarctic plate under the South American plate (Fig. 2.1; Fig. 2.2). Extensive magmatic activity and shortening of the crust by folding and faulting led to a thickening of the continental crust and uplift along of the Andes range (Jordan et al., 2001). The mountain range primary uplift took place during the Miocene but the emergence still continues today, as demonstrated by major earthquake and volcanic activity.

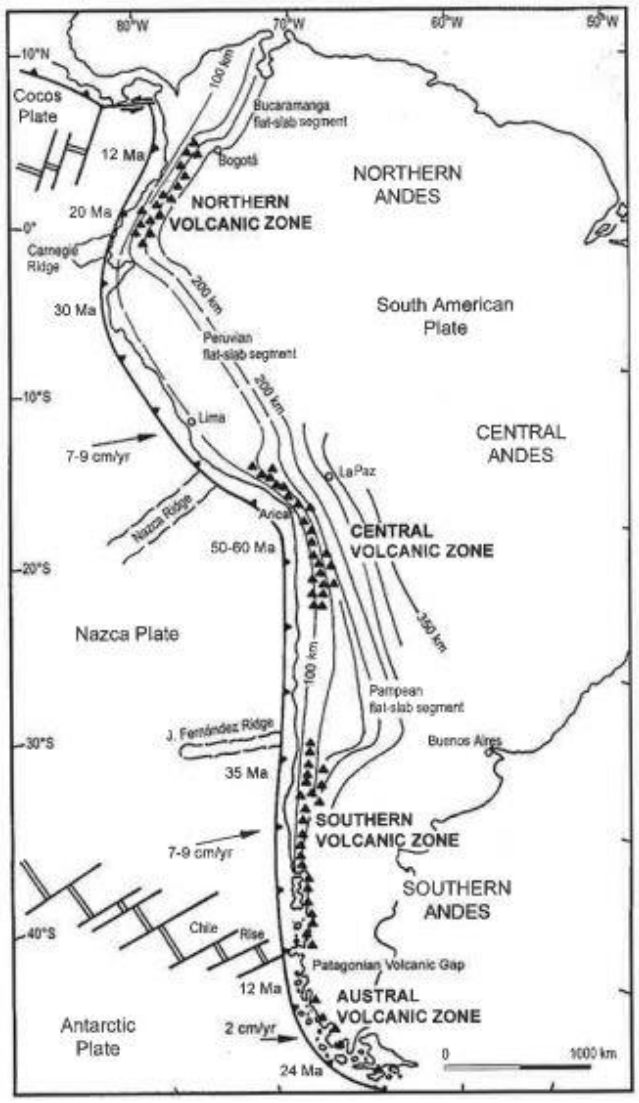

Figure 2.2 Schematic map of the Andes range divided in the four volcanically active zones. Subduction geometry as indicated by depth (in km) to the Benioff zone, oceanic ridges, ages of oceanic plates close to the trench, and convergence rates and directions along the length of the Andes. Volcanoes are represented with a black triangle (modified from Stern, 2004).

2.2 Volcanism in Chile

2.2.1 Tectonics

The convergence of two tectonic plates and the presence of a wedge of asthenospheric material are the main causes for the formation of a volcanic range. In the case of the Andes, there are areas characterized by both great volcanic and seismic activity, and areas within only an intense seismic activity. The reason for this difference is related to the subduction angle between the oceanic plate and the continental plate. With an angle of subduction greater than 25° there is enough asthenospheric material to generate volcanism, but with an angle of subduction lower than 15°, volcanism is absent, and only intense seismic activity occurs (González-Ferrán, 1994).

Variations in the subduction angle of the Nazca Plate under the South-American Plate require a North-South adjustment, which is expressed by the presence of the Liñique-Ofqui Fault System (LOFS), a fairly vertical fault along most of the Andes in south-central Chile. This point of weakness is where almost all the Southern-Volcanic-Zone (SVZ, see section 2.2.3) volcanoes are located. As a result, the volcanic arc has an almost North-South trend in southern Chile (39°S-46°S), although oblique alignments in NW-SE and NE-SW directions control the location of many of the volcanic complexes and large stratovolcanoes at the local scale (Stern et al., 2007).

2.2.2 Eruption types

In Chile, as along most of the segments along the Pacific Ring of Fire, the subduction process generates an andesitic magma that permits the formation of explosive volcanism (Fig. 2.3). The explosiveness is the result of a great viscosity, an abundant quantity of gases, and the presence of high quantities of groundwater. Viscosity is controlled by temperature, chemical composition, crystal content, concentration of dissolved volatiles, and the presence of bubbles (Orton, 1996). The viscosity increases proportionally to the content of silica and crystals and is inversely proportional to the temperature and the concentration of dissolved volatiles.

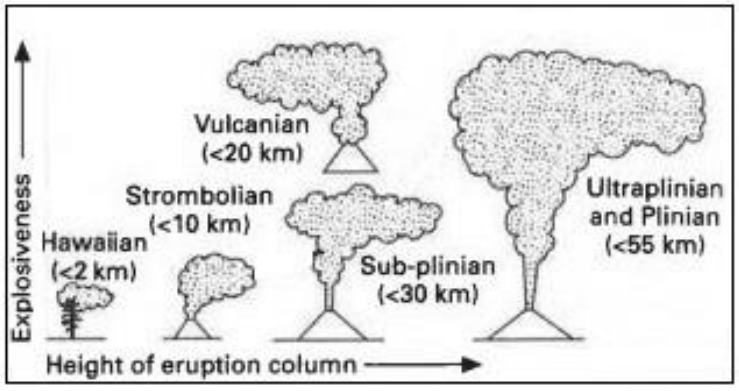

Figure 2.3 Classification of subaerial explosive volcanic eruptions based on explosiveness and the height of eruption column (figure modified from Orton, 1996).

Explosive magmatic eruptions vary according to magma composition, especially its volatile content and viscosity, and other factors. At least four types of eruptions are recognized (Orton, 1996; Figures 2.3 and 2.4):

a) **Hawaiian** eruptions are the least explosive. They alternate between extrusion of fluent magma and emission of liquid sprays high into the air as fire fountains.
b) **Strombolian** activity involves more viscous magmas. Strombolian eruptions are larger than the Hawaiian ones, and some extreme discharges can produce eruption columns more than 1 km in height.
c) **Vulcanian** eruptions are small in volume (less than 1 km^3) but very explosive. They involve higher viscosity, commonly crystal-rich, andesites.
d) **Plinian** eruptions are the most explosive. They produce high convecting eruption columns and involve high viscosity, mostly silicic lava (Walker, 1981).

Eruptions of volcanoes in the Chilean Andes encompass the entire range of eruption types, from explosive Vulcanian to the more extrusive Hawaiian type. For this reason, this paragraph should only be considered as a very general introduction on volcanic processes and types of eruptions.

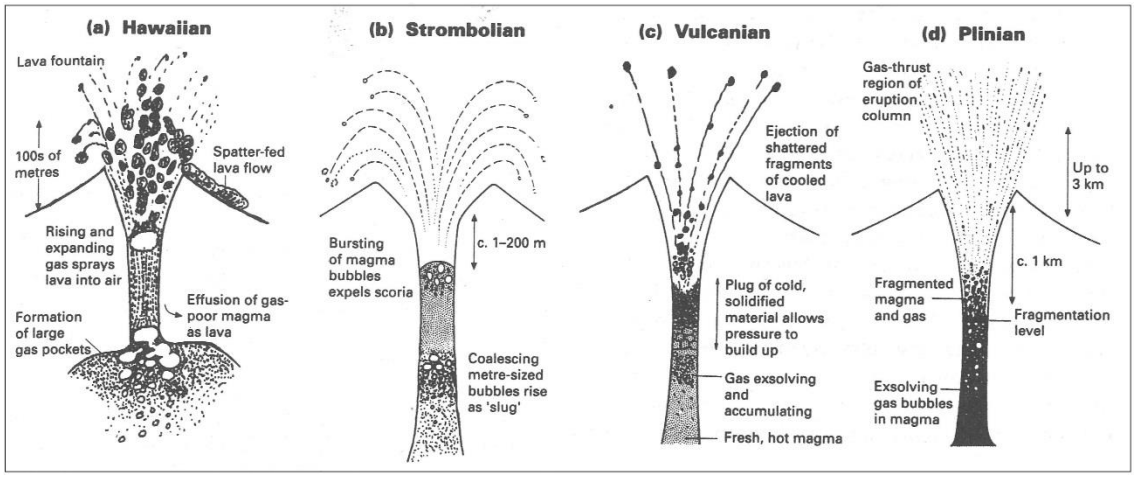

Figure 2.4 Types of magmatic eruptions. Diagrams are not all at the same scale. In general the depth to the fragmentation level and height of the gas-thrust portion of the eruption column increases from (a) to (d) (figure modified from Orton, 1996).

2.2.3 Chilean volcanic zones

The Andes range in South America contains four different volcanic zones (Fig. 2.2): the Northern (2°N-5°S), Central (14°S-28°S), Southern (SVZ; 33°S-46°S) and Austral (49°S-55°S) (Stern et al., 2007). Here, only the SVZ is described in details since the volcano of interest for this study – Villarrica – is located at 39.5°S.

The Southern Volcanic Zone (SVZ) is one of the most volcanically active areas in South America. It contains more than 70 Pleistocene and Holocene composite stratovolcanoes and large volcanic fields that are located along a continuous 1400 km long arc segment between 33.3°S and 46°S. The SVZ is limited to the North by the volcanic islands that constitute the Juan

Fernández Ridge (Fig. 2.2). Its southern limit corresponds to the triple junction point, i.e., the point where the Nazca, Antartic, and Pacific plates merge (Stern et al., 2007).

The behaviour of the volcanic arc changes long the SVZ. Between 33.3°S-34.4°S it consists in a narrow chain of volcanoes located along the Chile–Argentina border. Between 34.4°S and 39.5°S, the Cenozoic arc widens to more than 200 km. South of 39.5°S it turns into a relatively narrow chain of volcanoes mostly on the Chilean side of the border. South of 42°S all the volcanoes are located in Chile.

2.3 Products of volcanoes

2.3.1 General products of volcanoes

Products of volcanoes can be divided in two different types: the volatiles and lava.

The volatiles, or volcanic gases, consist in a great variety of dissolved gases that are part of the magma. They are mainly released during the eruption or when the magma reaches the earth's surface. The most abundant is the water steam, and it is followed by other gases like carbon dioxide, carbon monoxide, sulphuric anhydride, hydrogen sulphide, chlorine and fluorine.

When the magma reaches the earth's surface, it is called *lava*, an Italian word. Neapolitans applied the term lava to the magma flows from Vesuvius and now it is applied universally (González-Ferrán, 1994). Magma consist in a liquid with dissolved gases, which cools and degasses in contact with the atmosphere, resulting in a variety of volcanic rocks such as lava flows and pyroclasts of different sizes called tephra.

Tephra is derived from the Greek language meaning "ash". It encompasses all explosively expelled material, unconsolidated and fragmented products from a volcanic eruption. When they are found on earth they can originate from fallout of a volcanic plume or from pyroclastic density currents. The term can be applied to all volcanological grain sizes but a further subdivision is also available (a more extensive subdivision can be found in Table 2.1): ash (<2 mm in diameter), lapilli (2-64 mm), and blocks (angular) or bombs (rounded) (>64 mm).

	Pyroclastic deposits	
Grain size	Unconsolidated tephra	Consolidated pyroclastic rock
<1/16 mm	Fine ash	Fine tuff
<1/16–2 mm	Coarse ash	Coarse tuff
2–64 mm	Lapilli tephra	Lapillistone (or lapilli tuff or tuff-breccia)
>64 mm	Bomb (fluidal shape) tephra Block (angular) tephra	Agglomerate (bombs present) Pyroclastic breccia

Table 2.1 Grain-sized based nomenclature for common types of volcaniclastic rocks (from Orton, 1996).

Several different kinds of particles can compose a tephra whereby the most common ones are: pumice, glass shards, mineral crystals, and different lithics (igneous, sedimentary, and metamorphic). These fragments can have low densities, as is the case in vesicular pumice and glass, to being quite dense in crystals and lithics (Lowe, 2011).

The mechanism of spreading tephra is by air. It starts at the eruption column that is generated during a volcanic eruption. This column is able to reach several tens of kilometres into the atmosphere, sometimes even reaching the stratosphere. Then, the wind is the responsible of transporting the material until the density of the material reaches a similar level as its surrounding environment, resulting fallout, and deposit on the earth surface (Lowe, 2011).

The main characteristics of a lava-flow deposit are determined by the effusion and movement speed rates, controlled by the viscosity, and the slope. The effusion rate is the most important factor. For high-viscosity lavas, the effusion rate is always very low and it deposits forming a very thick with very steep walls dome, covering an up to few km^2. For low viscosity lavas, the effusion rate can vary. A low effusion rate (<10 m^3/s) produces a lot of small flows that pile nearby the emission centre; on the contrary, discharges of lava of tens of m^3/s cover areas of tens of km^2 (González-Ferrán, 1994). The flow velocity is linked to the viscosity degree, being inverse to the viscosity.

Lava flows can also produce a partial melting of snow and ice, generating subvolcanic products like lahars.

2.3.2 Lahars

Lahar is an Indonesian term originally used to describe mudflows containing volcanic debris, but the term has recently been extended to describe all rapidly flowing mixtures of rock debris and water from a volcano (Smith and Lowe, 1991). That rock debris refers to a combination of pre-existing fractured rocks remaining on the slopes of the volcano, fresh effusive materials and water.

The definition recognizes that some aspects of these events are unique to volcanic areas, but not all the lahars are a direct result of eruptive activity. Orton (1996) identified two types of lahars: those that occurred during an eruption and those between eruptions.

During eruptions water and the rest of materials can be released by:

1) Ejection of crater-lake water (Major and Newhall, 1989).
2) Melting of snow an ice by hot pyroclastic density currents, including subglacial pyroclastic eruptions (Maizels, 1989).
3) Liquefaction of just-deposited debris-avalanche deposits.

Between eruptions lahars can be triggered exclusively by rainfall (Rodolfo and Arguden, 1991). Seepage of rainfall or groundwater into hot pyroclastic debris can also cause violent steam explosions that further mantle the landscape with loose pyroclastic debris, which is later mobilized as lahars (Pierson, Janda *et al*., 1992).

These masses descend from the slopes, destroying and incorporating everything they find on their way. That allows the first lahar pulses to remove rough elements and create smooth channels that allow later lahars to travel faster. Therefore, their physical, dynamic and destructive power characteristics are controlled by the size of the fragments, the volume of water and the characteristics of the slope. Lahars are one of the most common indirect hazards related to volcanoes. González-Ferrán (1994) said that, generally, their density is higher than 2000 kg/m3; what means that it develops high energy and high velocities. Historical examples demonstrated varying velocities from 1.3 m/s to 40 m/s downstream the valley, with which can overcome significant topographic barriers. In consequence, the area of influence can reach several tens to hundreds of km depending on the characteristics of the lahar, the topographic features of the region and its initial velocity.

Wells and Harvey's (1987) model of subaerial lahar structure assumes that, based on the water/sediment ratio, it is possible to differentiate lahars into dilute streamflows (lower percentage of sediment), debris flows (higher percentage of sediment) and an intermediate type, which they call hyperconcentrated flow (Fig. 2.5; Fig. 2.6).

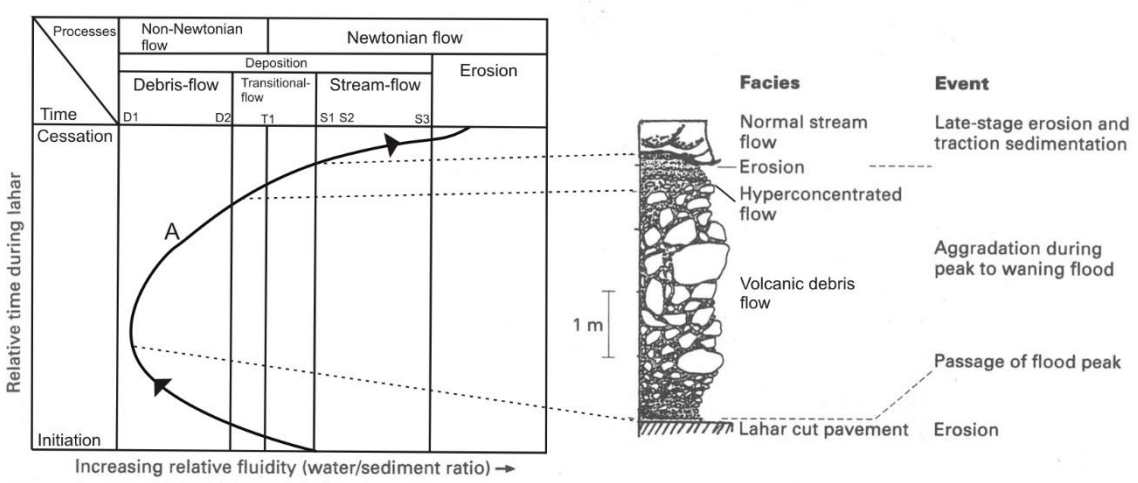

Figure 2.5 Conceptual model showing the changes in water/sediment ratio, and the sequence of deposicional and erosional processes observed in modern lahars. Line A and associated arrows illustrate the relative timing of facies deposition, resulting stratigraphic sequence, and relative timing and amount of erosion for an ideal lahar event. Column on right depicts an ideal lahar cross section and how it might be interpreted in this context (figure modified from Wells and Harvey, 1987).

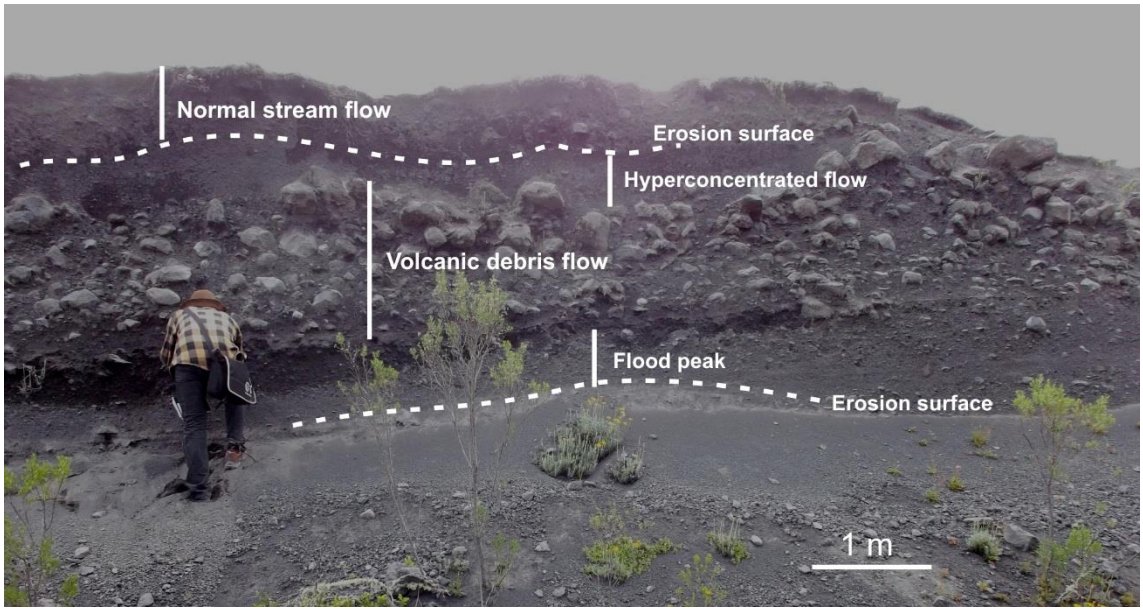

Figure 2.6 Picture placed at one of the historical lahar pathways of Villarrica Volano illustrating an ideal cross section of a sub-aerial lahar (Ferran Parera, January 2014).

In a normal streamflow, the sediment-water mixture is transported in a Newtonian flow. Turbulence is important and fluid and granular phases act independently, sand or gravel particles are free to settle grain by grain to develop traction structures or bedforms. It remains as a Newtonian flow as the concentration of suspended particles reaches a level where the particles start to interact and the fluid acquires a yield strength. That yield strength depends on the amount of clay and the clay mineralogy (with flocculated suspensions of smectite[1] it reaches the yield strength at concentrations of 3% by volume, while with coarse pumiceous suspensions can remain a Newtonian fluid until frictional interaction begins approximately the 50% by volume) (Fig. 2.5; Fig. 2.6).

Hyperconcentrated flows have an intermediate character with sediment concentrations of 20-60%. Turbulence is soothed by the higher sediment concentration (due to dispersive pressures generated by intergrain collision). Pierson and Scott (1985) classified the material typically carried in this kind of flow in two groups: (1) sand and low-density gravel transported in suspension, and (2) large boulders (up to 1 m in diameter) transported as bedload. Deposits are generally tens of cm to metres thick, generally massive and often normally graded with little to no stratification, which is a result of rapidly and commonly uninterrupted deposition from suspension. The upper fine-grained part may show some stratifications (Fig. 2.5; Fig. 2.6).

Volcanic debris flows consists on non-Newtonian fluids with a 10 to 25% of water content. They are generally clay-poor, few being mudflows, because most form by mobilization of fragmental pyroclastic and autoclastic[2] debris soon after eruption (Orton, 1996). There are two

[1] Smectite is a group of minerals of the group of the clay minerals (hydrous aluminium phyllosilicates).

[2] Autoclastic refers to the process of fragmentation produced by mechanical friction or gas explosion during the movement of a lava flow.

predominant types of facies in volcanic debris flows: (1) channel debris flows (if they are confined) or (2) unconfined debris flows (if they are unconfined, such as a floodplain):

- Channel debris-flow facies is basically composed by large clasts and a coarse matrix. One of the main characteristics of those deposits is that the clasts are randomly dumped, more than other matrix-supported debris flow deposits (Rodolfo, 1989). Brayshaw (1984) described the rheological behaviour of these deposits indicating that large clasts tend to accumulate as linear clusters of outsized boulders aligned to the direction of flow, sometimes forming "whale-back bars"[3]. The largest events sometimes include a basal episode called "sole layer" covering 10-15% of the deposits. Scott (1988) described it as inversely graded crudely stratified pebbly sands or clast-supported pebbles, attributed to cataclasis[4] and dispersive pressure within a basal shear zone, and is thought to be deposited near peak discharge.

- Unconfined debris flow facies are usually matrix supported and outsized clasts are common on tops of beds. Orton (1996) described that the thickness of that facies ranges between 1 and 6 m, and is proportional to the size of the flow.

Most lahars are affected by a mixture of these three modes of transport during their evolution (Fig. 2.5; Fig. 2.6). They generally start as transitional flows, evolve towards debris flows, and finally return to transitional and stream flow conditions. In a cross-section, this results in a massive unit that contains the coarsest and densest elements in its centre. This unit progressively fines upwards (hyperconcentrated flow deposits), and is finally capped by a thin unit of fine-grained floodplain deposits. Since the mode of transport also changes with distance downvalley, the same lahar can show different facies upstream and downstream.

2.4 Lakes in southern Chile

During the Last Glacial Maximum (LGM)[5], the southern part of the South-American continent (38°S – 56°S) was covered by the Patagonian Ice Sheet, the largest ice sheet in the Southern Hemisphere excluding Antarctica. The landform record indicates that the Patagonian Ice Sheet consisted of many outlet glaciers, local cirques[6] and independent ice domes (Glasser et al., 2008). In general, climate was cold and humid on the western side of the Andes south of 33°S, and mean summer temperatures were about 5-6°C below present.

[3] "Whale-back bar" it is defined in Scott (1988) as a term to describe a longitudinal streamlined bar of poorly sorted inverse to normally graded clast-supported gravels.

[4] Cataclasis consists on the deformation of a rock at low temperature produced by crushing tectonic fracturing and rotation of mineral grains or aggregates without chemical reconstitution, which causes fragmentation and disunity granulation crystal (structure of mortar or rock fragments surrounded by matrix crystals shattered), the rock texture becomes thin and acquires a schistose structure, occurs with a certain amplitude, without reconstitution chemical and mechanical consequence of actions that have performed after their formation.

[5] The LGM corresponds to a period in the Earth climate history, between 26,500 and 19,000–20,000 years ago when ice sheets were at their maximum extension (Clark, et al., 2009).

[6] Cirques are large amphitheatre-shaped depressions carved in mountain flanks or incised into plateau edges (Glasser et al., 2008).

During the deglaciation, most of those glaciers, especially the glaciers located on the western side of the Andes, were warm-based (Glasser et al., 2008). The retreat of these glaciers generally results in the formation of proglacial lakes through processes such as damming by moraines[7], formation of depressions by melting ice (kettle lake), or the reversal of regional slope due to isostatic depression caused by glacial build-up.

Large piedmont glaciers were developed during glacial periods at the Chilean side of the southern part of the Andes Range. The maximum positions of these glaciers are, in general, marked by arcuate terminal moraines. The glaciers eroded deep basins at the front of the Andean mountains and nowadays their terminal moraines enclose the lakes that give their name to the Chilean Lake District (39°S – 42°S and 72°30'W – 71°30'W) –where the area of interest of this study (lakes Villarrica and Calafquén) is located– (Fig. 2.7). Laugenie (1982) described at least four first-order glacial periods in the Chilean Lake District, but the innermost moraines around the lakes were formed during the last glaciations, also called the Llanquihue glaciation (75000–14000 cal a BP).

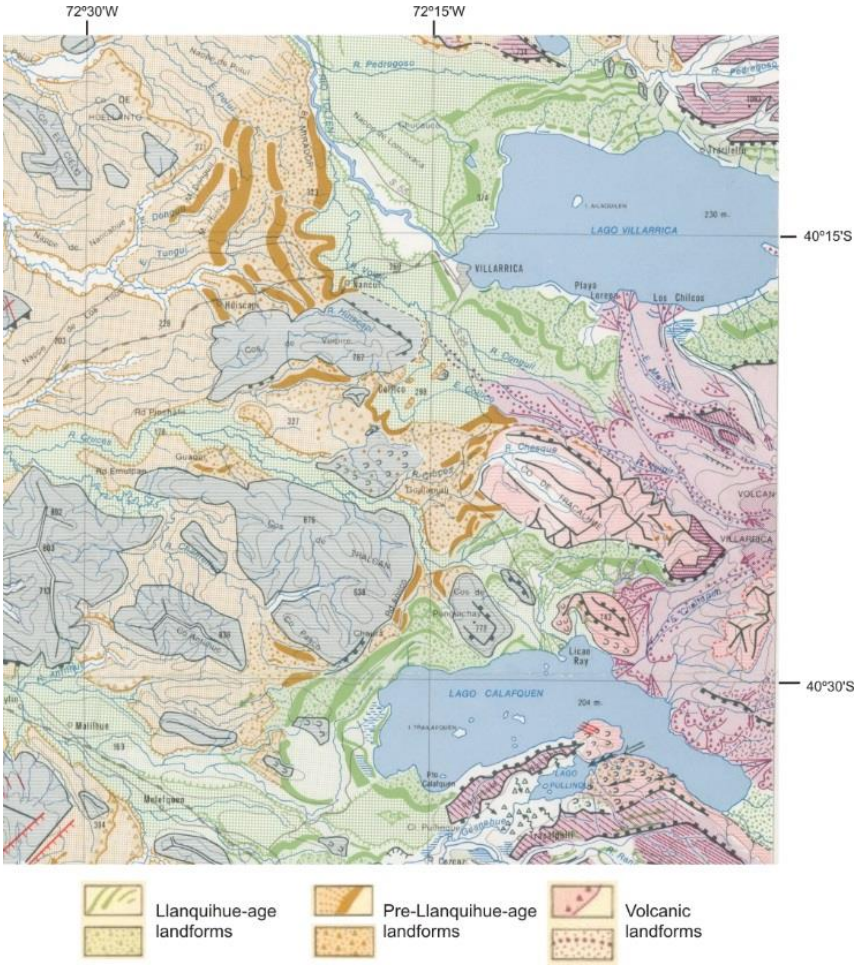

Figure 2.7 Geomorphological map of the study area in the northern Chilean Lake District: 1:250,000 (figure modified from Laugenie, 1982).

[7] A moraine is a form of glacial accumulation consisting in a mass of detritus fallen on a glacier, or torn by ice, transported and deposited by the same glacier, poorly classified and without stratification; which retains its original morphology and depositional situation regarding the glacier.

2.5 Lacustrine sedimentation

2.5.1 Lake stratification

Dynamic processes in lakes are regulated to a large extent by differences in water density. The density of water is a function of temperature and to a lesser extent of suspended sediment concentration (Talbot and Allen, 1996).

The greatest source of heat to lakes is solar radiation. During the hottest periods of the year, solar energy warms the surface waters, generating a vertical temperature gradient in the lake (Fig 2.8). The upper part of the water column, which is the warmest and least dense layer, is called the epilimnion. The lowest part is termed hypolimnion. It is cooler and denser than the layers above. The transition between the epi- and hypo-limnion occurs in an intermediate layer termed metalimnion (Fig 2.8). The corresponding zone where temperature decreases most rapidly with depth is called thermocline. Talbot and Allen (1996) described that the extent of thermal density stratification and resistance to mixing (that is, the stability) of a lake is very strongly influenced by its size and morphology.

Thermal stratification is well developed in temperate lakes such as Villarrica and Calafquén, but seasonal changes in air temperature and wind can also trigger an "overturning" process, especially in autumn, which consists in homogenizing the water masses after disparition of the lake stratification (Talbot and Allen, 1996).

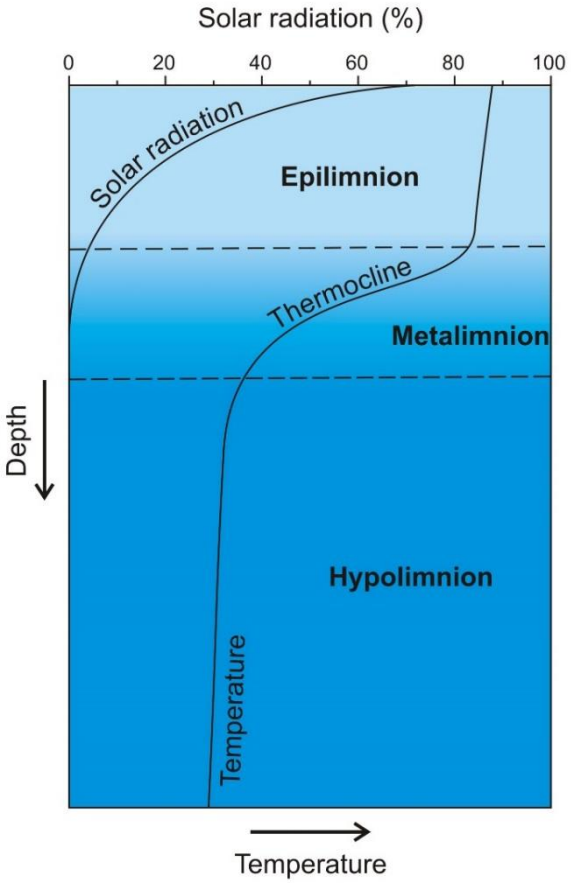

Figure 2.8 Vertical profile of solar radiation and temperature in the water column of a temperate lake. The thermocline marks the zone of maximum temperature change (from Bertrand, 2005; based on Wetzel, 1983).

Other than thermal stratification, sedimentary stratification can be of great importance in lakes. Sturm and Matter (1978) described that, in general, the quantity of sediment material in suspension increases with depth, and the density of the water is proportional to the percentage of sediment in suspension.

2.5.2 Lake sedimentation

2.5.2.1 Types of sediment

There are two types of sediment depending of their origin: Autochthonous and allochthonous. On one hand, autochthonous sediment it is composed by organic matter and authigenic minerals. Organic matter is originated by the decomposition of lacustrine organisms such as plankton and benthos and its quantity depends of the lake productivity that in turn it depends on the amount of nutrients available. According to the nutrient productivity parameter, Cohen (2003) classified lakes in two different types: oligotrophic and eutrophic, with low organic matter productivity and high organic matter productivity rates, respectively.

On the other hand, allochthonous sediment corresponds to all the material brought into the lake by sediment transport processes such as aeolian, fluvial, glacial and gravity processes. The transport mechanisms are controlled by meteorological factors such as precipitation or ice cover, the characteristics of the surrounding area (amount of vegetation and geomorphology) and other local features (Cohen, 2003). For example, the study area of this thesis –lakes Villarrica and Calafquén– is located in an active volcanic area encircled by volcanoes.

2.5.2.2 Sediment transport and distribution

Mulder and Alexander (2001) described that the distribution of material by non-aeolian mechanisms can take place through fluid gravity flows or sediment gravity flows.

In temperate lakes the sedimentation process is controlled by the thermal stratification of the lake water (Fig. 2.8) and the difference in density between the incoming flows with sediment and the lake water.

Onshore fluid gravity flows start at some place due to gravity and drag sediment of different sizes and densities along their pathway with them. Subaqueous sediment-transporting density flows (fluid gravity flows when they interact with the lake) can be subdivided according to the difference of densities between the inflow (ρ_f) and the surrounding water (ρ_w) (Mulder and Alexander, 2001) (Fig. 2.9 and Fig. 2.10). If the density of the river is the same as the lake water ($\rho_f = \rho_w$) the flow is called homopycnal. It consists in a cloud of sediment where heavy fractions (grave, sand) are deposited at the stream mouth. When the incoming flow has a density higher than the lake water ($\rho_f > \rho_w$) it forms an underflow (hyperpycnal flow), that remaining at the hypolimnion (Fig. 2.8), follows the bathymetry of the lake until the deepest part. Density flows that transport large volumes of sediment to deep water are probably mostly underflows. However, in temperate lakes with a well-developed thermal stratification (Fig. 2.8) two different

situations can occur: on one hand, when $\rho_f < \rho_w$ the flow behaves as an overflow, also called hypopycnal flow, where sediment is dispersed as a buoyant plume cross the epilimnion (Fig. 2.8, Fig. 2.9 and Fig. 2.10). On the other hand, when the density of the incoming flow is lower than the epilimnion but higher than the hypolimnion ($\rho_{w1} < \rho_f < \rho_{w2}$), it travels through the area called metalimnion as an interflow (of mesopycncal flow) above the thermocline (in terms of temperature that corresponds to the pycnocline, what refers to the same but in terms of density) of the lake acting as a sediment trap (Fig. 2.8, Fig. 2.9 and Fig. 2.10).

All these cases are not strictly opposite and they can occur at the same time during a single event because the density and the sediment concentration is not homogeneous along the gravity flow.

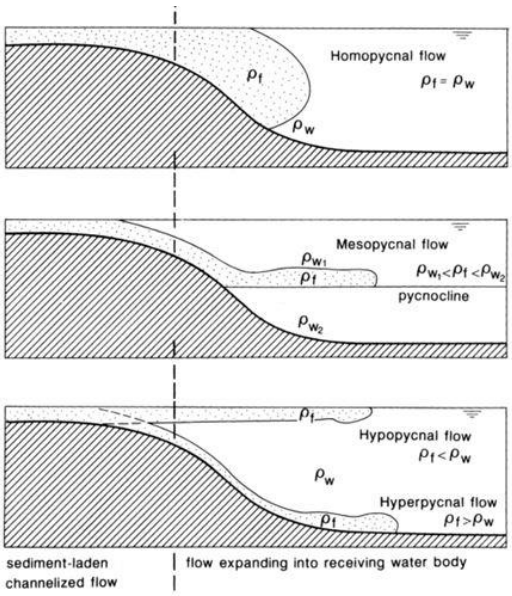

Figure 2.9 Types of density flow (from Mulder and Alexander, 2001).

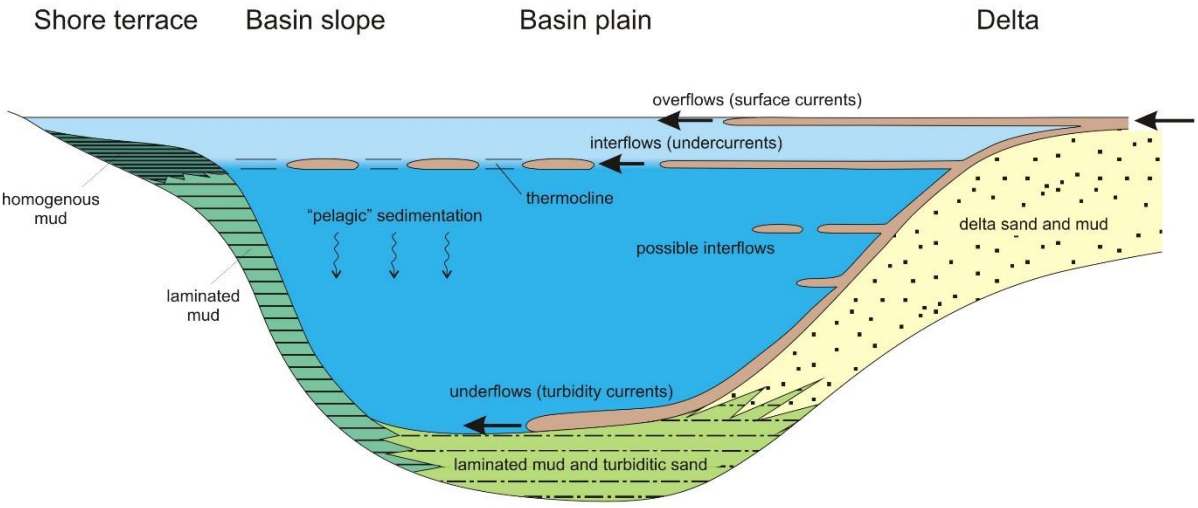

Figure 2.10 Distribution mechanisms and resulting types of proposed for clastic sedimentation in oligotrophic lakes with annual thermal stratification. Width of basin and sediment thickness are not to scale (from Bertrand, 2005; based on Sturm and Matter, 1978).

There is a complex variety of sediment gravity flows operating in subaqueous environments. Mulder and Alexander (2001) classified the most relevant ones based on physical flow properties and grain-support mechanisms. Since the deposits studied in this thesis are not thick enough to tell these different types of deposits apart, this aspect will not be developed here.

2.5.2.3 Volcanic sedimentation in lakes

As previously described in section 3.3.2, lahars are affected by a mixture of different modes of transport during their evolution. These transport processes vary both in time and space. As a result, lahar deposits are represented by sedimentary facies that are different upstream than downstream. When a lahar enters into a lake, the coarsest grains (coarse silts and coarser) are transported in a hyperpycnal flow and further deposited on deltaic fans and in (proximal) deep basins (Van Daele, 2013; Fig 2.11). Medium silts and finer grains are transported by means of a homopycnal flow, an interflow or an overflow (depending on lake stratification) and distributed over the entire lake.

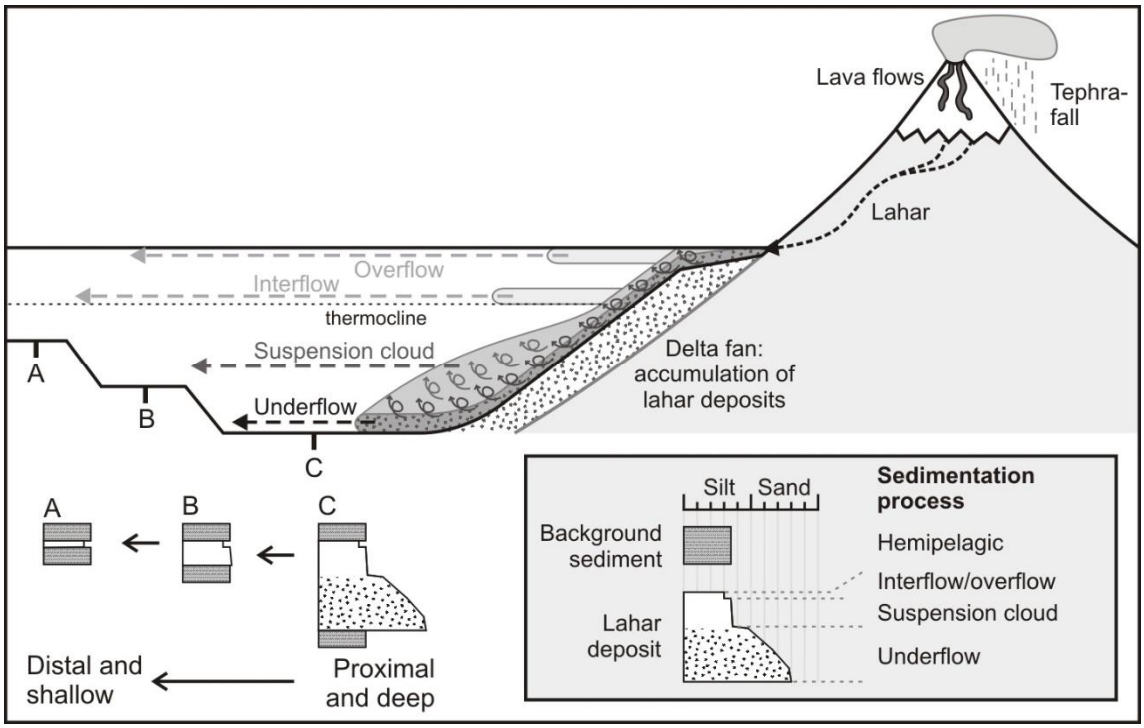

Figure 2.11 Schematic illustration of the formation of lahar deposits in lacustrine environments (Van Daele et al., 2014).

Tephra is generally deposited in lakes through direct fallout. Particles of tephra settled in the lake surface and remain floating, being transported by currents and the swell generated by wind. After a certain time, they sink to the bottom of the lake at a rate depending on their density and shape.

Recently, Bertrand et al. (2014) demonstrated that another way whereby particles of tephra can reach lakes, especially for lakes located upwind from volcanoes in south-central Chile, is by rivers; which gather tephra from the watershed previously distributed by wind. With this mechanism, when tephra particles make contact with the lake water, its distribution and

deposition gets controlled by thermal stratification of the lake and the density contrast between the feeding river and the lake water (Fig. 2.11). Then, the sedimentation process is the same as with lahars.

Chapter 3: Regional Setting

3.1 Study area

3.1.1 Lake origin

The study area consists of two lakes (Villarrica and Calafquén), which are belong to the "Región de los Ríos" and the "Región de la Araucania", in south-central Chile. As previously described in section 2.4, the origin of these lakes is associated to the last Andean glaciation and both lie in glacially overdeepened valleys dammed at their western border by large frontal moraines (Fig. 2.7 and Fig. 3.1). The landscape surrounding the lakes is dominated and highly influenced by Villarrica Volcano, one of the most active volcanoes of the SVZ in Chile.

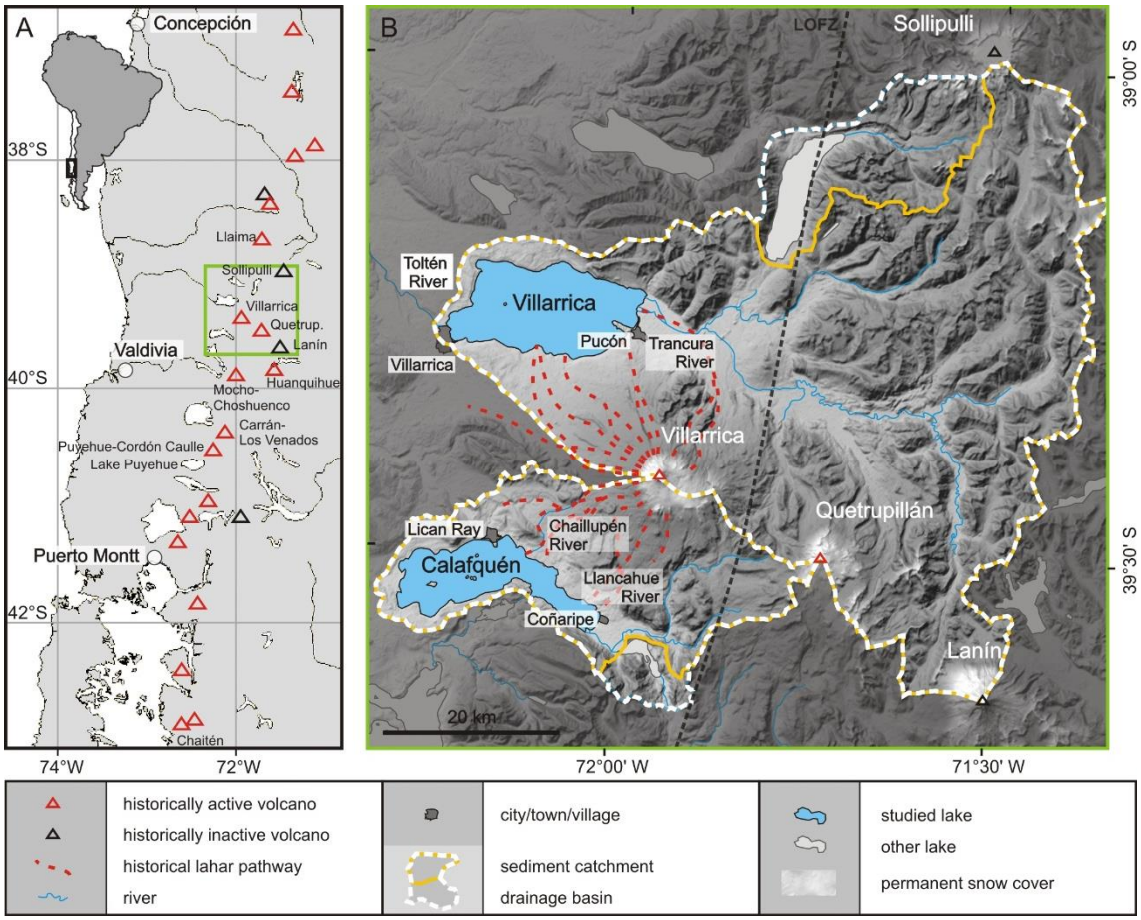

Figure 3.1 (A) Location of the study area in South-Central Chile. (B) The two studied lakes (in blue) and their drainage basins and sediment catchment. Historical active (red triangle) and inactive (black triangle) volcanoes in the region and historical lahar pathways from Villarrica Volcano (red dashed line) are indicated (modified from Van Daele, 2013).

3.1.2 Limnology

The climate in this area of Chile is humid-temperate, with a mild summer and most precipitation occurring during austral winter (Heusser, 2003). Lakes are temperate with winter circulation and summer stratification. A study accomplished by Campos et al. (1983) in Lake Villarrica shows that superficial layers began to get warm at the beginning of spring penetrating to the deep layers until 80 m of depth. The variations of seasonal temperature at different depths show a division which was found at a depth of 30 m during spring-summer, with a warm upper layer and a cold beneath. The isotherms show that the epilimnion fluctuates from 12° to 22°C, the thermocline from 13.4° to 20.9°C and the hypolimnionfrom 9.5° to 10°C (Fig. 3.2). Due to the proximity, we can infer that similar mechanisms apply for Lake Calafquén.

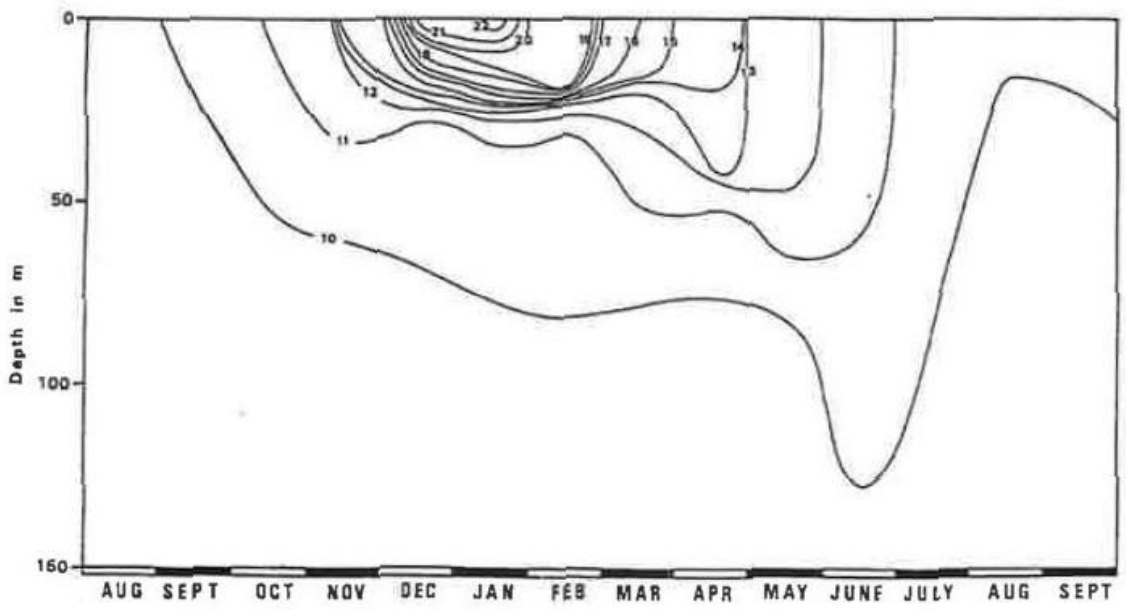

Figure 3.2 Chronological distribution of the isotherms in Lake Villarrica from the winter of the year 1978 until the same season in 1979 (Campos et al., 1983).

Van Daele (2013) suggested that these weather features, like the perennially high amount of winter precipitation, enable that the availability of easily erodible material in the sediment catchment is the controlling factor on sediment transport to the lakes. Bertrand and Fagel (2008) described the superficial material in the study area as andosols that developed in volcanic ash, and amorphous clays (allophanes) that are the product of post-depositional weathering of this ash, which mainly consists of volcanic glass and plagioclase.

3.1.3 Bathymetry and catchment area

Lake Villarrica is located at a latitude 39°18'S and a longitude 72°05'W (Fig. 3.1). It consists of a single, deep central basin with a subrectangular morphology, with its biggest axis that run in an East to West direction (Tab. 3.1). A small rocky island (Allaquillén) marks the transition between the mean deep basin to a shallower area in the SW part of the lake. Villarrica's catchment (2650

km^2) comprises the northern slopes of Quetrupillán (2360 m a.s.l) and Lanín (3776 m a.s.l) and Villarrica (2847 m a.s.l) volcanoes, and the southern slopes of Solipulli volcano (2282 m a.s.l). Its main tributary (the Trancura River) reaches the lake from the East and its main outflow is the Toltén River, which discharge the lake towards the Pacific Ocean.

Lake Calafquén is located at a latitude 39°31'S and a longitude 72°11'W (Fig. 3.1). It consists of a narrow, elongated and deep basin in the East and a wider area in the West (Tab. 3.1). As Moernaut (2010) described, many topographic highs, including some islands, separate the eastern part from the western area of the lake, which is more complex. This western part consists of a flat-bottomed deep basin (210 m deep basin), a SW sub-basin (150 m deep) and a SW basin. Two small E-W oriented valleys are located east of the SW basin. Calafquen's catchment (554 km^2) comprises the southwestern slopes of Quetrupillán Volcano and the southern slopes of Villarrica Volcano. Its main tributary is the Llancahue River.

Lake	Altitude (m asl)	Maximum length (km)	Maximum width (km)	Shore line (km)	Surface area (km^2)	Maximum depth (m)	Volume (km^3)
Villarrica	230	23.05	11.20	71.20	175.87	165	20.987
Calafquén	203	25.1	7.80	76.30	120.60	212	13.91

Table 3.1 Morphometric parameters of Lake Villarrica and Lake Calafquén (from Campos, 1984).

The landscape of the study area has been shaped by numerous megathrust earthquakes. As previously described in section 2.1, Chile is close to an important subduction area in which the current convergence rate of the Nazca Plate under the South American Plate is estimated between 66 mm/y (Angermann et al., 1999) and 78 mm/y (DeMets et al., 1994). The largest earthquake ever recorded occurred in the study area in 1960 (M_w 9.5), along the Valdivia rupture zone, with a rupture length of 1000 km (Cifuentes, 1989). Other main documented earthquakes occurred in 1575, 1737 and 1837. And more recently, in February 2010, the Maule earthquake (M_w 8.8) ruptured about 500 km of the megathrust just north of the study area (Moreno et al., 2012).

3.2 Villarrica Volcano: Geology and eruptive history

Villarrica Volcano (39°25'12"S – 71°56'23"W, 2847 m asl) belongs to the SVZ in Chile. It is located at the western edge of the Villarrica–Quetrupillán–Lanín volcanic complex, which is oblique to the Liñique-Ofqui Fault System (Fig. 3.1). It consists of a Middle Pleistocene–Holocene compound stratovolcano with a basaltic to andesitic composition (González-Ferrán, 1994). Historic eruptions that have occurred at Villarrica Volcano have been mainly Hawaiian to Strombolian (Clavero and Moreno, 2004).

The evolution of Villarrica Volcano is known since 300 ka, and it has been divided into three stages (units) according to geochronological, stratigraphical and morphostructural criteria (Clavero and Moreno, 2004):

- During the first stage (Villarrica 1, middle to upper Pleistocene) an ancestral stratocone was built ending with an explosive eruption that shape a caldera (caldera 1) of 6.5 x 4.2 km in diameter and 1900 m asl at 14.5 ka.

- During Villarrica 2 (upper Pleistocene to Holocene, 14.5 – 3.7 ka), of postglacial age, a new stratocone located on the northwestern edge of the caldera 1 was built. It consists of a succession of lavas and more than ten pyroclastic flows up to 10 km^3. This stage finished with a great eruption, associated to the Pucón Ignimbrite eruption (Clavero and Moreno, 2004), and the corresponding formation of a new caldera (caldera 2) of 2.2 km diameter at a 2400 m asl.

- During Villarrica 3 (covers the Holocene until nowadays, 3.7 ka to present) the modern cone with a height of 450 m above its base was formed in caldera 2. This new cone has been built through successive effusive and explosive eruptions. The last large explosive event occurred in 1620 (Clavero and Moreno, 2004).

Before the arrival of the Spanish colonist, there is no more detailed information about the eruption history of the Villarrica Volcano. Nevertheless, since the Spanish settled in the region in 1551, Villarrica Volcano is considered as one of the most active volcanoes in Chile, Having more than 50 reported eruptions (Petit-Breuilh, 2004; Tab. 3.2), on top of which Van Daele et al. (2014) discovered another 36 eruptions within that time period. The same authors also show that Villarrica Volcano has been constant during the last 600 years. There have been eruptions of great importance, either by their destructive power and deaths caused, by the amount of ejected material or duration. For example, the eruptions of 1558 and 1575 destroyed the town of Villarrica, killing 350 people in the second case (Gonzalez-Ferrán, 1994).

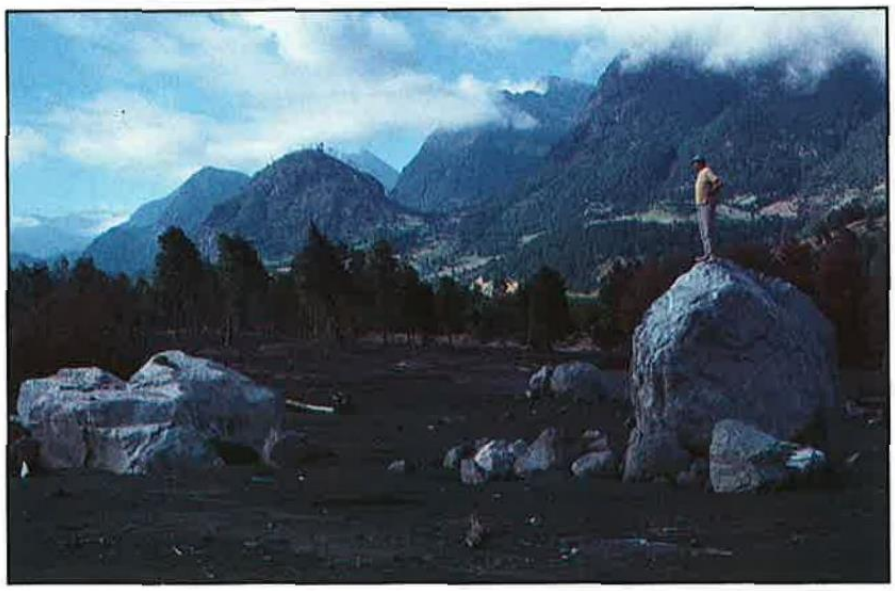

Figure 3.3 Granit blocks with a volume up to 40 m^3, dragged some kilometres by the power of a lahar during 1971 Villarrica Volcano eruption (González-Ferrán, 1994).

Year		Calafquén				Villarrica			
	Rep. VEI	VY	FeL	TEF	LAH	VY	FeL	TEF	LAH
2009	1								
2008	1								
2004	1								
2003	1								
1998	1								
1996	1								
1995	1								
1994	1								
1992	1								
1991	2					1993			X
1984	2	1984	X						
1983	1								
1980	2	1982	X						
1977	1								
1971	**2**	1971			X	1974			X
1964	**2**	1965			X	1965			X
1963	**3**	1963			X	1964			X
1961	1								
1960	1								
1960	EQ	1960	LT-1			1960	LT-1		
1958	1								
1956	1								
1949	**3**	1948			X	1949			X
1948	2?								
1947	1								
1938	2	1938			X				
1935	1								
1933	2					1935	X		
1929	1								
1927	2	1929	X						
1922	2	1924	X						
1921	2?								
1920	**2**					1927			X
1915	1	1918	X						
1909	**2**	1910	X			1918			X
1908	**2**					1916			X
1907	2								
1906	2	1906	X						
1904	**2**	1904	X			1910			X
1902						1908	X		
1897	2					1902			X
1893	2	1894			X	1897			X
1890						1891	X		
1883	2	1887	X						
1880	2					1880			X
1879	2					1878			X
1877	2					1876	X		
1875	2								
1874	2					1872	X		
1871		1877	X						
1869	2	1875	X			1867	X		
1864	2								
1859	2								
1853	2	1860	X			1848		X	
1852						1846			X
1850						1843	X		
1841		1846	X						
1837	2	1841	X						
1837	EQ	1839	LT-2			1830	LT-2		
1836		1839	X						
1832	2	1834	X			1821			X
1826		1829	X			1815	X		
1822	2	1825			X	1811			X
1815	1					1807	X		
1806	2	1807	X			1796			X
1798		1799	X						
1790	1								
1787	2	1790		X		1781			X
1780	1					1775	X		
1777	1								
1775	**2**	1782			X	1772			X
1771		1777	X						
1767		1773	X						

Year		Calafquén				Villarrica			
	Rep. VEI	VY	FeL	TEF	LAH	VY	FeL	TEF	LAH
1761		1766	X						
1759	1	1764	X						
1751	1	1750	X			1753			X
1745	1								
1742	2					1742	X		
1737	2	1734		X		1739	X		
1737	EQ	1732	LT-3			1739	LT-3		
1730	2	1725			X	1728			X
1721		1717			X				
1716	1	1712		X		1715			X
1715						1713	X		
1709		1707	X			1707		X	
1708		1706			X				
1705		1703			X				
1688	**1**	1690			X	1691			X
1682		1684		X		1684			X
1675	?	1676	X						
1672		1673	X						
1669						1672			X
1657	1								
1647	1	1648		X		1651			X
1645						1649	X		
1642						1647	X		
1640	(3-4?)	1639			X	1645			X
1638		1637	X						
1632						1638			X
1625		1627	X						
1617		1620			X	1625			X
1612		1617			X	1619			X
1610		1614		X					
1604						1612	X		
1600		1606	X						
1594	2	1601	X			1603	X		
1584		1590	X			1592			X
1582		1587	X						
1579						1587	X		
1576						1584	X		
1575	EQ	1579	LT-4			1583	LT-4		
1564						1577			X
1562	2					1575			X
1558	**2**	1576		X		1571		X	
1553		1571	X			1566	X		
1543		1560	X			1557			X
1539						1551			X
1538						1548	X		
1537						1545	X		
1526		1544	X			1533			X
1523		1541	X						
1521		1539	X						
1516		1534	X						
1515		1533			X				
1509		1527	X						
1503		1521	X						
1497		1515	X						
1494		1512	X						
1492		1510			X				
1483		1501			X				
1479		1497	X						
1474		1492	X						
1471		1489			X				
1466		1484	X						
1463		1481			X				
1454		1472	X						
1448		1466	X						
1433		1451	X						
1417		1435	X						
1413		1431	X						
1410		1428			X				
1404		1422		X					
1392		1410	X						
1388		1406	X						
1384		1402	X						

erosion

Table 3.2 (Previous page) historically reported eruptions of Villarrica Volcano including reported VEI (volcanic eruption induced) and lahars (bold), and the volcanic event diposits (EDs, in light grey) attributed to Villarrica Volcano with varve year and inferred calendar year. Historical earthquakes (EQ) and their lacustrine turbidites (LT; dark grey). Rep.: reported; VY: varve year; FeL: Fe-rich lamina; TEF: tephra; LAH: lahar (modified from Van Daele, 2013; based on Siebert et al., 2010).

Records of 20th century eruptions are more or less complete, and show that the main related hazards are generation of lahars, lava flows, tephra fallout and small-volume pyroclastic flows; but only lahars have produced casualties in Villarrica's history (Stern et al., 2007). For example, in 1948, lahars generated during an eruption destroyed the town of Coñaripe resulting in 23 casualties and 31 missing people (González-Ferrán, 1994; Petit-Breuilh, 2004; Fig. 3.1). These large lahars reaching the villages on the shores of lakes Villarica and Calafquén also reach the lakes itself and will leave a permanent imprint in the lake bottoms. For example, lahars from eruptions in 1908 and 1920 affected only Lake Villarrica, and in 1963/64 and 1971 they reached both lakes –Villarrica and Calafquén– (Fig. 3.3).

For the last century, 10 lahar deposits were observed in the sediment record considering both lakes, and related to a specific eruption (Fig. 3.2). Turbidites and tephra fallout deposits, were identified as well and linked to an eruptive event too (Van Daele et al., 2014).

Chapter 4: Material and methods

4.1 Material

The material used in this study was collected during 4 different expeditions between 2008 and 2012, in two lakes (Villarrica and Calafquén) in the Chilean "Región de la Araucania" and "Región de los Ríos", respectively. Twenty-two short sediment cores were taken using either a UWITEC gravity coring system (BAS and Limnology Unit, Ghent University) or a Swiss corer (Universidad Austral de Chile, Valdivia), and 6 long cores were obtained using a UWITEC piston coring system operated from a floating platform (Figure 4.1). The three coring systems use the same type of transparent PVC liner with an external and internal diameter of 63 mm and 59 mm, respectively. The length of the short cores varies from 25 to 130 cm and the long cores varies from 8 to 13.75 m (Table 4.1).

The dating of the long cores is based on ^{14}C analyses made in the framework previous studies. All the ^{14}C ages were calculated using the Southern Hemisphere 2013 calibration curve (SHCal13; Hogg et al., 2013) from samples of macroscopic organic matter and bulk organic matter obtained from the two master long cores of lakes Villarrica and Calafquén (VIL1 and CAL2, respectively), and reported historical data. For VIL1, an age model was updated using ages of Heirman (2011) (Heirman, 2011; personal communication) (Fig. 4.2a). For CAL2, dates of Viel (2012) and Moernaut (2010) were combined into a preliminary age model of CAL2 (Van Daele et al., 2014; personal communication) by correlation of cores CAL2 and CAL1 (Fig. 4.2b).

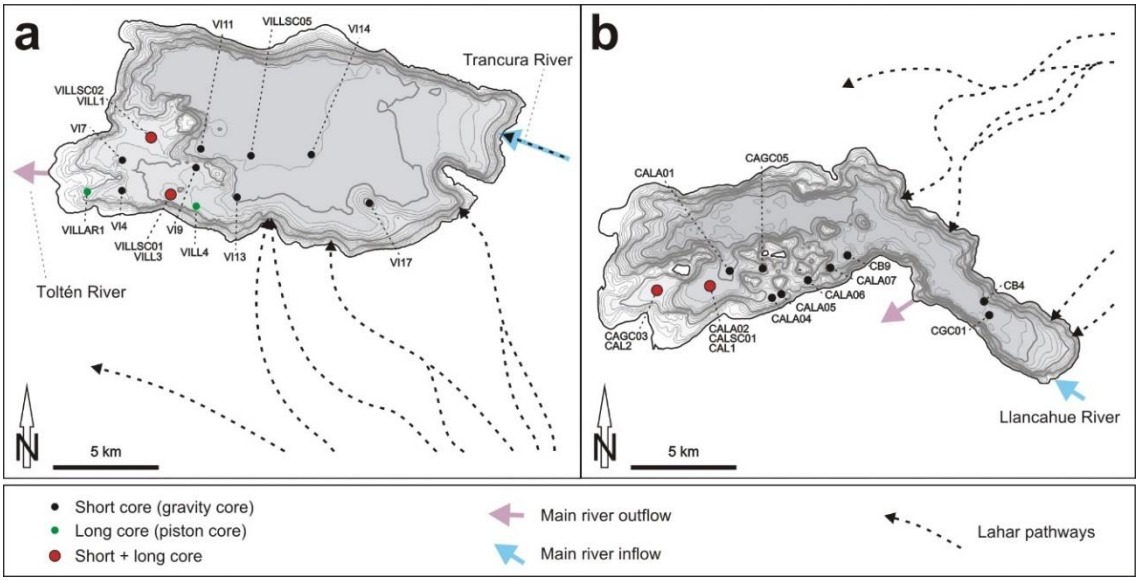

Figure 4.1 Location of the sediment cores used in this thesis in lakes Villarrica (a) and Calafquén (b). The cores were taken during four different expeditions between 2007 and 2012 (Heirman, 2008; Moernaut, 2009; Vandoorne, 2011; Moernaut, 2012). Figure modified from Van Daele, 2013.

Core name	Lat (°N)	Long (°E)	Measured depths (m)	Depth (m)	Length (cm)	Sampling year
	Lake Villarrica					
VILLSC01	-39.28111	-72.15838	112	114	81	2009
VILLSC02	-39.25664	-72.17123	81	82	86	2009
VILLSC05	-39.26319	-72.11601	158	161	49	2009
VI4	-39.28075	-72.1871	85	88	81	2011
VI7	-39.27097	-72.18065	98	98	110	2011
VI9	-39.26934	-72.14557	109	111	106	2011
VI11	-39.26147	-72.14358	160	162	130	2011
VI13	-39.28201	-72.12283	148	150	55	2011
VI14	-39.26218	-72.08209	160	161	59	2011
VI17	-39.28264	-72.04797	90	90	62	2011
VILLAR1	-39.28339	-72.21002	30	30	800	2011
VIL1	-39.2566	-72.1724	81	–	1375	2008
VIL3	-39.28119	-72.15843	112	–	1125	2009
VIL4	-39.28611	-72.14705	117	–	879	2009
	Lake Calafquén					
CALSC01	-39.54583	-72.2191	145	–	122	2009
CAGC03	-39.54917	-72.25014	63	64	51	2008
CAGC05	-39.53685	-72.18983	112	114	76	2008
CB4	-39.5482	-72.06489	173	171	54	2009
CB9	-39.53046	-72.14298	170	189	45	2009
CGC01	-39.55566	-72.06033	177	176	25	2009
CALA01	-39.5397	-72.2099	160	157	123	2011
CALA02	-39.54577	-72.21890	147	147	110	2011
CALA04	-39.55054	-72.18385	93	93	120	2011
CALA05	-39.54848	-72.17941	88	90	119	2011
CALA06	-39.54146	-72.16435	94	93	123	2011
CALA07	-39.53595	-72.15231	172	167	96	2011
CAL1	-39.54582	-72.21911	145	–	890	2009
CAL2	-39.54851	-72.24942	63	–	923	2009

Table 4.1 Locations, length, sampling year and depths of sediment cores discussed in this study. Depth is the column with the values obtained from the bathymetry maps and used for the calculations in this study, and measured depths are the values from the field reports. (–) are those cores that have not been used as a short core in the first part of the study (table modified from Van Daele, 2013).

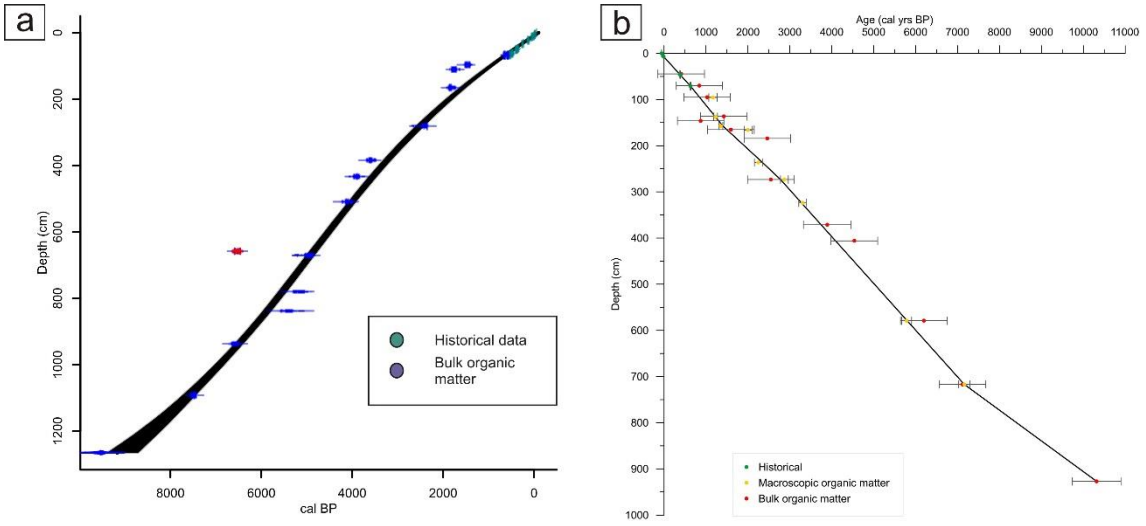

Figure 4.2 Calibration models based on 14C ages using the calibration curve SHCAL13 from Lake Villarrica (a) and Lake Calafquén (b) (figures from Heirman, 2011; and Van Daele et al., 2014, personal communication).

4.2 Methods

Before starting this study, cores were opened in the core-opening lab at Ghent University (Hydrogeology Unit), cleaned, described and photographed. Then, image acquisition, image analysis and high-resolution magnetic-susceptibility (MS) were done before initiating this thesis. For this thesis, new data has been obtained by carrying out other analysis like X-ray computed tomography (CT) and more image analysis using different software packages. All these methods are described in this section.

4.2.1 Image acquisition and image analysis

All the images of the cores used in this study were taken by Dr. Maarten Van Daele with a special self-designed setup to make pictures with homogenous illumination. This setup consisted in a 120 x 50 x 60 cm wooden box with black walls and 25 x 12 cm openings on each end to slide the core through. The box was closed using an adjustable height (>60 cm) lid with a cylindrical opening in its centre (above which the camera was installed; diameter: 15 cm). On each side of the box, two 1.5 m long, white-light emitting fluorescent tubes were installed, resulting in a homogenously scattered white light inside the setup. This setup results in >99% homogenous illumination in the central 20 cm (along axis) of the setup. Pictures were taken at 15 cm intervals with fixed diaphragm and exposure time, and the central parts of the pictures (15 cm long) were stitched using the Corel PHOTO-PAINT software (Van Daele, 2013).

4.2.1.1 Histogram equalization (HE)

Contrast enhancement techniques are used in image processing to achieve better visual interpretation. Histogram equalization (HE) is a specific case of a histogram remapping method and it is one of the most widely used techniques to achieve contrast enhancement, due to its simplicity and effectiveness (Gonzalez and Woods, 2002).

In this study, HE was applied on the original pictures using the Corel PHOTO-PAINT software. Before the equalizing procedure, original images were processed to delete remaining reflections and smearing. This problem was solved by applying an adjustment to reduce the noise using the tool in Corel PHOTO-PAINT: Effects-noise-medium.

HE is based on contrast enhancement that is attained through the redistribution of intensity values of an image. When applying HE, the global contrast of the image is increased by expanding the range of close contrast values. The images used in this study are based on the RGB colour model[8], and with colour images based on RGB colour model, HE applies the same method separately to the Red, Green and Blue components of the image. The result is a new histogram of each colour channel re-distributed over each entire spectrum, thus equally distributing the histogram over the respective spectrum (Fig. 4.3). Because of that, the proportion between the colours bands also changes and that produces unrealistic effects and fake colours. However, that fact didn't represent a problem, because the purpose of using this method was to distinguish the different layers present in the core.

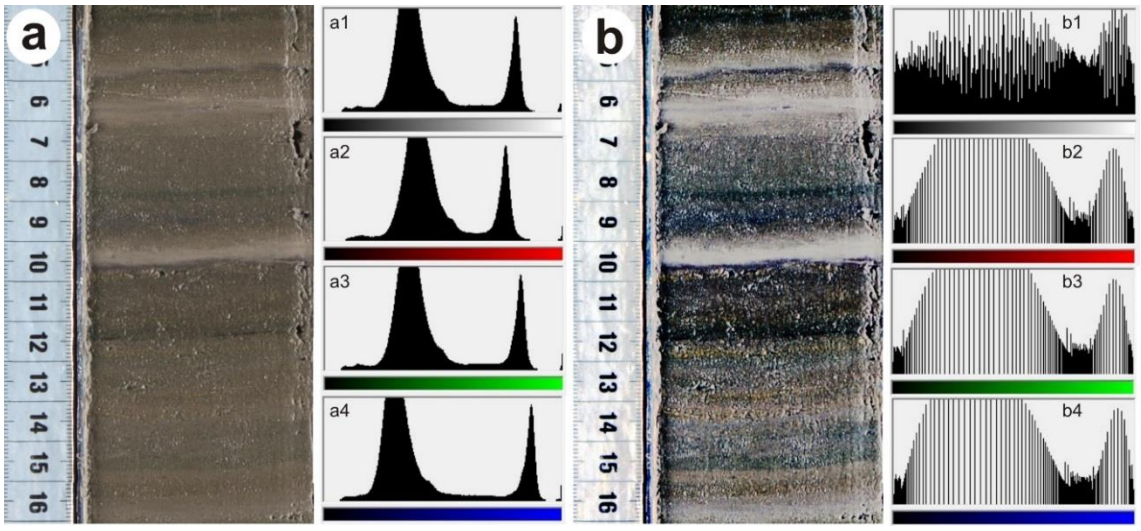

Figure 4.3 Example of a processed core image. (a) Original picture, i.e., before applying a histogram equalization and histograms of the unequalised image corresponding to the cumulative Red-Green-Blue channels (a1), Red (a2), Green (a3) and Blue (a4) channels. (b) The same core image after applying histogram equalization (processed picture) and its corresponding histograms.

[8] The RGB colour model is an additive colour model in which red, green, and blue light are added together in various ways to reproduce a broad array of colours. The name of the model comes from the initials of the three additive primary colours: red, green, and blue.

4.2.1.2 ImageJ (Fiji) software

Computer vision-based image processing methods has been developed as an alternative to provide solutions to practical measurement, identification and size distribution analysis. ImageJ is a very useful and versatile public software for processing images. For this study, ImageJ was used to measure the thickness of the lahars using the pictures of the short cores taken by Dr. Maarten Van Daele in the framework of his PhD thesis (Van Daele, 2013; Van Daele et al., 2014).

The procedure consists in several steps. First, each image is scaled by measuring the number of pixels corresponding to 10 cm on the ruler that was photographed along the sediment core. Then, each lahar is digitized by drawing a polygon along its contours, and the surface area of the polygon is automatically calculated by the program. The average thickness of each lahar is finally obtained by dividing its surface area by the width of the core, which is also measured on the photograph. It is important to note that since the thickness of the lahars is generally variable laterally, the thickness values calculated here represent averages over the width of the sediment core (Fig. 4.4).

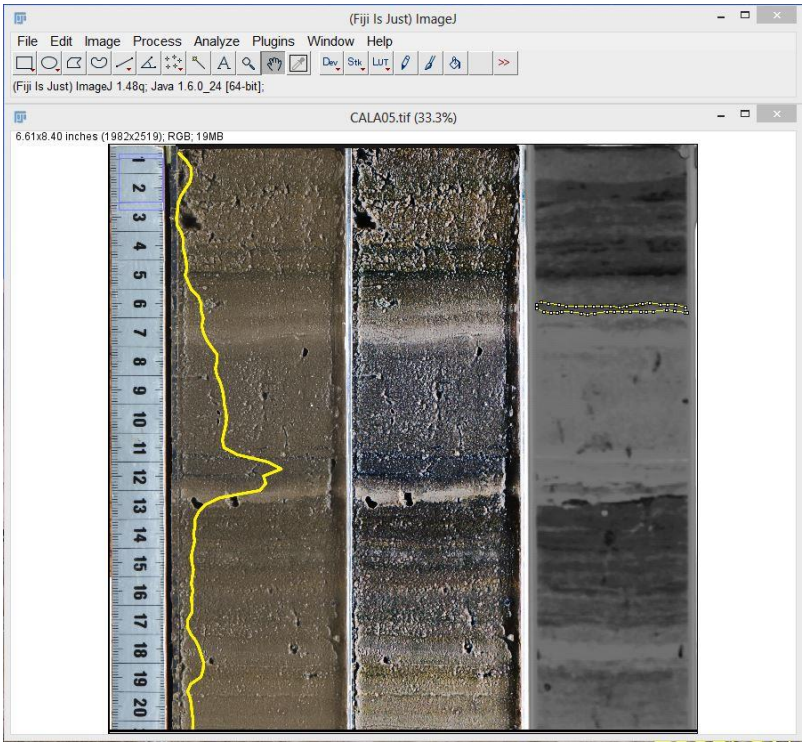

Figure 4.4 Screenshot of the program ImageJ during the digitization process of the lahars clay cap. There are 3 different images of the same core. From left to right: normal picture, processed pictured (applying a HE) and CT scan image. There are 2 yellow lines: Magnetic susceptibility curve on the left, and the one on the right is the contour resulting of digitize a lahar. The ruler is used to scale the figure.

4.2.1.3 Corelyzer

Corelyzer is a scalable, extensible visualization tool developed to enhance the study of geological cores. The strength of Corelyzer is the ability to display large sets of core imagery with multi-sensor logs, therefore it was used to compile original and processed pictures of the long cores with the magnetic susceptibility (MS) values with the goal of making a correlation (Fig. 4.5).

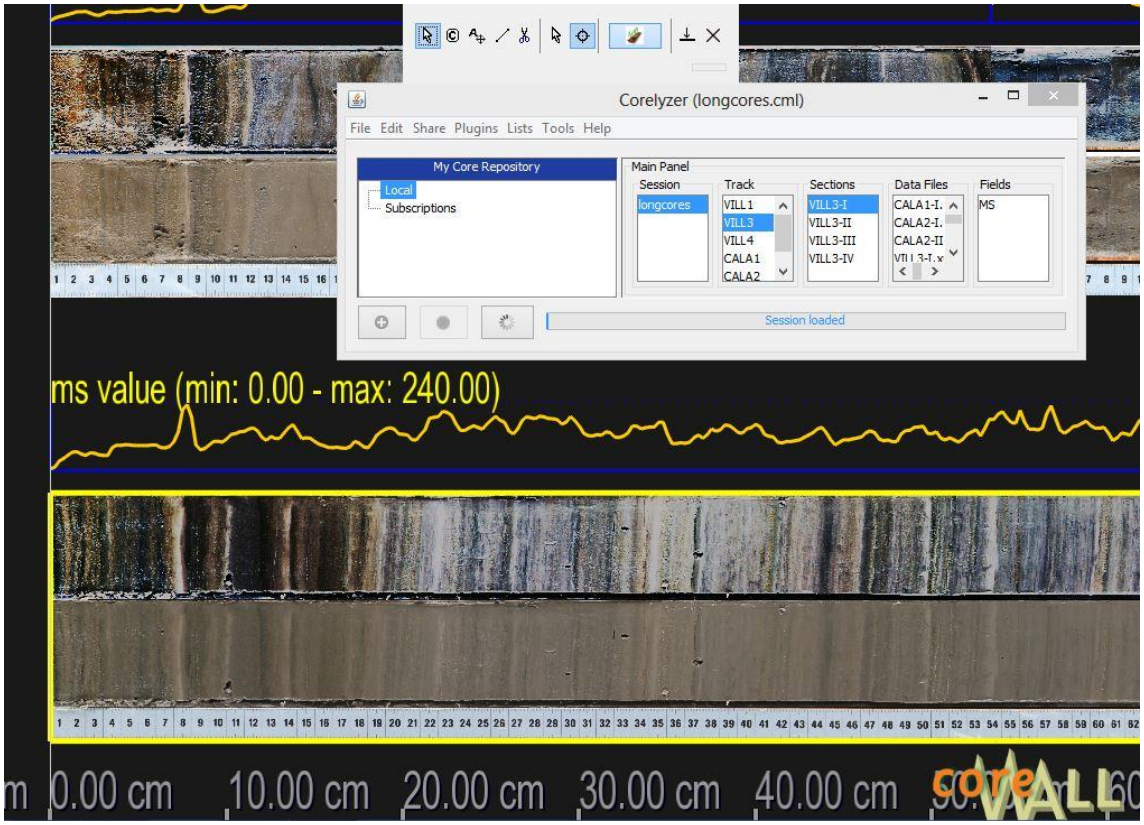

Figure 4.5 Screenshot of the program Corelyzer during the processing of the long cores.

4.2.2 High-resolution magnetic-susceptibility (MS)

Low field or initial magnetic susceptibility is a measure of how easily a material can be magnetised (Thompson & Oldfield, 1986). MS varies with the content of iron-bearing minerals (Zolitschka et al., 2001). It is particularly high for materials with ferrimagnetism behaviour like magnetite and a few other Fe-bearing minerals such as nickel and cobalt (Dearing, 1999).

The results used in this study were obtained in 2008-2012 on split-core surfaces with a Bartington MSE2 surface sensor (Royal Observatory of Belgium and Department of Soil Management, UGent). The along-core resolution of this sensor is 3.5 mm, and the step size during the measurements was 2.5 mm, resulting a 1 mm overlap between successive

measurements (Van Daele, 2013). In this study, MS was used to classify different types of materials and to correlate the sediment cores with each other.

4.2.3 X-ray computed tomography (CT)

A CT scanner uses digital geometry processing to generate a 3-dimensional (3-D) image of the inside of an object. CT stands for computerized tomography. Tomography is the process of generating a 2-dimensional image of a slice or section through a 3-dimensional object. That process consists in emitting a series of narrow beams through the sample while it moves through an arc. The 3-D image is computed from many 2-dimensional (2-D) X-ray images that are taken around a single axis of rotation.

A CT scanner is composed of an X-ray source and an X-ray detector, which can measure different levels of density, one of which is able to rotate. This data is transmitted to a computer, which builds up a 3-D cross-sectional picture of the sample and displays it on the screen (Fig. 4.6).

Figure 4.6 Pictures of the Siemens SOMATON Definition Flash medical X-ray CT scanner (a) and the control room (b) at Ghent University Hospital. October 2013.

The CAT-scan[9] uses a pixel intensity scale to quantify and map X-ray attenuation coefficients of the analysed object on longitudinal (topograms) or transversal (tomograms) images. The resulting images are displayed on a grey scale, darker and lighter zones representing lower and

[9] CAT and CT scans refer to the same type of diagnostic examination. CT scan is the newer term, while CAT scan is the older term. The term ´CT´ refers to 'Computed Tomography', while ´CAT´ stands for 'Computed Axial Tomography'.

higher X-ray attenuation, respectively (St-Onge & Long, 2009). This attenuation is a function of the material composition (effective atomic number) and bulk density (Cnudde et al., 2004).

In this study, this method was applied in October 2013 to the short sediment cores using a Siemens SOMATON Definition Flash medical X-ray CT scanner (Ghent University Hospital). The scanner was set to 120 kV, with an effective mAs of 200 and a pitch of 0.45. The reconstructed images have a voxel size of 0.5 mm and a down core step of 0.6 mm with a delay of 2 s. The results were visualised and examined using the VGStudio MAX 2.0 software[10].

4.2.4 Lahars pathway length measuring method

The most likely pathway of each individual lahar was identified on the bathymetric maps of Van Daele (2013). The length of each pathway was then measured between the point where the lahar entered the lake as retrieved from historical data (Van Daele et al., 2014) and the location of the short core of interest, using the Global Mapper 13 software.
The procedure consist on drawing a line following the most probable pathway of the lahar based on the morphology of the isobaths generated by Global Mapper.

[10] VGStudio MAX is a software for the visualization and analysis of CT data providing slice images along all three axes as well as a 3D image. It was developed by the company Volume Graphics GmbH.

Chapter 5: Results

5.1 Short cores

Before presenting the results obtained from the analysis of the short cores, it is important to consider some aspects already discussed and published in Van Daele (2013) and Van Daele et al. (2014):

- In all cores, two main types of event deposits (EDs) were identified and classified in two main types: lacustrine turbidites and volcanic-eruption-induced EDs. Volcanic-eruption-induced EDs were further subdivided into three main groups: Fe-rich clay to fine silt laminae (FeLs), tephra-fall, and detrital fining-upwards EDs (interpreted as lahar deposits); but only the last two were considered in this study.

- All nine historically documented lahar-creating eruptive events at Villarrica Volcano in the 20th certury were identified in the lake sediment record in lakes Calafquén and Villarrica as a lahar deposit and related to its corresponding eruptive event. All of them are represented by a detrital fining-upwards event deposit. The most recent ones, in 1948, 1949, 1963, 1964 and 1971 are present in both lakes; while the oldest, in 1904, 1908, 1909 and 1920 were only observed in Lake Villarrica sediment record, even though only in 1908 lahars were reported to have reached the lake shore.

- Two other non-reported lahar deposits have been observed in the lake sediments and can be linked to two less important eruptive events (1938 and 1991).

- In some cores, lahars from 1948 and 1949 were considered as a singular event due to the two lahar events occurred in a short period of time and it is not possible to distinguish between each other. The same happens with the events of 1963 and 1964.

- The strongest earthquake that ruptured the Valdivia rupture zone occurred in 1960, and recently, another great earthquake occurred in 2010. These earthquakes are represented by lacustrine turbidites in the lake's sedimentary sequence. In some of the cores 2010 turbidite is not found because they were taken before the 2010 earthquake (Tab. 4.1).

- MS values are always high for tephra and lahar layers. Turbidites have always a high peak at the bottom and it decreases until the top, which has the lowest values. All other sediments are being considered as background throughout this thesis.

5.1.1 Counting of the last century lahar events

In a first set of analysis, the cores were examined and the main EDs present in each short core of both lakes were identified. Original pictures, processed images, the images obtained from the CT-scanner and the MS values were compared for ED identification.

The tree different types of EDs were identified in the sediments: lacustrine turbidites, tephra and detrital fining-upwards, or lahar deposits. These EDs were distinguished from the

background sediments based on the colour of the pictures and Ct-scan images and the MS values (Table 5.1). When possible, the event deposits were correlated with historical events in the region, such as earthquakes and volcanic eruptions of Villarrica Volcano.

	Characteristic	Color	MS values
Type of event	**Image**		
Lahar	N	Light brown/beige to white.	High to very high. Represented with a high peak.
	HE	The lowest part is brown or dark blue and the clay cap on top white.	
	CT	Light grey to white.	
Tephra-fall	N	Black.	High to very high. Represented with a high peak.
	HE	Dark blue to black.	
	CT	Light grey to white.	
Turbidite	N	Dark brown to greish brown.	High at the bottom and decreases up to the top to low values.
	HE	The lowest part is brown and the clay cap on top white.	
	CT	White to light grey and top.	

Table 5.1 Main features of the most important sedimentary deposits present in the short core record. (N) Corresponds to the photographs of the cores, (HE) corresponds to the processed images applying a Histogram Equalization, and (CT) corresponds to the images obtained from the CT-scanner. (MS) corresponds to Magnetic susceptibility values.

In total, 10 short cores taken in Lake Villarrica with a maximum and minimum length of 130 and 49 cm, respectively; and 11 short cores from Lake Calafquén with a maximum and minimum length of 123 and 25 cm, respectively, were analysed (Fig. 4.1; Tab. 4.1). Figure 5.1 is an example of how the analysis has been done and how the results are shown. Results on all the other short cores are attached in appendix A.1.

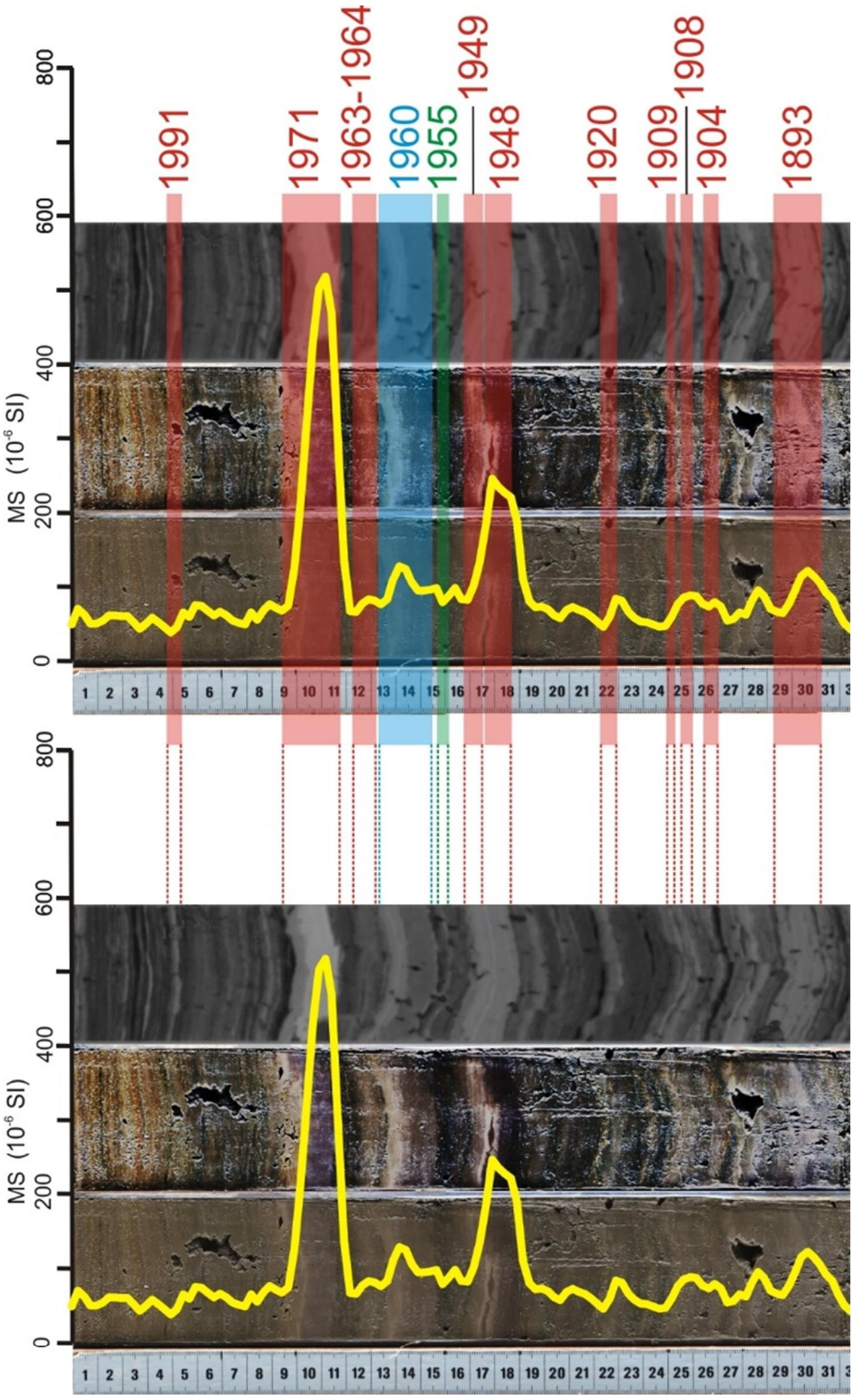

Figure 5.1 Picture (N), Histogram Equalization processed image (HE), X-ray CT-scan image (CT) and Magnetic Susceptibility (MS) graph of core VI11; before being analysed (Left) and after being analysed (Right). The three different types of EDs are indicated with colored bars: lacustrine turbidites (blue), tephra-fall layers (green) and detrital fining-upwards, interpreted as lahar deposits (red). When possible, EDs are correlated with strong historical earthquakes in the region and eruptions of Villarrica Volcano (Tab. 3.2). Material that is not colored is considered as background. Slumps are also indicated (orange) and Magnetic susceptibility values (MS) are represented by a yellow line graph. 10 lahars have been identified and correlated in VI11 (1893, 1904, 1908, 1909, 1920, 1948, 1949, 1963/64, 1971 and 1991), a thin tephra layer (1955) and a lacustrine turbidite (1960).

5.1.2 Thickness of the lahars clay cap during the 20th century.

After measuring the thickness of the clay cap of the lahars that occurred during the 20th century (appendix A.2), the results show that almost half of the volcanic events, with a volcaninc eruption index higher or equal than 2, related to Villarrica Volcano produced lahar deposit in lakes Villarrica and Calafquén, but Lake Villarrica contains more lahar deposits than Lake Calafquén. E.g. the oldest events (1904, 1908, 1909 and 1920) were not present in the sediment core record in Lake Calafquén, and 1991 either (Fig. 5.2). Van Daele (2013) attributed this discrepancy to the higher amount of lahar pathways in Lake Villarrica catchment and Lake Calafquén.

The thicknesses of the lahar clay cap range from 0.047 to 0.93 cm. Only when a major lahar reached the shore of the lake (1908, 1948/49, 1963/64 and 1971) the lahars clay cap deposits thicker than 0.3 cm have been identified in the sediment core. Caps of deposits in cores located in front of the lahar inflow point, in general, are thicker than 0.6 cm. For example, in 1948/49 lahars reached the shore of Lake Villarrica mainly from the South, and cores VI14 and VILLSC05, located just in front the inflow point, contain a very thick deposit (> 0.7 cm) compared to the rest of the cores.

None of the reported lahars reached the lakes shore in 1904 and 1991. This corresponds to no thicker clay caps or fine-silt caps (< 0.3 cm) in the sediment record during these events.

Cores located at the western part of Lake Villarrica have thicker clay caps in 1908 and 1971, when a reported major lahar reach the lake shore from the East.

Core VI17, situated on the top of a hill in the South-eastern part of Lake Villarrica (Fig. 4.1; Fig. 5.2), always shows a clay cap with a thickness below 0.30 cm, except in 1971 that increases up to more than 0.6 cm.

In Lake Calafquén, the cores situated at the south-eastern part of the lake (CB4 and CGC01) during the events of 1963/64 and 1971 registered the thickest lahar clay cap deposits (up to 0.6 cm) of the 20th sedimentary record of the Lake Calafquén. The most striking result is the one obtained in the core CB4 in 1963/64 event, with a thickness of the clay cap higher than 0.9 cm (appendix A.2; Fig. 5.2). At the same points, the lahar clay caps from 1948/49 event could not be identified because a slump modified the sedimentary record (appendix A.1).

The lahar clay caps in the cores CAGC03 and CALA05, which are the shallowest cores taken in the lake (Fig. 4.1; Tab. 4.1), never exceed a thickness of 0.3 cm, despite this fact, the values obtained on the shallower areas (up to 100 m depth) do not show any apparent trend.

The cores CALA07 and CB9, which are located in front of two lahar pathways, always register a thickness of the lahars clay cap higher than 0.3 cm; except in the core CB9 during the event of 1948/49, that a slump modified the sedimentary record at that point and it was impossible to identify the lahar clay cap corresponding to that event (appendix A.1).

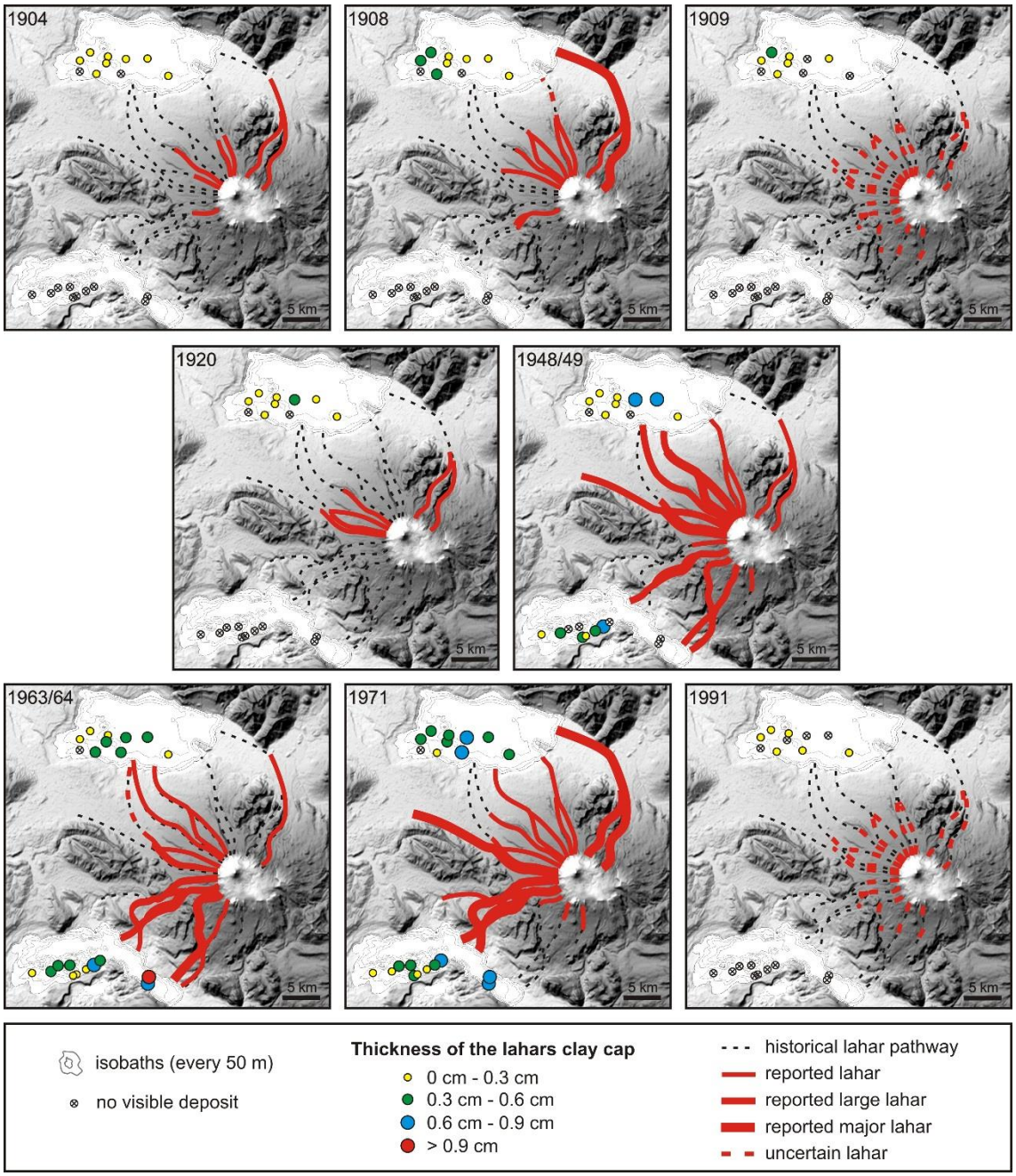

Figure 5.2 Historical lahar pathways compared with the thickness of the linked lahar's clay cap deposits (illustration inspired from Van Daele, 2013).

5.1.3 Depth and distance measurements

Once the thickness of each clay cap was measured, the purpose was to compare those measurements to the different characteristics of each location. For that, the depth of each core and the straight distance between each core and the main lahar inflow points were measured. The pathways of the lahars to the cores located in the deepest parts were also determined, due to those core locations could be affected by an underflow deposition.

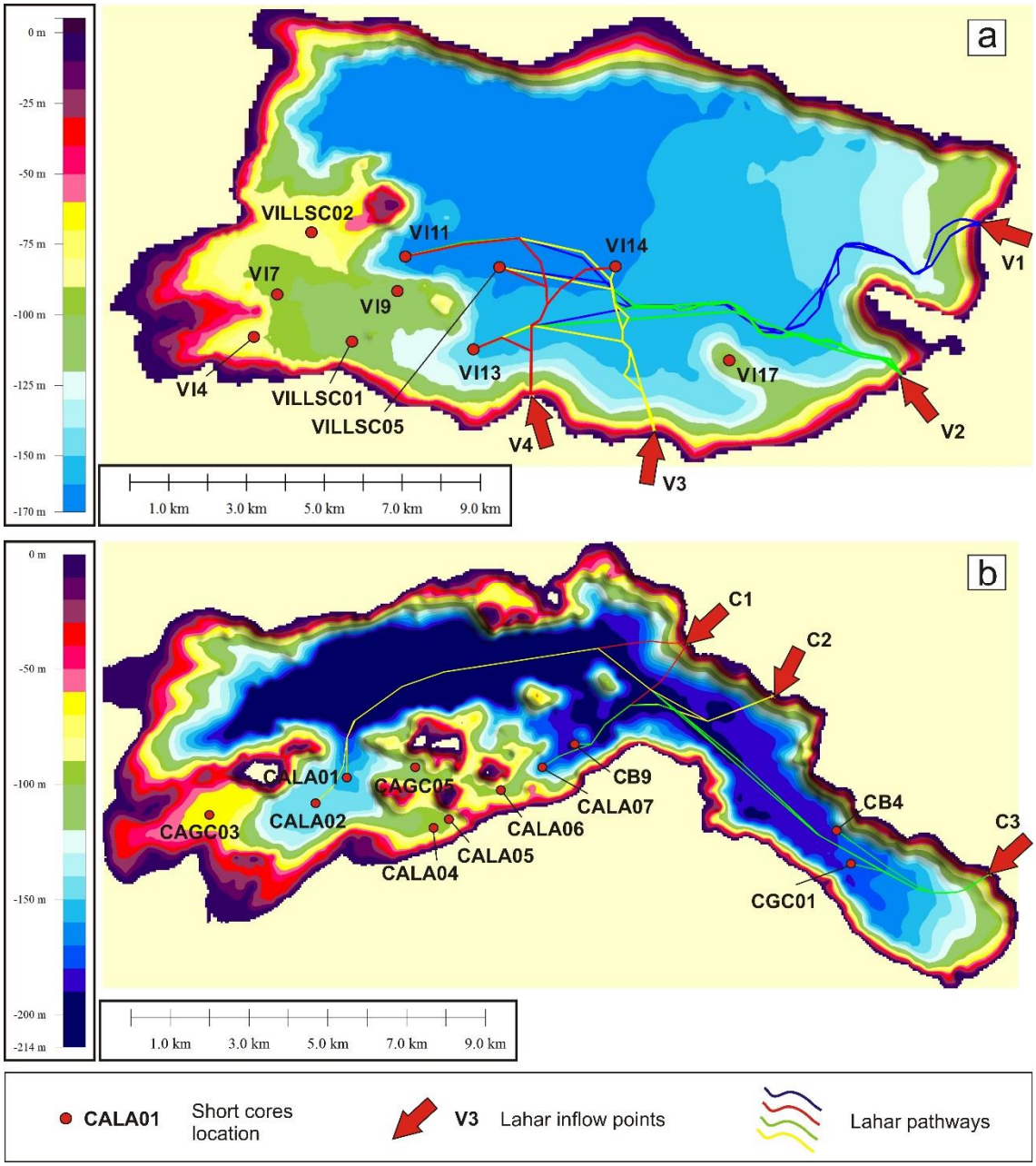

Figure 5.3 Bathymetry of Lake Villarrica (a) and Lake Calafquén (b). The different pathways of the lahars from the lahar inflow points to the deepest cores are represented in different colors: V1 to VI11, VI13, VI14 and VILLSC05 (blue); V2 to VI11, VI13, VI14 and VILLSC05 (green); V3 to VI11, VI13, VI14 and VILLSC05 (yellow); V4 to VI11, VI13, VI14 and VILLSC05 (red); C1 to CALA02, CALA01, CALA07 and CB9 (red); C2 to CALA02, CALA01, CALA07 and CB9 (yellow) and C3 to CALA02, CALA01, CALA07, CB9, CB4 and CGC01 (green).

In Lake Villarrica, four cores are located at the deepest parts (between 140 and 180 m depth; Tab. 4.1) of the lake in the central basin (i.e. VI1, VI13, VI14 and VILLSC05). Five cores are situated on a western shallower basin (between 70 and 120 m depth; i.e. VI4, VI7, VILLSC01, VILLSC02 and VI9), and the core VI17 is located on top of a hill at the south-eastern part of the lake.

In Lake Calafquén there are three cores located at different depths along an East-West subbasin (between 60 and 160 m depth; i.e. CAGC03, CALA02 and CALA01), four more cores are located in a central steep area between four main hills (i.e. CAGC05, CALA04, CALA05 and CALA06), cores CB9 and CALA07 are located at the western side of a small hill, and the cores CB4 and CGC01 are

situated at the south-eastern extreme of the lake, on the slope of the lake platform and in the middle of a channel, respectively.

Seven lahar inflow points were estimated between both lakes considering the historical lahar pahtways, four in Villarrica (V1, V2, V3 and V4) and three in Calafquén (C1, C2 and C3) (Tab. 5.2a and Tab. 5.2b; Fig. 5.3). These are located at the Eastern and Southern shore of Lake Villarrica, and at the North-Eastern and South-Eastern shore of Lake Calafquén.

Lahar inflow point	**V1**	**V2**	**V3**	**V4**
Short cores Lake Villarrica				
VILLSC01	16.142	13.879	7.985	4.696
VILLSC02	16.896	15.301	10.04	6.866
VILLSC05	12.201	10.489	5.745	3.287
VI7	17.844	15.868	10.151	6.866
VI9	14.82	12.88	7.423	4.243
VI11	14.549	12.855	7.717	4.685
VI13	13.188	10.81	5.047	1.829
VI14	9.284	7.701	4.333	3.857
VI17	7.216	4.352	2.637	5.079

Table 5.2a Straight distance between the lahar inflow points and each of the cores in Lake Villarrica, measured on the bathymetry map. Distances measured in km.

Lahar inflow point	**C1**	**C2**	**C3**
Short cores Lake Calafquén			
CAGC03	12.893	14.621	19.858
CAGC05	7.594	9.261	14.826
CB4	6.069	3.772	4.036
CB9	3.842	5.182	11.03
CGC01	6.957	4.688	3.528
CALA01	9.293	11.014	16.493
CALA02	10.275	11.926	17.199
CALA04	7.965	9.242	14.159
CALA05	7.524	8.802	13.792
CALA06	6.027	7.311	12.585
CALA07	4.845	6.129	11.668

Table 5.2b Straight distance between the lahar inflow points and each of the cores in Lake Calafquén, measured on the bathymetry map. Distances measured in km.

After measuring the straight distance from each core location to the different lahar inflow points it can be observed that the most distal cores from any of the inflow points are VI7 (17.8 km away from point V1) in Lake Villarrica and CAGC03 (19.9 km away from point C3) in Lake Calafquén. On the other hand, the closest cores from an inflow point are, in Lake Villarrica, VI13 from V4 (1.8 km) and CGC01 from C3 (3.5 km) in Lake Calafquén (Tab. 5.2a and Tab. 5.2b).

Thirty different lahar pathways have been measured: sixteen in Lake Villarrica (there are four inflow points and four cores in areas that can be affected by an underflow) and fourteen in Lake Calafquén. There are six cores in the deepest areas, but not all of them were interpreted to be affected by lahars coming from all the inflow points (Fig. 5.3; Tab. 5.3a and Tab. 5.3b).

Lahar inflow point	**V1**	**V2**	**V3**	**V4**
Short cores Lake Villarrica				
VILLSC05	15.4	11.041	6.761	4.145
VI11	17.15	13.929	9.838	7.209
VI14	12.74	8.914	4.795	4.447
VI13	15.301	11.241	6.414	2.672

Table 5.3a Lahar pathways from the lahar inflow points to the deepest cores measured on the bathymetry map of the Lake Villarrica. Distances measured in km.

Lahar inflow point	**C1**	**C2**	**C3**
Short cores Lake Calafquén			
CB4	–	–	4.48
CB9	4.001	5.652	12.652
CALA01	10.339	13.175	20.207
CALA02	11.248	14.09	21.11
CALA07	4.961	6.612	13.61
CGC01	–	–	3.79

Table 5.3b Lahar pathways from the lahar inflow points to the deepest cores measured on the bathymetry map of the Lake Calafquén. (-) means that the pathway from the inflow point to the core location was not measured. Distances measured in km.

5.1.4 Comparison of clay cap thickness with depth and inflow distance

In this section the results of lahars clay cap thickness, depth of the cores and distance-to-inflow measurements are compared.

5.1.4.1 Thickness-depth comparison

Comparisons between the thickness of the lahars clay cap and the depth of each core present different trends.

In Lake Villarrica the results of the 1904 deposits show that the thickness, apparently, does not depend on the depth. All the cores have more or less the same thickness, varying from 0.1 to 0.25 cm (Fig. 5.4). On the other hand, during 1908, the deposits in the shallowest cores are thicker than in the deepest (ranging from 0.2 to 0.5 and 0.1 to 0.2, respectively), with the exception of VI17, which is located in the other side of the lake and is thinner than 0.05 (Fig. 5.5). This trend can be also identified in the event of 1909, but with thinner deposits; the thickest one is lower than 0.35 cm and corresponds to core VILLSC02 (Fig. 5.6). In 1920 the trend of previous years remains in the more shallow cores, whereas in the case of the deeper cores thickness increases; being above 0.3 cm in the case of core VILLSC05 (Fig. 5.7). The most striking result to emerge from the graph of 1948-1949 are the high values of the cores VI14 and VILLSC05 (higher than 0.8 cm) compared with those of the more shallow cores (lower than 0.4 cm), with the exception of VI11 (Fig. 5.8). Except for VI17, all shallow cores and VI11 have a very similar thickness. In the event of 1963-1964 the trend is the same than in the previous event, with two main differences: the highest values are less thick (they range from 0.35 to 0.5), and the thicknesses in the shallow cores gradually increase with depth (which is opposite as for the 1908 and 1909 events (Fig. 5.9). Results in the 1971 event clearly confirm a change of the trend from events previous of 1948 to 1949. Larger thicknesses can be observed in all the deeper cores (below 140 m depth) with respect to the shallower cores (Fig. 5.10). Within the shallower cores, a similar trend as for the 1908 and 1909 deposits can be observed. A remarkable fact is that in this event is the first time the thickness in the core VI17 exceeds the 0.2 cm. In 1991 the results are very similar to the ones obtained in 1904, not showing any relation between the thickness and the depth (Fig. 5.11).

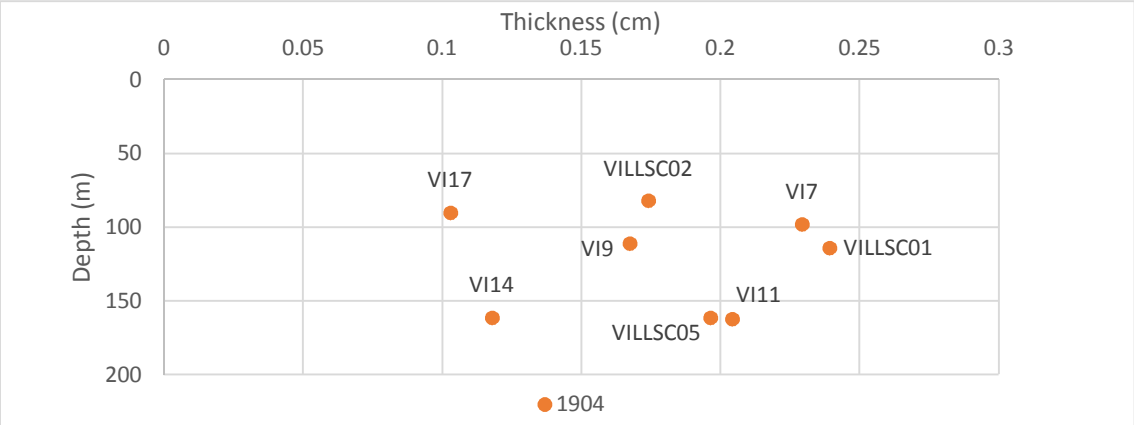

Figure 5.4 Relation between the thickness of the lahar clay cap and the depths of the cores in Lake Villarrica in the eruptive event of 1904.

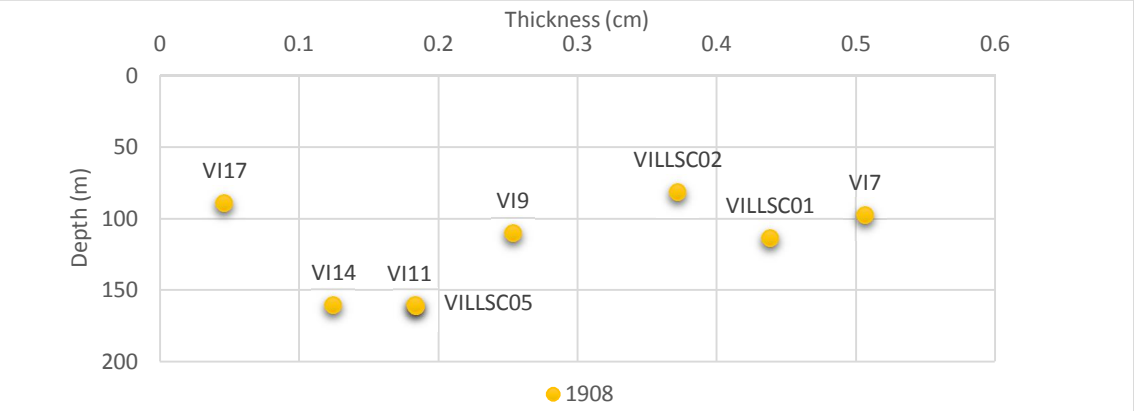

Figure 5.5 Relation between the thickness of the lahar clay cap and the depths of the cores in Lake Villarrica in the eruptive event of 1908.

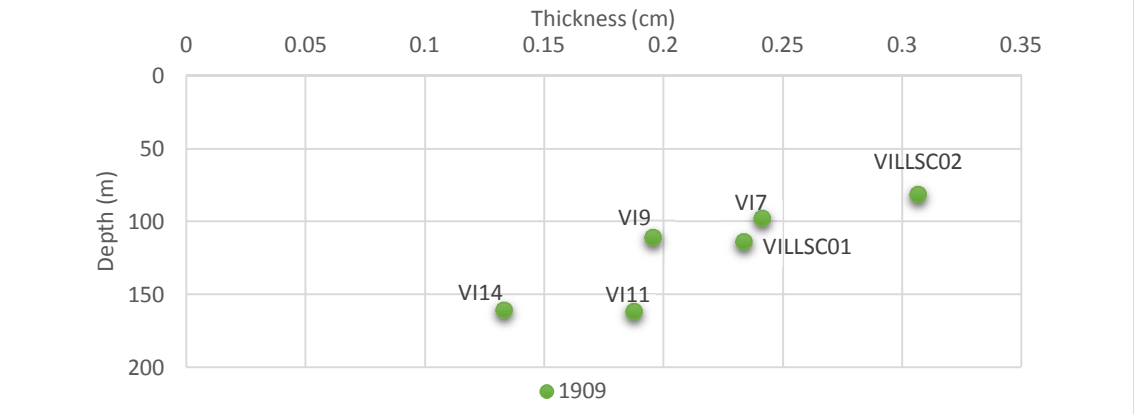

Figure 5.6 Relation between the thickness of the lahar clay cap and the depths of the cores in Lake Villarrica in the eruptive event of 1909.

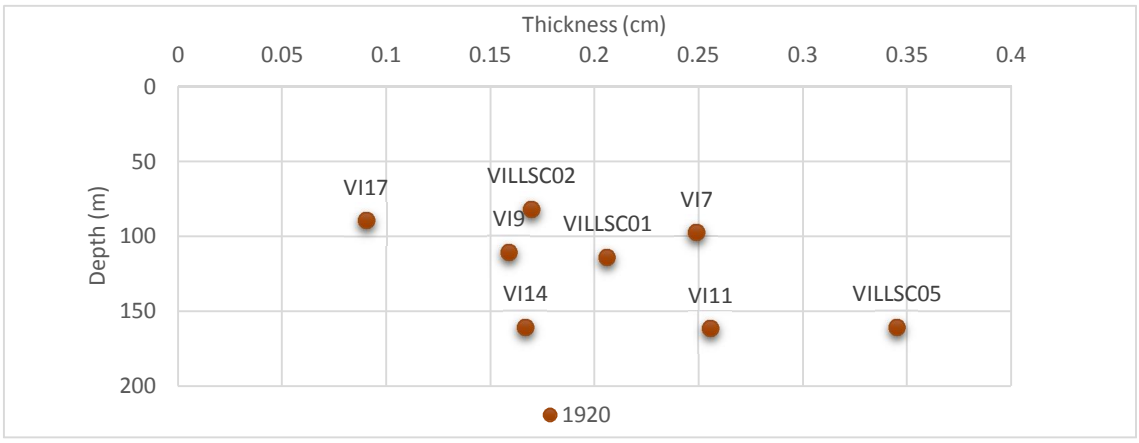

Figure 5.7 Relation between the thickness of the lahar clay cap and the depths of the cores in Lake Villarrica in the eruptive event of 1920.

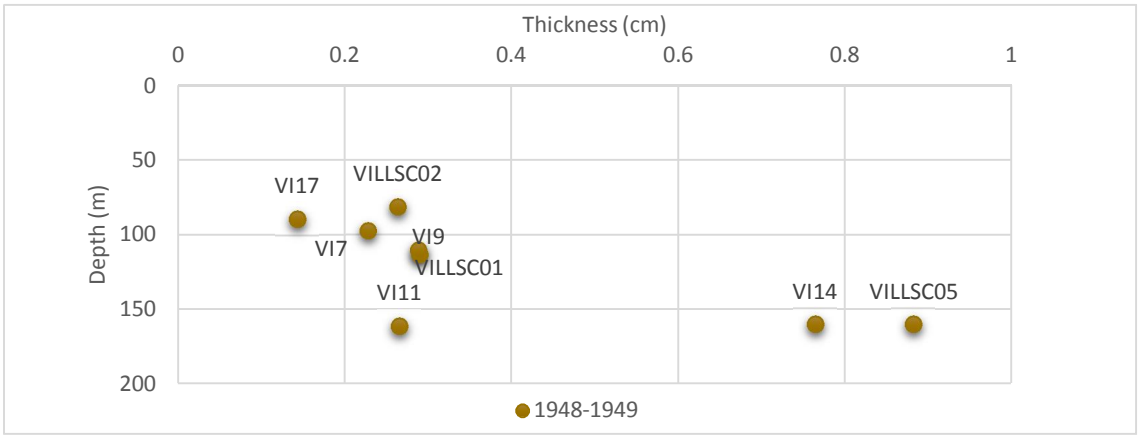

Figure 5.8 Relation between the thickness of the lahar clay cap and the depths of the cores in Lake Villarrica in the eruptive event of 1948-1949.

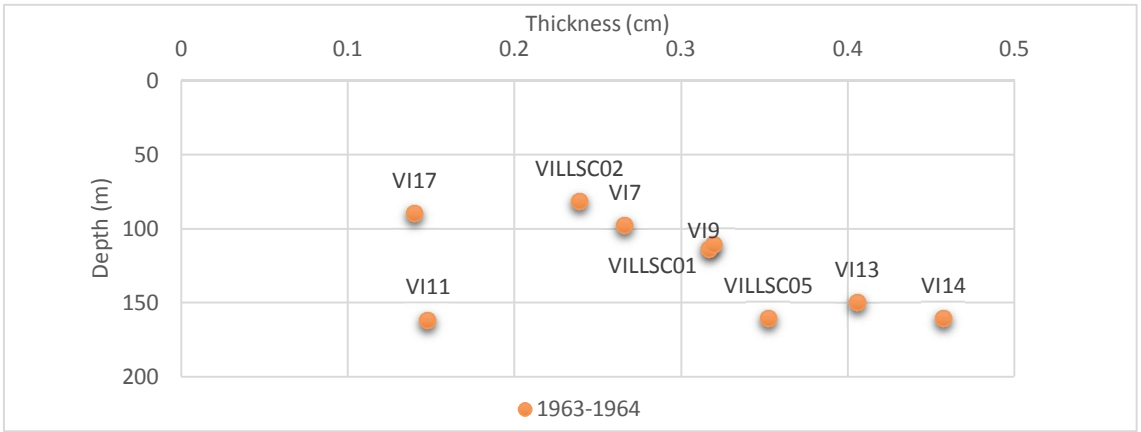

Figure 5.9 Relation between the thickness of the lahar clay cap and the depths of the cores in Lake Villarrica in the eruptive event of 1963-1964.

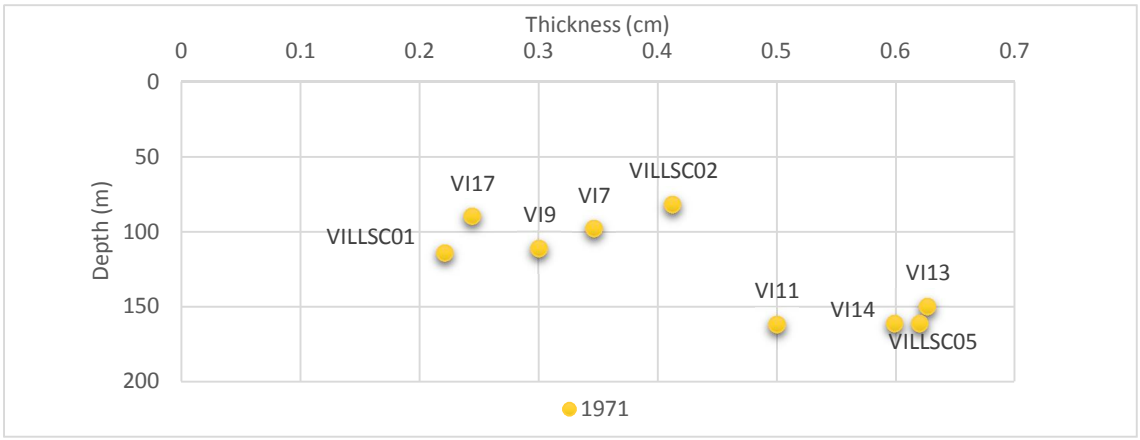

Figure 5.10 Relation between the thickness of the lahar clay cap and the depths of the cores in Lake Villarrica in the eruptive event of 1971.

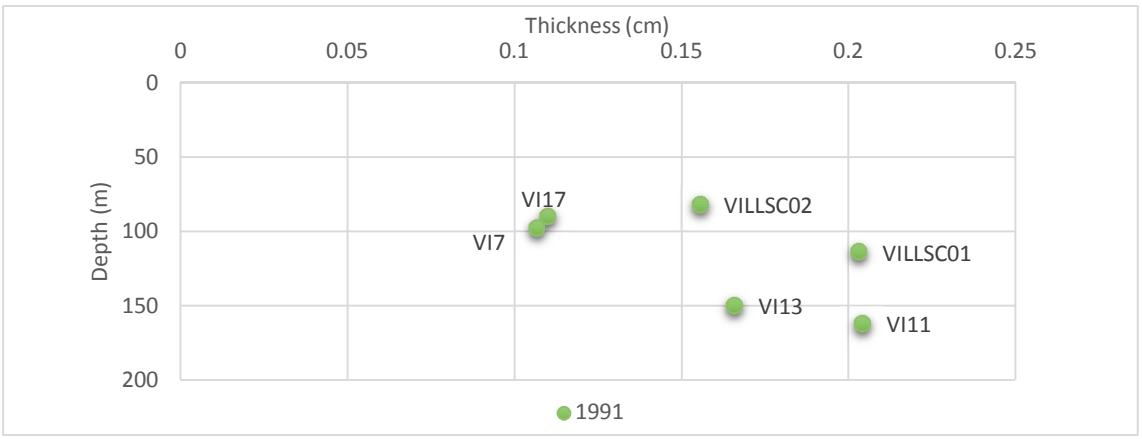

Figure 5.11 Relation between the thickness of the lahar clay cap and the depths of the cores in Lake Villarrica in the eruptive event of 1991.

In Lake Calafquén there is only information of the thicknesses in the events of 1948-1949, 1963-1964 and 1971. The three events share a common fact which is that the core CAGC03 (the shallowest) contains the thinnest deposit (Fig. 5.11; Fig. 5.12 and Fig. 5.13). The events of 1963-1964 and 1971 show a similar trend, in which the cores can be grouped by thickness into three groups: a first group consists of cores at a depth shallower than 100 m, which are those with thinnest deposits (from 0.15 to approximately 0.4 cm). A second group is composed of the cores located at an intermediate depth (between 115 and 160 m deep) with a range of thicknesses between 0.3 and 0.5 cm. And finally, the deeper cores, more than 160 m deep, with thicknesses greater than 0.5, except in 1971 the core CALA07 having a thickness of less than 0.4 cm.

In group 1 and 2 there is a trend of increasing thickness with depth. Especially in 1971, the thickness increases mainly strongly in group 1, and only slightly in group 2.

In group 3, the thickness is very variable, both for the different cores within one event, as for the same cores between different events. These variations do not seem to be influenced by depth variations, but probably more by distance from the inflow.

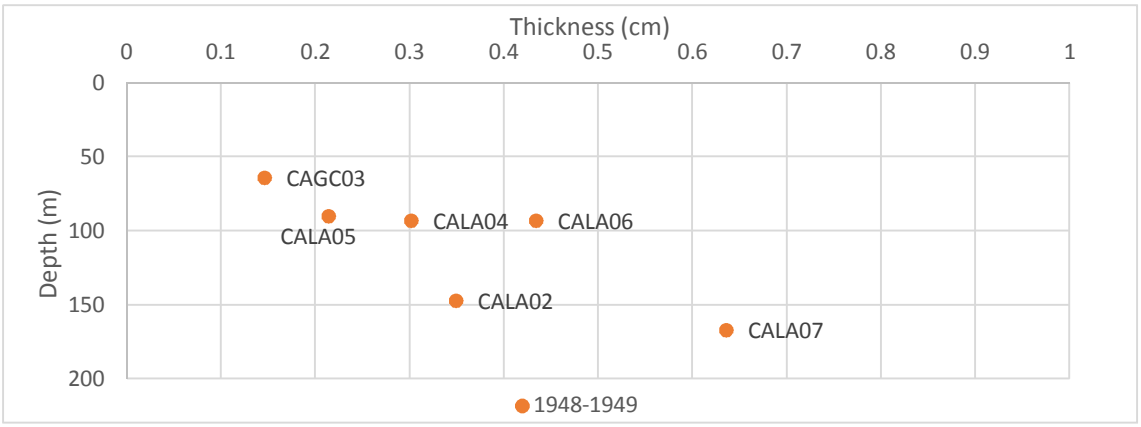

Figure 5.12 Relation between the thickness of the lahar clay cap and the depths of the cores in Lake Calafquén in the eruptive event of 1948-1949.

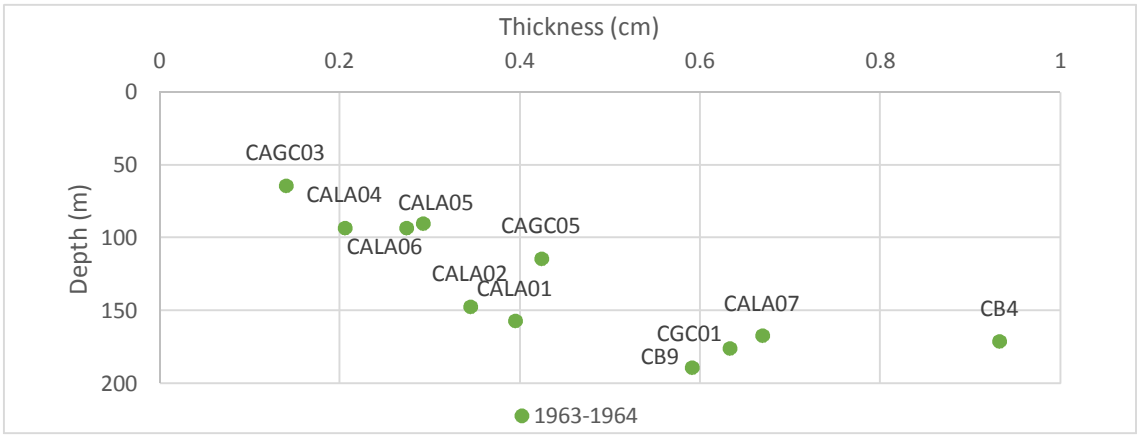

Figure 5.13 Relation between the thickness of the lahar clay cap and the depths of the cores in Lake Calafquén in the eruptive event of 1963-1964.

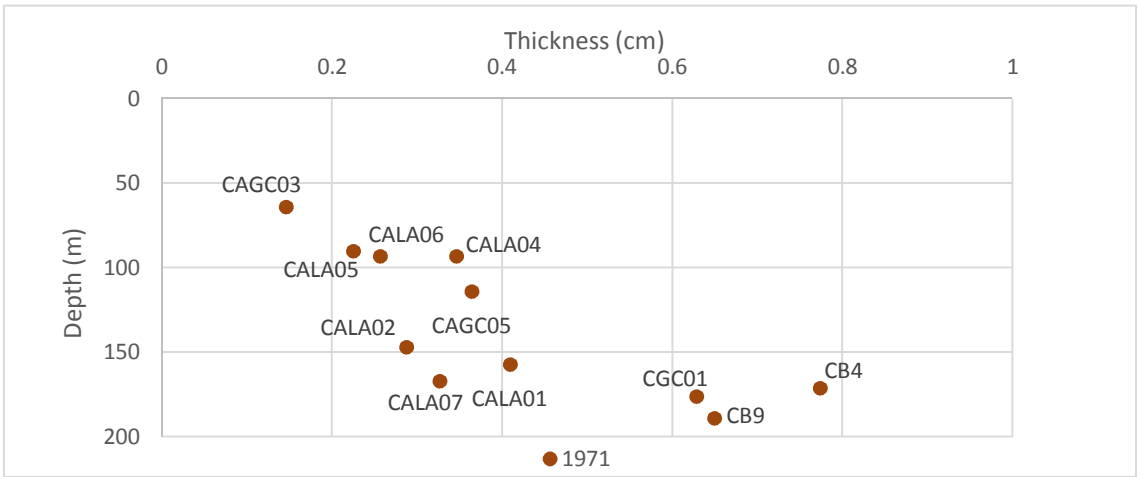

Figure 5.14 Relation between the thickness of the lahar clay cap and the depths of the cores in Lake Calafquén in the eruptive event of 1971.

5.1.4.2 Thickness-distance comparison

Considering the events when the historical lahar pathways reached the lakes during the 20th century (1908, 1948/49, 1963/64 and 1971; Fig. 5.2 and Fig. 5.3), the results after comparing the thickness values with the straight distance from the lahar inflow points and the cores show different trends (Fig. 5.15). For example, looking at the results obtained in Lake Villarrica during the event of 1908 it can be observed that the thickness increases with the distance. On the other hand, looking at the events of 1948/49, 1963/64 and 1971 the trend observed is to get thinner with distance. The only exception is the core VI17 that is always situated in a completely different location on the top of a hill close to the lahar inflow points (Fig. 4.1; appendix A.2).

From the point of view of Lake Calafquén a common trend is observed in the three different episodes (Fig. 5.16). It is very clear that the thickness decreases with the distance, being the thinnest deposits at the more distal cores; and that, in general, the thickness decreases fastest in the proximal areas.

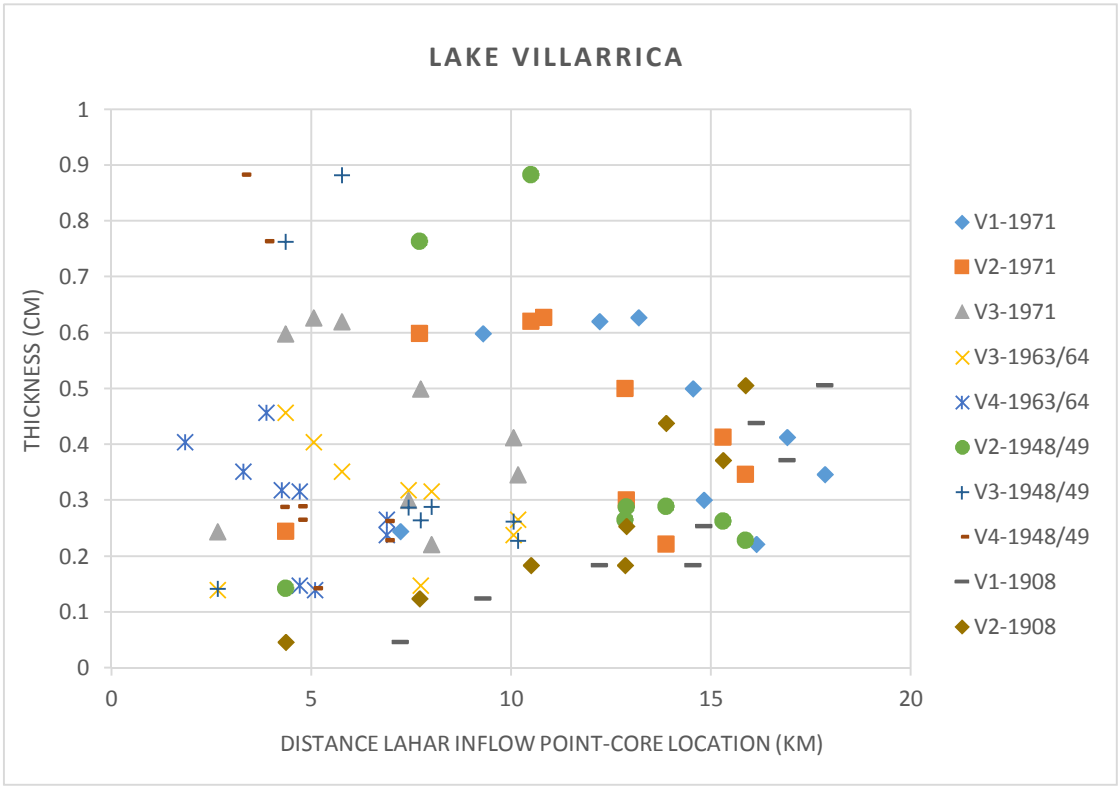

Figure 5.15 Relation between the thickness of the lahar clay cap and the straight distance from the lahar inflow points, where the lahars reached the lake each year, to the cores in Lake Villarrica during the 20th century.

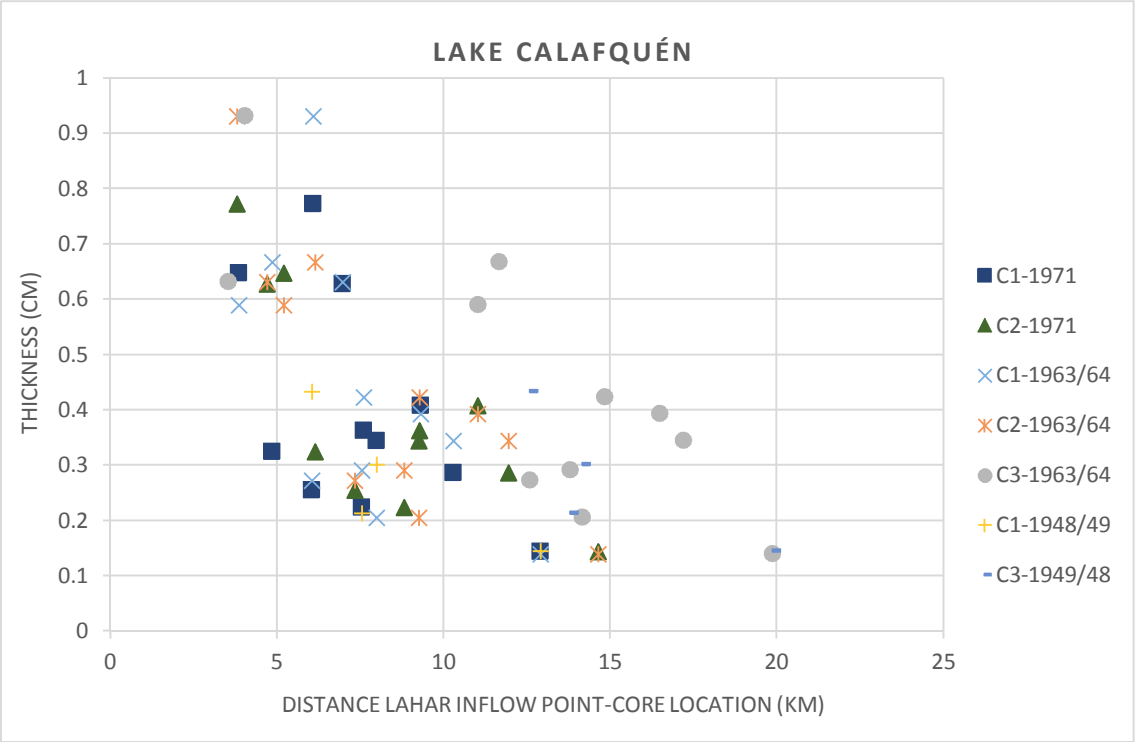

Figure 5.16 Relation between the thickness of the lahar clay cap and the straight distance from the lahar inflow points, where the lahars reached the lake each year, to the cores in Lake Calafquén during the 20th century.

As can be seen from the graphs (above), after comparing the different lahar pathways in both lakes with the thickness of the lahars clay cap deposits in the deepest cores, different trends have been observed. The general trend observed is that thickness of the lahar clay cap is thicker near the inflow and decreases with increasing distance.

In Lake Villarrica, on one hand, the results show that during the events of 1963/64 and 1971 the points where the lahars reached the lake did not affect the sedimentation, since a similar trend is observed for the distance from each inflow (Fig. 5.17). In 1948/49 the tendency is the same, but the difference between the thicknesses of the distal cores and the close ones is wider than in the other events. On the other hand, in 1908 the tendency flips and the distal cores have the thicker deposits.

In Lake Calafquén the trend is the same than in Lake Villarrica, i.e. that the closest cores from the inflow points have the thickest deposits (Fig. 5.18).

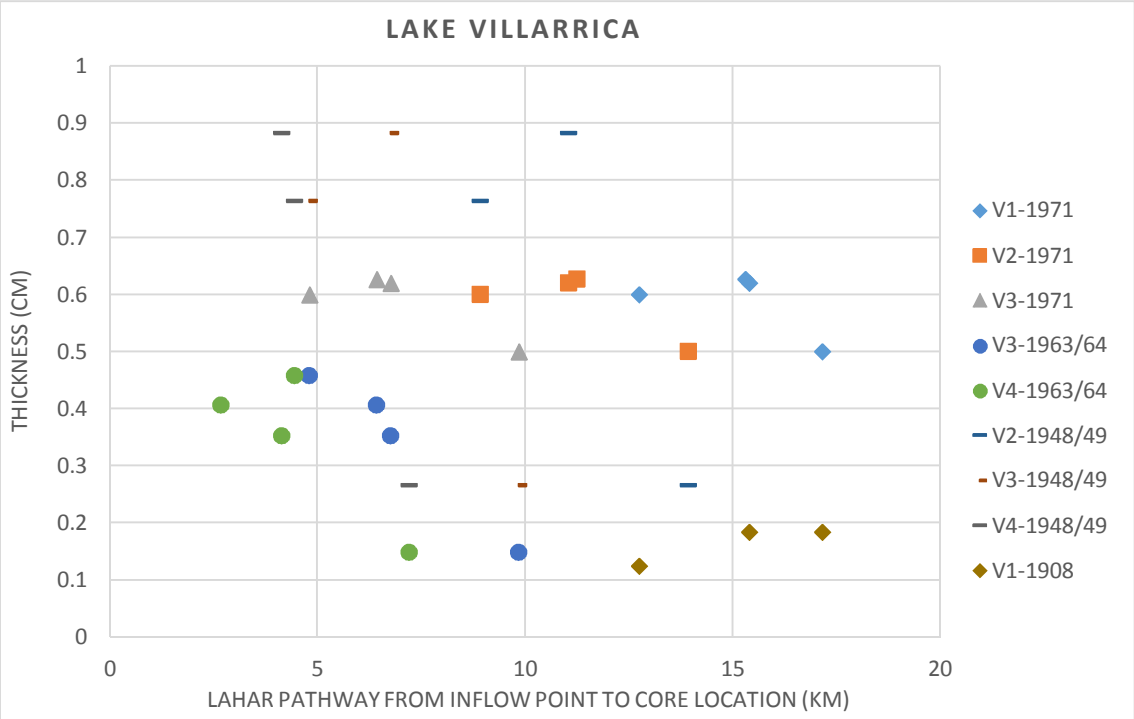

Figure 5.17 Relation between the thickness of the lahar clay cap and the pathways from the lahar inflow points, where the lahars reached the lake each year, to the cores in Lake Villarrica during the 20th century.

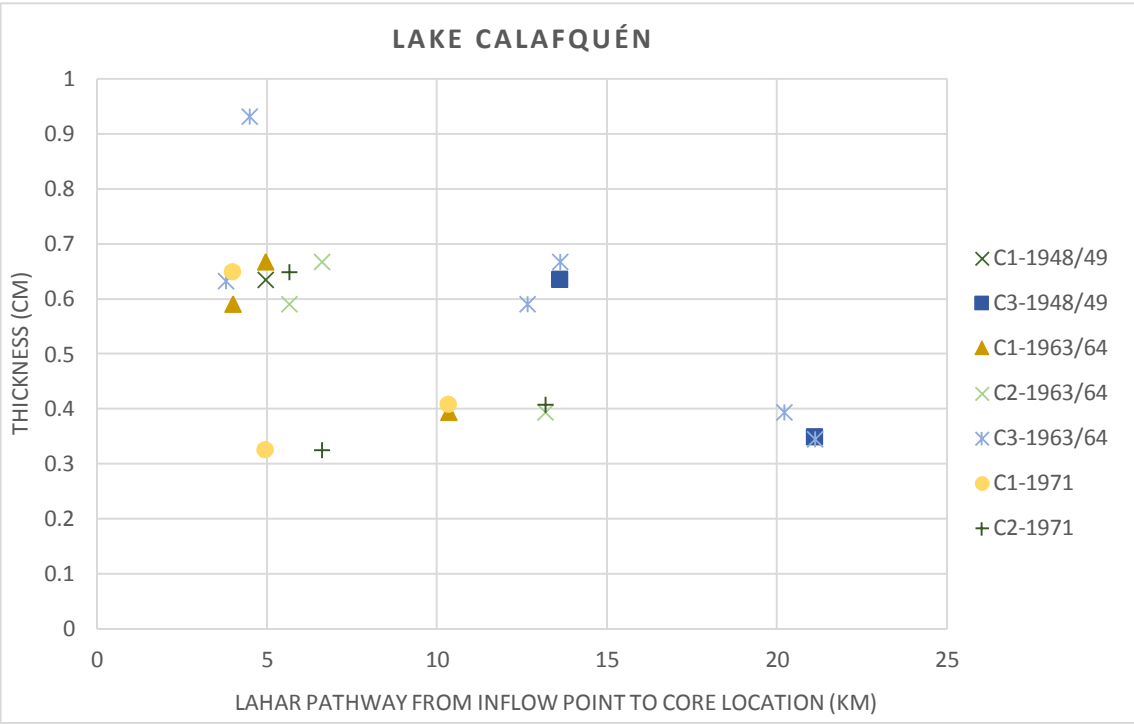

Figure 5.18 Relation between the thickness of the lahar clay cap and the pathways from the lahar inflow points, where the lahars reached the lake each year, to the cores in Lake Calafquén during the 20th century.

5.2 Long cores

From the study of the long cores taken in lakes Villarrica and Calafquén (Fig. 4.1), more than 300 lahar deposits were identified, described, and the complete thickness and depth were measured. Pictures of the cores, processed images applying a HE, and MS values were used for the identification of the lahars. The main characteristics that those deposits present in the pictures and the MS were the same as for the short cores (Tab. 5.1).

After identifying the lahars, most of them were correlated between cores of the same lake (Appendix B.1). Some tephra-fall deposits have been also identified and correlated as key levels for the further correlation of the lahars.

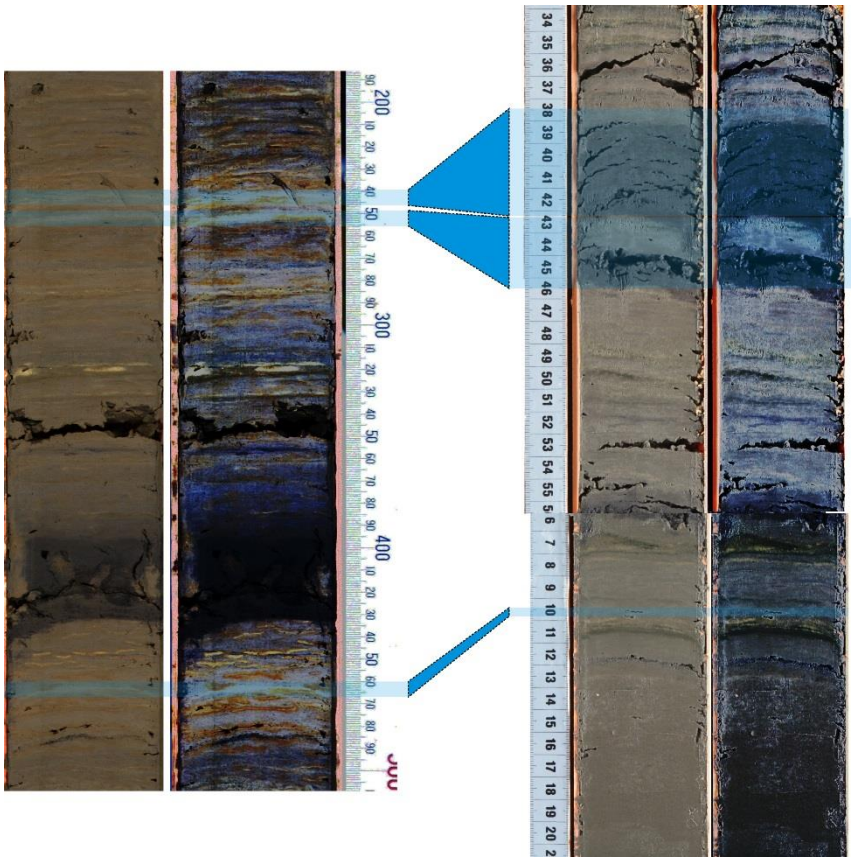

Figure 5.19 Pictuare and processed image applying a HE of the cores CAL2, left, and CAL1, right. Blue rectangles show three of the lahars correlated in Lake Calafquén.

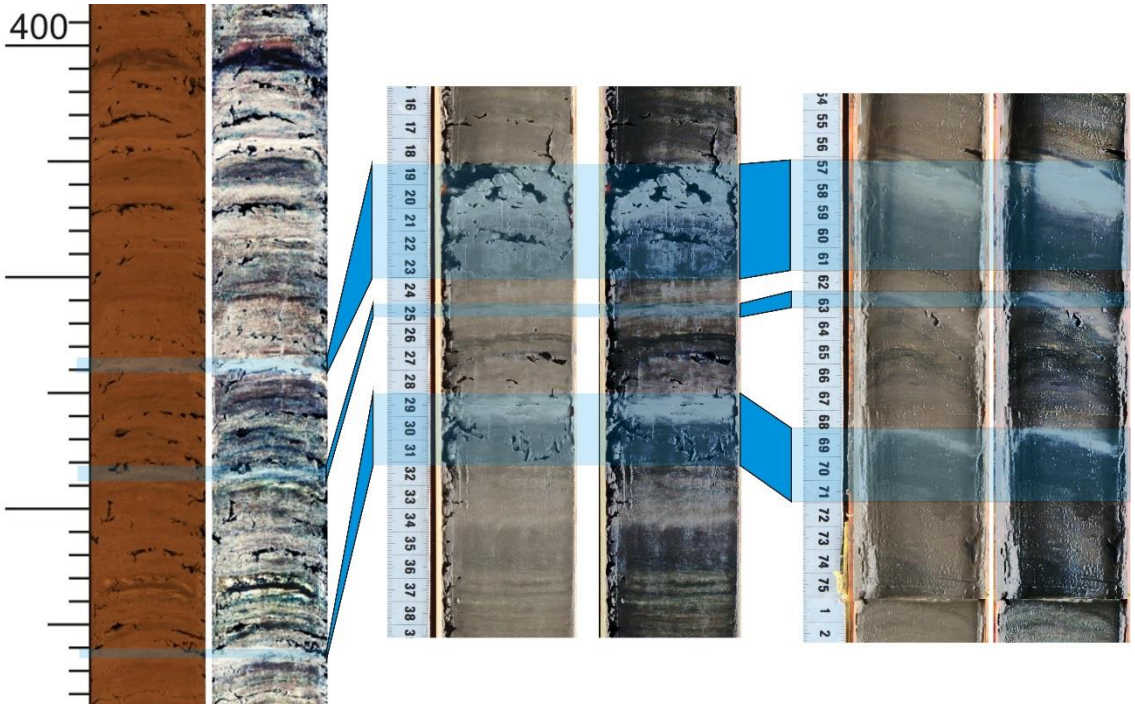

Figure 5.20 Pictuare and processed image applying a HE of the cores VIL1, left, VIL3, middle, and VIL4, right. Blue rectangles show three of the lahars correlated in Lake Villarrica.

For the correlation of the lahars the data from Heirman (2011), Moernaut (2010), Van Daele (2013) and Viel (2012) were taken as a starting point. For the tephras, correlations made by Fontijn, K.[11] using geochemical analysis of samples obtained from the cores CAL1 and CAL2 in Lake Calafquén and VILLAR1 and VIL1 in Lake Villarrica, were used.

In each of the lakes, a master core was chosen (VIL1 in Lake Villarrica and CAL2 in Lake Calafquén), to which the lahars in the other cores in that lake were correlated. The main reason of having a master core is because for further correlations and dating a reference is needed. The cores that are oldest and less influenced by earthquake-induced event deposits such as mass-wasting deposits, were chosen as master cores.

VILLAR1 was not a candidate for being a master core since it is located in a very shallow area, resulting in no lahar deposits (appendix B.1).

Of the more than 300 identified lahar deposits, 117 in VIL1, 88 in VIL3, 86 in VIL4, 37 in CAL1 and 52 in CAL2. About 100 lahars have been correlated between cores VIL1, VIL3 and VIL4; and 25 between CAL1 and CAL2 (Fig. 5.19; Fig. 5.20; Appendix B.1).

[11] Fontijn, K., volcanologist at the Department of Earth Sciences, University of Oxford, South Parks Road, Oxford, OX1 3AN, UK.

5.2.1 Description of the lahars in the sedimentary record of Lake Villarrica.

For the correlation of the lahars in Lake Villarrica, three cores were considered (VIL1, VIL3 and VIL4) and VIL1 was chosen as the master core. VIL1 was taken at a depth of 81 m and it has a length of 13.75 m. It is located at the northern part of the secondary basin on the western side of Lake Villarrica. VIL3 and VIL4 are shorter (11.25 and 8.79 m, respectively) and deeper (112 and 117 m, respectively) than VIL1 (Tab. 4.1), and both are located at the southern part of the secondary basin on the western side of Lake Villarrica (Fig. 4.1).

About 106 lahars were identified in VIL1. Forty-seven were correlated with the core VIL3 and fifty-six with VIL4.

The oldest lahar correlated between the master core and any of the other cores occurs around 7 m depth in VIL1. Below this depth, all the information is only based in VIL1 (Fig. 5.21; Fig. 5.22 and Fig. 5.23). Considering this, the sedimentary record can be divided in three stages with each a different trend.

In the first interval, below 7 m depth, in general the lahar deposits are evenly distributed along the core, with a relatively low frequency and thicknesses. The number of lahars per 50 cm is always between 1 and 5; and the cumulative thickness is mostly lower than 3 and has a maximum of ~5 cm at a depth of 9.75 m. Between 12.5 and 13.5 m more lahars occur then on average, followed by a zone with less lahars (11-12.5 m). In the upper meters of this interval the frequency of lahars has a spiky appearance but shows a generally decreasing trend. At the top of this interval (7-7.5 m) the first lahars of the core VIL3 appear. It consist in a group of 4 lahars with a cumulative thickness of 13 cm.

The second interval is located at a depth ranging from 5 to 7 m. It can be divided in two parts: (i) from 7 to 6 m and (ii) for 6 to 5 m:

(i) The trend of the first part shows in 0.5 m of the sediment record a group of 9 lahars, present in all the cores, but with different cumulative thickness. At VIL4 more than 10 cm of sediment from the lahars was accumulated, in VIL3 a little bit more than 5 cm and in VIL1 less than 5 cm.

(ii) In the upper part the most striking result is the great quantity of material deposited, around 113 cm of sediment between the three of the cores (the highest amount of lahar sediment accumulate along the 14 m sedimentary record). The lahars trend to accumulate a lot of material but are well distribute along a meter of sediment with only a few events.

Just on top of the second stage there is a gap of approximately 80 cm without lahars, but then the average frequency increases to 7 lahars per 50 cm decreasing the average cumulate thickness to 6.5 cm. Then there is a decrease of the frequency of the lahars (until 3 and 4 lahars per 50 cm) towards 2-2.5 m depth, after which there is a gradual increase again (6 lahars at 1.75 m, 8 lahars at 1.25 and 0.75 m depth and finally, 9 lahars at the 25 upper meters of the core). The average of the cumulative thickness along the upper 1.75 m is 3 cm per 50 cm of core, except at 1.25 m depth where it increases to 6 cm.

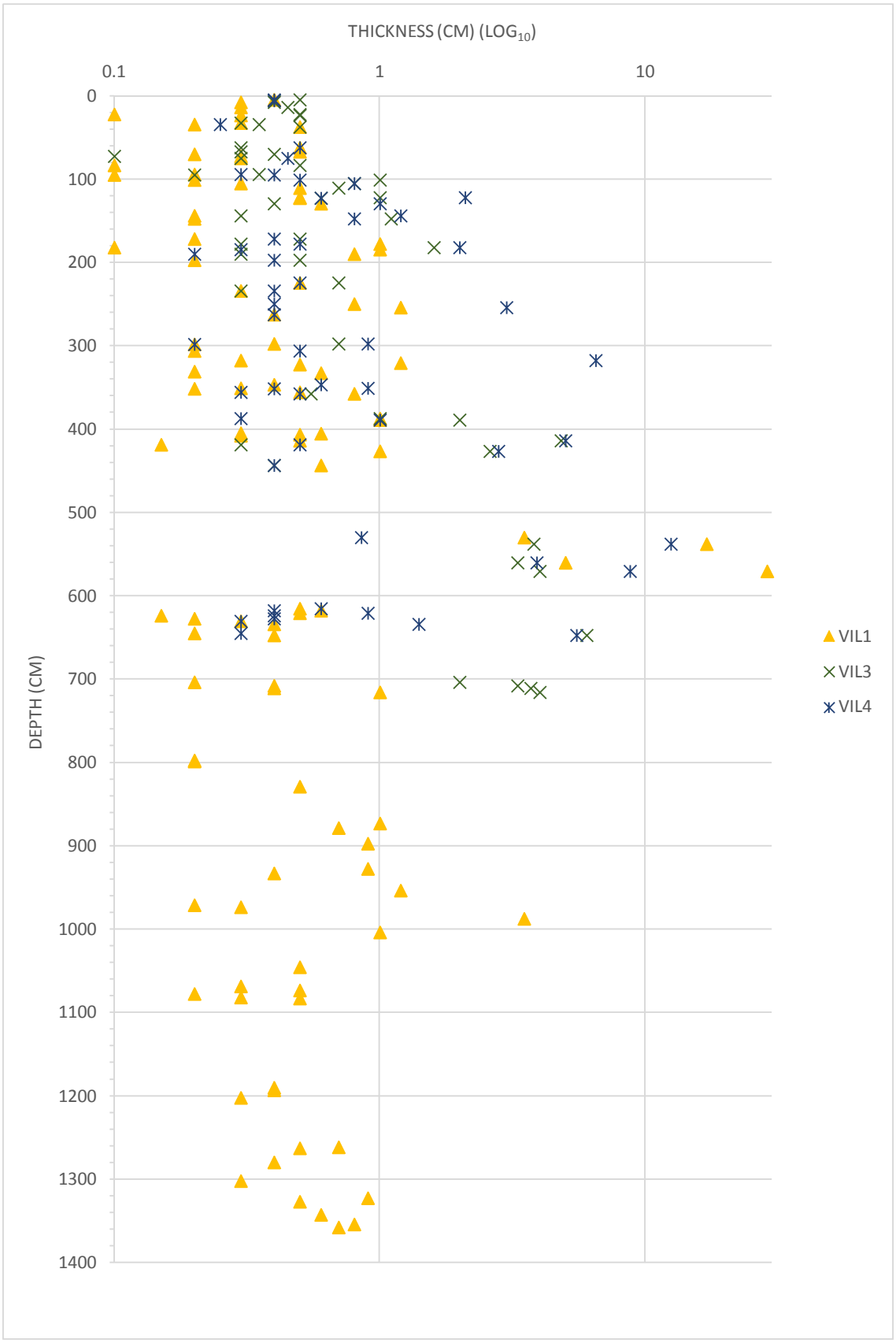

Figure 5.21 Thickness of the correlated lahars of all cores projected on the depth of the master core (VIL1) in Lake Villarrica.

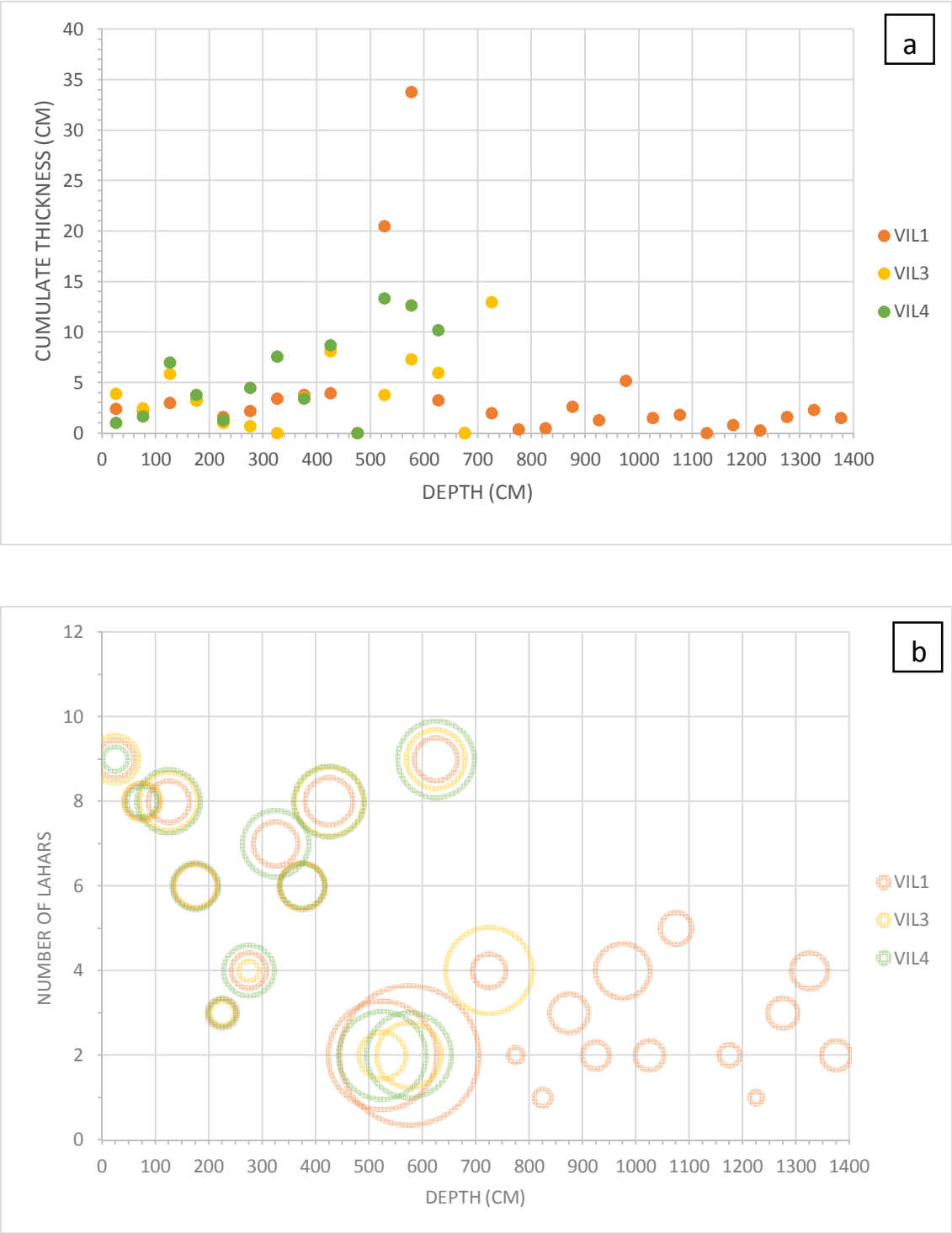

Figure 5.22a Relationship between the cumulative thicknesses of the correlated lahars and depth based on the master core (VIL1) in Lake Villarrica. The sum of the thicknesses was calculated gathering lahars in intervals of 50 cm length. The result is set at the average distance of each interval. **Figure 5.22b** Relation between the number of lahars each 50 cm, the depth based on the master core (VIL1), and the cumulate thickness of the lahars each 50 cm, represented by the size of the colored circles, in Lake Villarrica.

5.2.2 Description of the lahars in the sedimentary record of Lake Calafquén.

For the correlation of the lahars in Lake Calafquén, two cores were considered (CAL1 and CAL2). Master core CAL2 was taken at a depth of 63 m and it has a length of 9.23 m. It is located in a shallow area at the western side of Lake Calafquén. CAL1 is shorter (8.9 m) and deeper (145 m) than CAL2 (Tab. 4.1).

About 45 lahars and 53 tephra fall-out deposits were identified in CAL2. The 25 youngest lahars were correlated the core CAL1.

In general, the lahars of the master core are evenly distributed along the whole sedimentary record. However, at least two trends are clearly visible throughout the core (Fig. 5.23; Fig. 5.24a and Fig. 5.24b).

From the bottom of the core (9.5 m depth) until 3.5 m depth, there is a depositional frequency of 2 lahars per meter, except in two zones (6-7 m and 7.5-8.5 m) where the frequency increases to 10 and 6 lahars per meter, respectively. The average cumulative thickness of the events tend to be lower than2 cm, but in three cases the cumulative thickness of the lahars exceeds the 2 cm (at 8.25, 6.75 and 6.25 m depth).

In the upper three meters of the core, both the depositional frequency and cumulative thickness are higher than in the lower part. The most striking result is the high values of the cumulative thickness between 1.5 and 2.5 meters depth in the core CAL1. Up to 21 cm of cumulative thickness by 8 lahars at a depth ranging from 2 to 2.5 m, and 19 cm of cumulative thickness by 3 lahars at a depth ranging from 2 to 1.5 m. The same lahars in CAL2 cumulative a total thickness of approximately 5 cm.

Between 1 and 1.5 m depth there is a cumulative thickness of 14 and 8 cm in CAL1 and CAL2, respectively. From 1.5 m depth towards the top of the core, the number of lahar deposits gradually increases from 3 to 6 deposits per 50 cm, while the cumulative thickness stays rather similar.

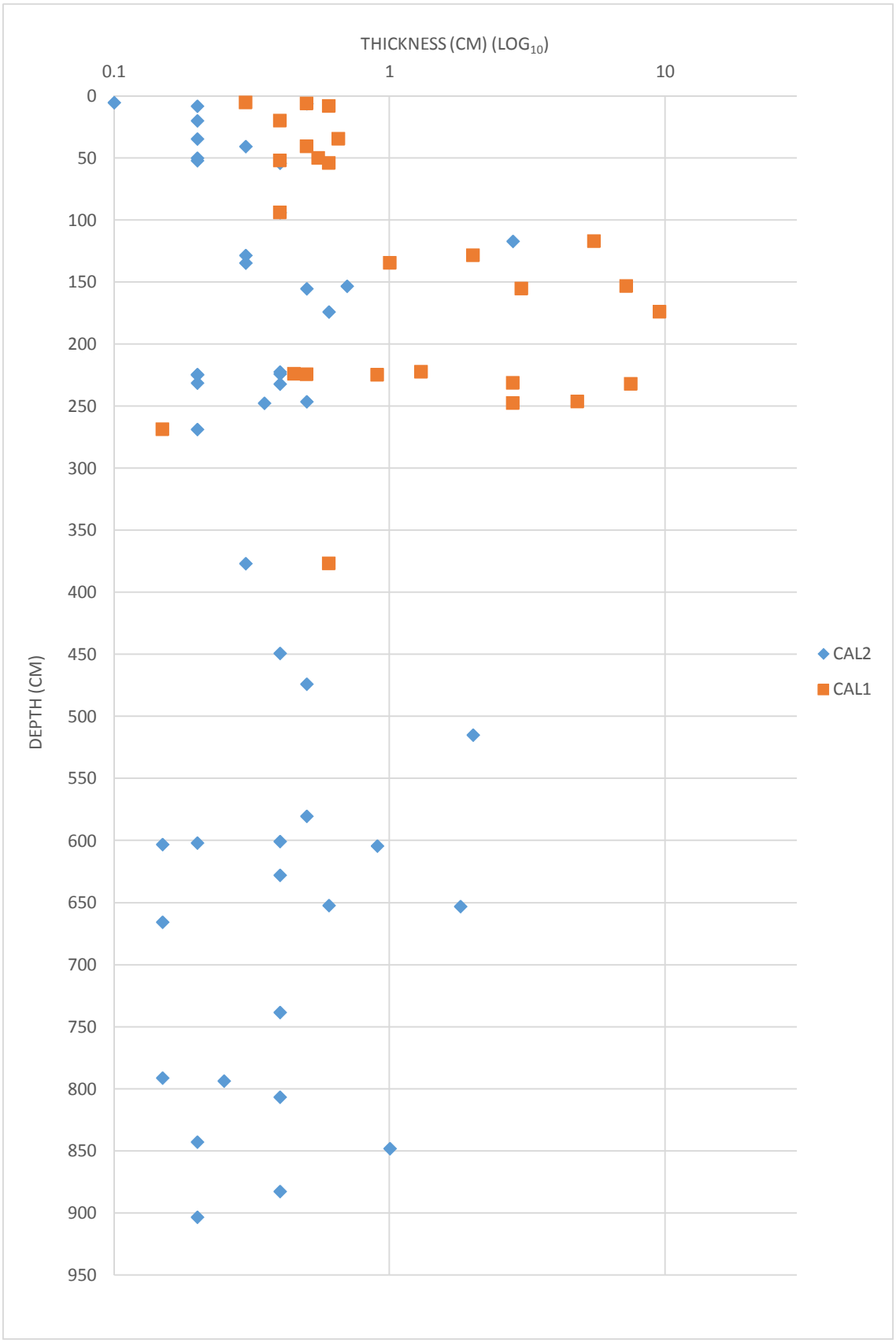

Figure 5.23 Thickness of the correlated lahars of all cores projected on the depth of the master core (CAL2) in Lake Calafquén.

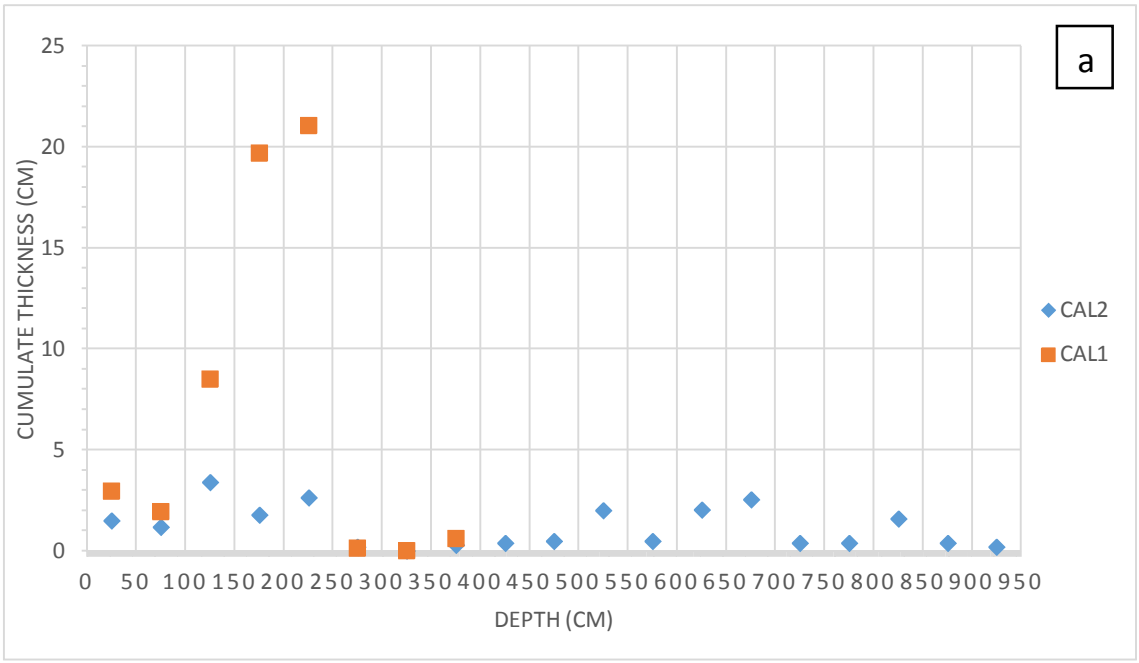

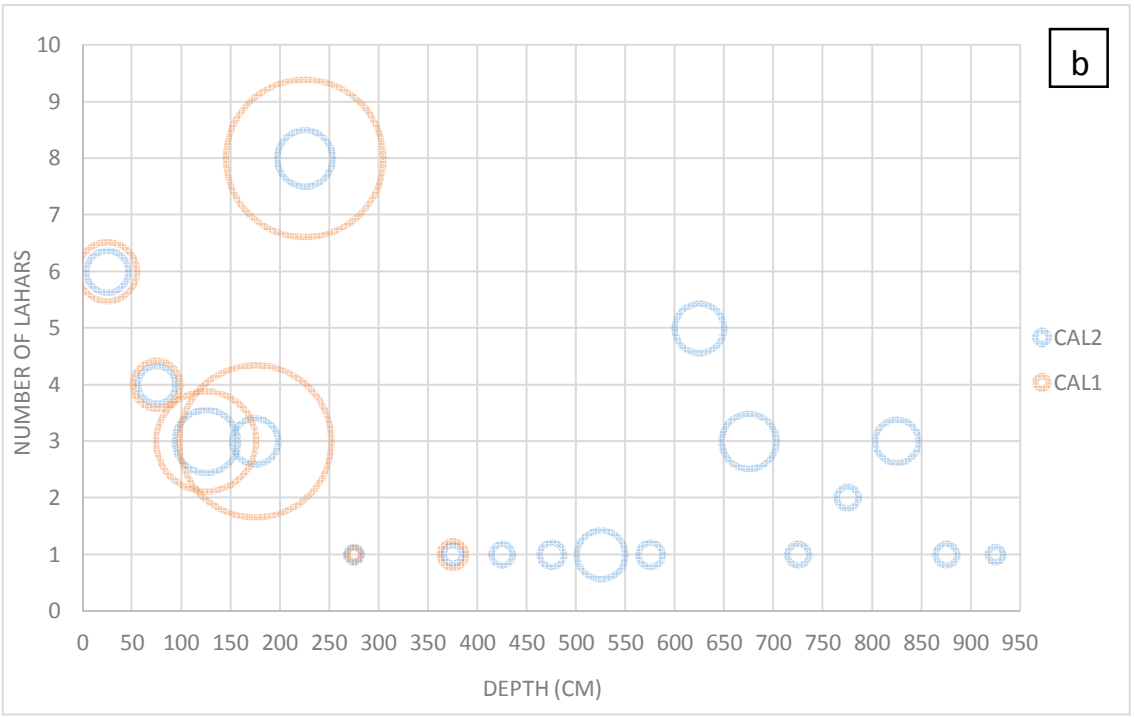

Figure 5.24a Relationship between the cumulative thicknesses of the correlated lahars and depth based on the master core (CAL2) in Lake Calafquén. The sum of the thicknesses was calculated gathering lahars in intervals of 50 cm length. The result is set at the average distance of each interval. **Figure 5.24b** Relation between the number of lahars each 50 cm, the depth based on the master core (CAL2), and the cumulate thickness of the lahars each 50 cm, represented by the size of the colored circles, in Lake Calafquén.

Chapter 6: Discussion

6.1 Short cores

This study builds further on the study of Van Daele et al. (2014), in which the main lahars that reached the lakes Villarrica and Calafquén during the 20th century were identified and correlated to the major eruptive events of Villarrica Volcano. Many other authors have described these events in detail, for example the season, magnitude, casualties and pathways (González-Ferrán, 1994; Petit-Breuilh, 2004).

Before discussing the results, some aspects of the stratification and sedimentation in lakes must be emphasised. Temperate lakes, like Villarrica and Calafquén, experience different periods of stratification throughout a year (Fig. 3.2). It is well known that during austral summer months, such lakes experience a thermal stratification, separating the colder water (bottom) to the warmer (top) by a thermocline. This feature might be very important for the lahar sedimentation in the lakes, because a thermal stratification imply a difference of the density of the water. Therefore, when the lake is stratified, the lacustrine sedimentary process of a lahar that reaches the shore of the lake might be completely different than when it is not stratified (see chapter 2.5 of this thesis).

Considering the previous premises, it can be deduced that if the thickness of a deposit increases with depth, this would mean that there is no relevant stratification and therefore all the sediment would has been deposited by an underflow. However, if the lake is stratified, the material denser than the lake water would be deposited by an underflow, but inflowing water with suspended sediment that is less dense than the water below the thermocline would be dissipated through an interflow above this layer, flowing through the lake to be deposited by fall-out when a balance is reached between the density of the suspension and the water surrounding it. This process would allow the cores located furthest from the source, and in shallower areas to equate or exceed the thicknesses of the deposit from the same event in cores located at deeper or closer from the source areas. These hypotheses will be tested in this chapter.

6.1.1 Lake Calafquén

The interpretation of the sedimentation process in Lake Calafquén takes as a starting point the results of the events of 1963-1964 and 1971 (Fig. 5.2, Fig 6.1 and Fig 6.2). The thicknesses of the deposits in the cores closest to the inflow of the lahars (CB4, CB9 and CGC01; Fig. 5.2 and Fig. 5.3; see chapter 5.1.2 of this thesis) are, by far, the largest. This can be explained as a direct consequence of the great magnitude of the lahars that reached the lake right in front of the points where these cores were taken. Hence, there was a contribution of very dense material possibly being deposited by underflow traveling along the lake slopes and floor. According to the results shown in Fig. 6.3, as the underflow travels in the lake, it loses energy, resulting in thinner deposits in cores CALA01 and CALA02.

On the other hand, in the cores located in the shallower areas (CAGC03, CALA04, CALA05 and CALA06; Fig. 5.3) the lahar deposits could not have been deposited there if part of the sediment was not transported by an interflow or overflow (Fig. 6.1 and Fig 6.2). The results show that in the cores located in a range of depths around 90 m (CALA04, CALA05 and CALA06), lahar clay caps have a thickness ranging from 0.2 to 0.3 cm. In core CAGC03, which is taken on a shallower location (63 m water depth), the lahar clay cap has a thickness that is approximately half of that in the ~90-m-depth cores (Fig. 5.13; appendix A.2). The interpretation of the sedimentation process of the lahar, according to the results, is that an interflow travelled at a depth ranging from 50 to 100 m. One of the reasons why the thickness of the lahar clay cap of the core CAGCO3 is half of the other cores, is because CAGC03 is located at a depth of 63 m (Tab. 4.1), so only the top-few meters of the interflow deposited material at that point. However, when the sedimentation process involves an interflow, also the distance from the source will influence the sedimentation process. As shown in Figure 6.4, as the distance travelled by the flow increases, the thickness of the lahar clay cap decreases. That would be another explanation why on CAGC03 the thickness of the lahar clay cap is thinner, because this core is the more distal core from the lahar inflow points (Tab. 5.2b; Fig. 6.3).

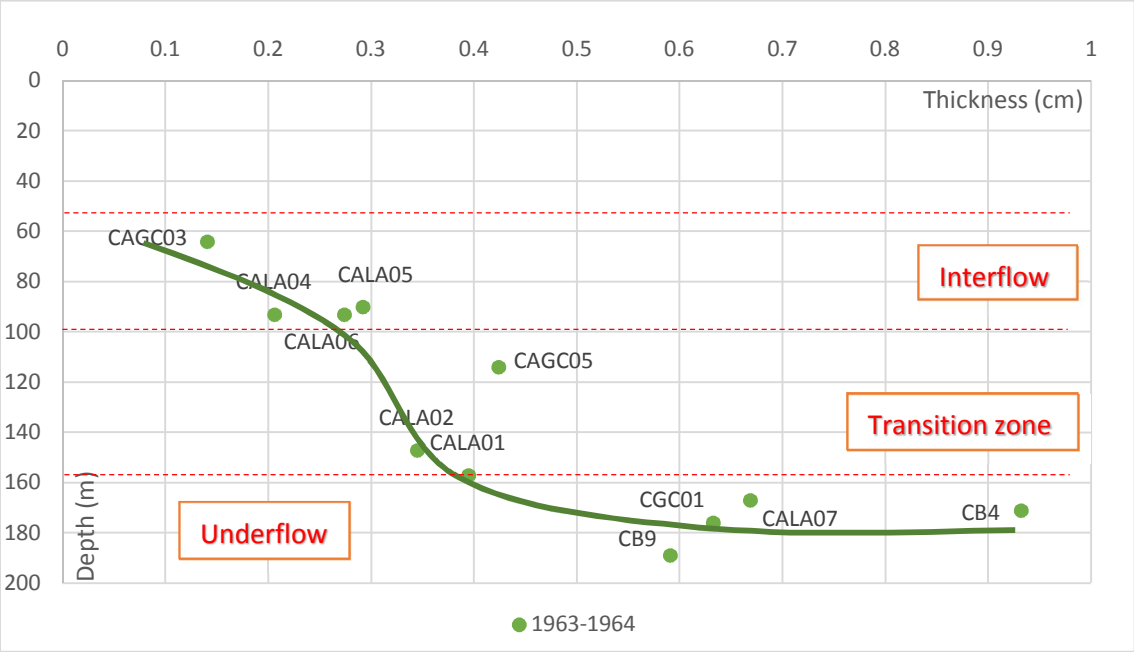

Figure 6.1 Interpretation of the sedimentation process based on the relation between the thickness of the lahar clay cap and the depth of the short cores in the event of 1963-1964 in Lake Calafquén.

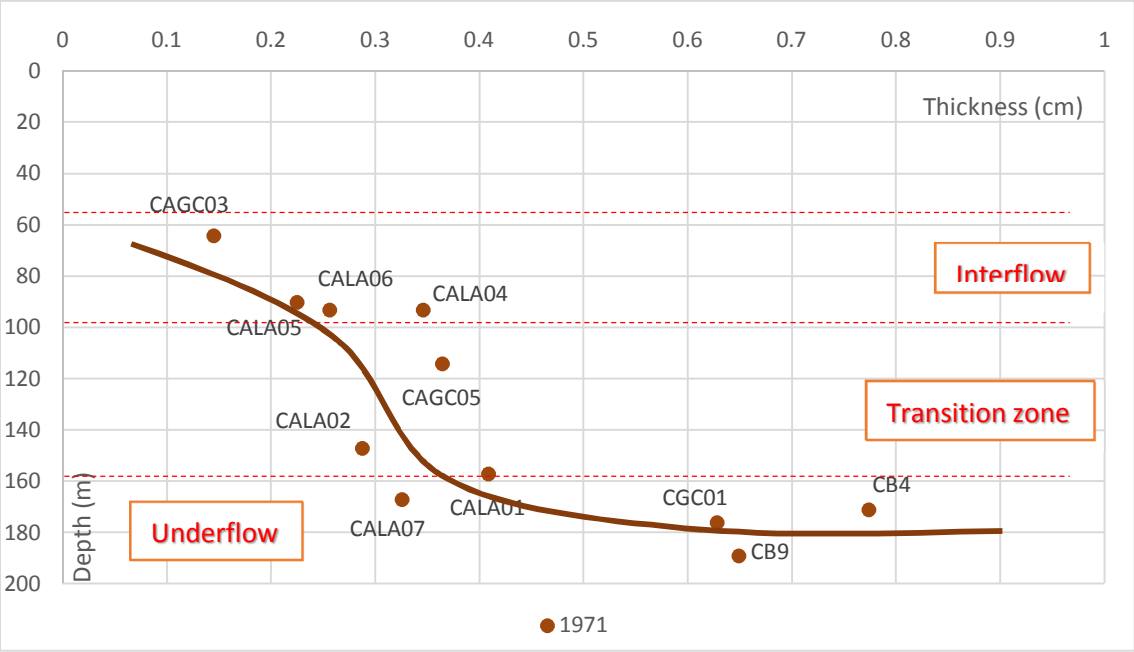

Figure 6.2 Interpretation sedimentation process based on the relation between the thickness of the lahar clay cap and the depth of the short cores in the event of 1971 in Lake Calafquén.

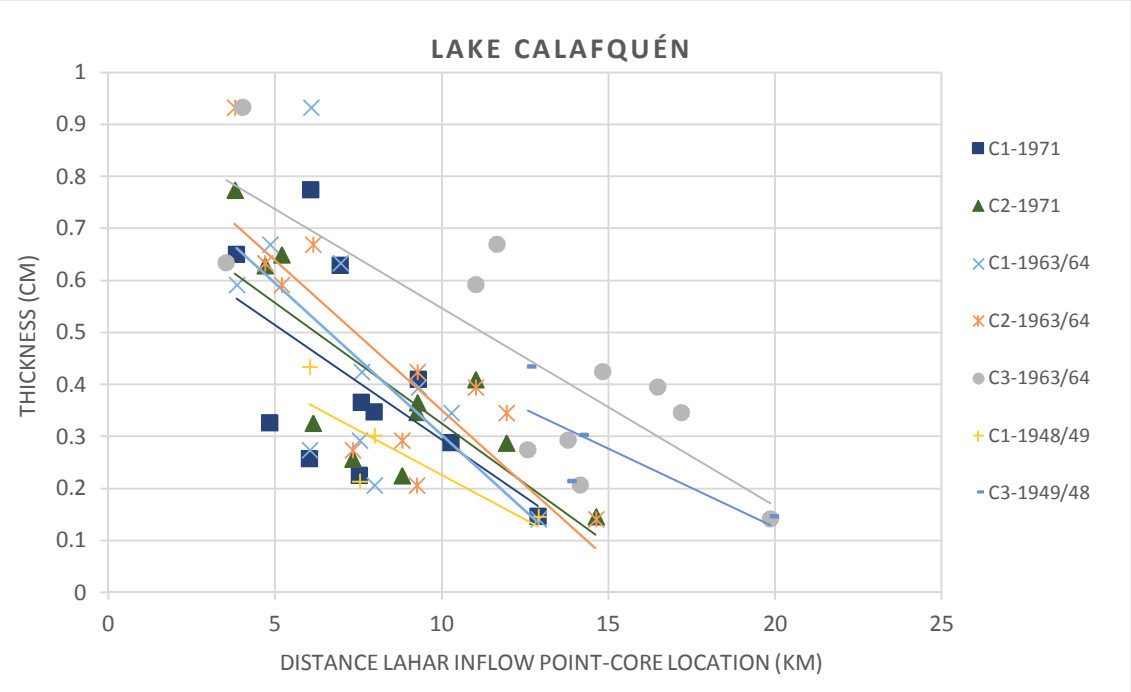

Figure 6.3 Relation between the thickness of the lahar clay cap and the straight distance from the lahar inflow points, where the lahars reached the lake each year, to the cores in Lake Calafquén during the 20th century. The trend lines show by colors a common behaviour of the lahars, being thinner deposits according the distance travelled by the interflow increases, independently from the point where the lake was reached.

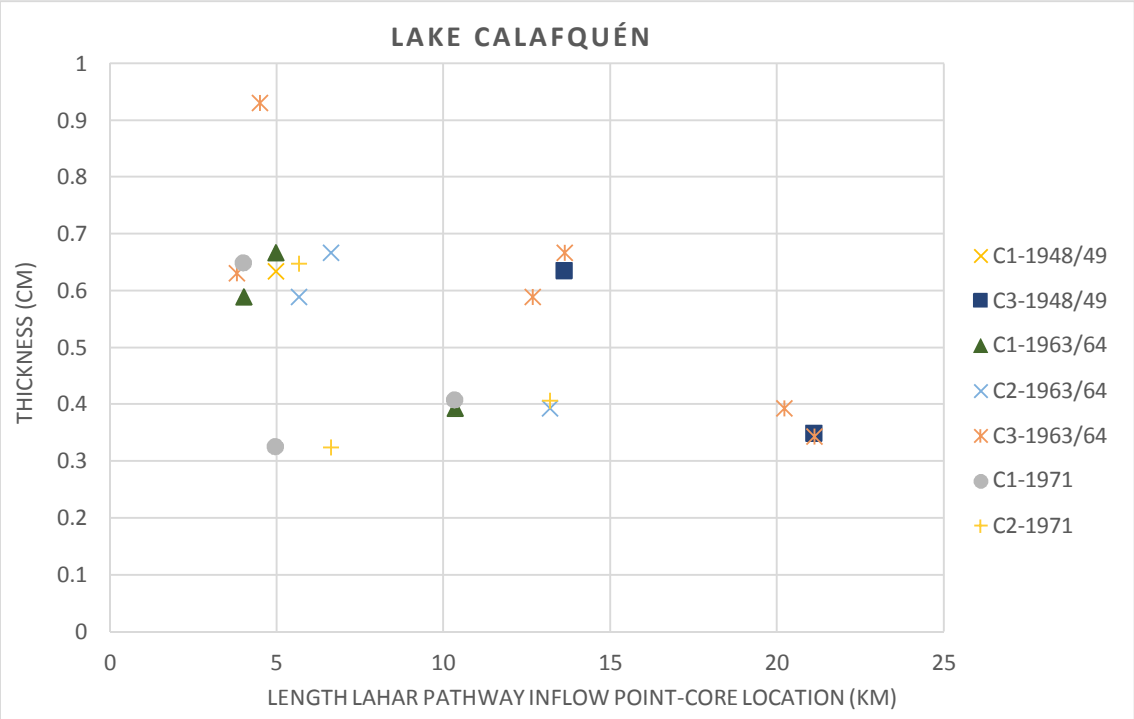

Figure 6.4 Relation between the thickness of the lahar clay cap and the pathways from the lahar inflow points, where the lahars reached the lake each year, to the cores in Lake Calafquén during the 20th century. The trend lines show by colors a common behaviour of the lahars, being thinner deposits according to the distance travelled by the underflow increases, independently from the point where the lake was reached.

When the density/temperature of the inferflow stabilized with the surrounding water the sediment settles. This means that the complete area of the lake with a depth of more than 50 m was influenced by the interflow, also the deepest parts, where the sedimentation is mainly controlled by the underflow. Considering this, the transition zone (Fig. 6.1; Fig. 6.2) was interpreted as a depth area from which its base is influenced by both the top of the underflow and the interflow. Below this zone mainly the underflow determines the thickness, while its upper part, which coincides with the base of the thermocline, is only affected by the behaviour of an interflow traveling above.

Considering the reports, in 1963 the events were formed in May 1963 and in March 1964, while in 1971, the lahars reached the lake at the end of December, i.e., during the austral summer (González-Ferrán, 1994; Fig. 2.8). This is the season of the year which a peak in lake stratification is registered (Campos et al., 1983; Fig. 3.2). This situation reaffirms the theory that in the shallower areas of Lake Calafquén the sediment was deposited by interflows.

Due to erosion by slumps and turbidites triggered by the 1960 earthquake (Van Daele et al., 2014), less cores with a deposit of the 1948/49 events are available in Lake Calafquén, and therefore the depth-thickness plots (Fig. 5.2; Fig. 5.12; appendix A.1 and appendix A.2) are harder to interpret. However, they do link with and thus confirm the sedimentation processes during the 1963/64 and 1971 events.

6.1.2 Lake Villarrica

In the following paragraphs the highlights of the results obtained from the sedimentary record of Lake Villarrica are discussed in detail.

The 1908 and 1971 events share certain characteristics and differ in others. Comparing them helps to understand how the lahars were sedimented during those events. The first common factor is that in both cases there is a reported major lahar that reached the lake at point V1, in the east end of the lake (Fig. 5.2). In 1971 two other lahars were reported, reaching the lake at the V2 and V3 points (southeast; Fig. 5.2). Finally, the last factor to consider is that in 1908 the event took place in the early austral spring, so the lake stratification was only poorly developped, and in 1971 it occured during the summer (end of December), meaning that the lake was stratified (Campos et al., 1983; Fig. 3.2).

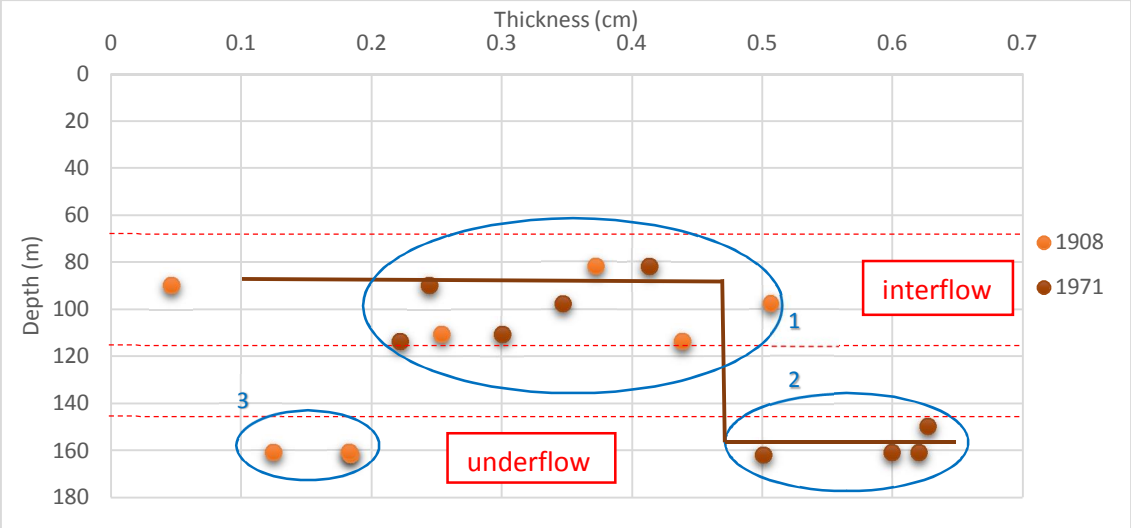

Figure 6.5 Relation between the thickness of the lahar clay cap and the depths of the cores in the eruptive events of 1971 and 1908, and interpretation of the sedimentation process based on the relation between the thickness of the lahar clay cap and the depth of the short cores in the event of 1971 in Lake Villarrica. In both cases the shallower cores have a thickness ranging from 0.2 to 0.4 cm (1). On the other hand, the deepest cores in 1971 have a thickness greater than 0.4 cm (2) and during 1908 are thinner than 0.2 cm (3).

With these premises, in 1908, considering the point V1 as the lahar entry point, the sediment was transported by an interflow that travelled with the lake currents to the most western area of the lake -where the outflow of the lake is located-, where sediments were trapped and subsequently settled. Such process explains why western and shallower cores have the thickest deposits (Figs 6.5 and 6.6). The possibility of the existence of an underflow is very small, since in the sedimentary record of the core VILLAR1 (the shallowest core; Fig. 4.1; Tab. 4.1; appendix B.1) there are no deposits identified as a lahars, i.e. that there is no trace of laharic material distribute from the surface of the lake through an overflow.

During the 1971 event, the lake was stratified and the sedimentation process was divided in two: (1) by an underflow that struck the deepest cores, and (2) by an interflow that transported the material to the westernmost area where the shallower cores were taken. Unlike the case in Lake Calafquén, a transition zone is not observed for the 1971 event (Fig. 6.5). The reason can

be that there are two distinct basins with very different depths, and at the transition from one to the other there is a generally steep slope covering a depth difference of 30 m in less than a kilometre. Hence, in this case a possible underflow in the deep basin cannot reach the shallower western subbasin. The fact that the thickness of the lahar clay cap from the 1971 event in the deepest located cores is so large compared to the 1908 event, is interpreted to be a consequence of the two other active lahar pathways that reached the lake from the South. Right in front the points where those cores are located.

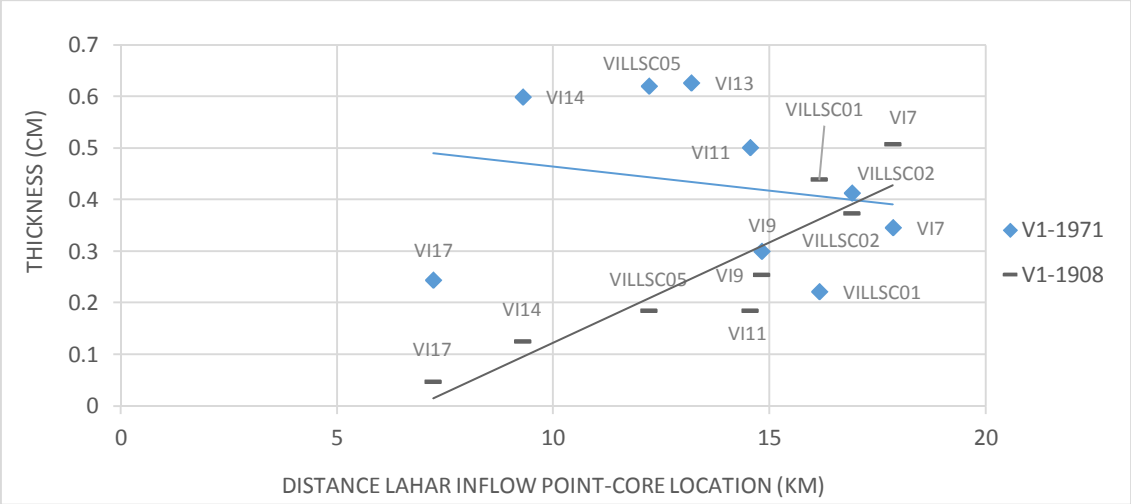

Figure 6.6 Relation between the thickness of the lahar clay cap and the straight distance from the lahar inflow point V1, where a major reported lahar reached the lake, to the cores in Lake Villarrica during the events of 1908 and 1971. The difference of the trends can be appreciated by the tendency lines. During the event of 1971 the influence of other lahars that reached the lake in front of the cores VI14, VILLSC05, VI13 and VI11 supposed a differential factor on the sedimentation.

The 1948/49 event took place during October of 1948 and January of 1949, what means that the vertical profile of the lake would be stratified when the lahar reached the lake. Deposits related to this event clearly show an influence of the points where the lahars reached the lake (V2, V3 and V4) in the sedimentation process (Fig. 5.3, Fig 5.8). Considering this, the material deposited at the points VILLSC05 and VI14 appears to have been transported by an energetic underflow which carried a lot of the material from the lahars. The thinner lahar clay cap in VI11, which has a similar depth as VI14 and VILLSC05, can be explained by its position in the lake that is sheltered from the lahars coming from the south, as is the case for this event. Moreover, the thickness in the shallower cores ranges from 0.2 to 0.3 cm without showing any trend. In this case, sedimentation is considered to be due to an interflow situated between 50 and 80 m depth, because if they all have the same thickness and there is no trend, it means that everything fell out of an interflow which is shallower as the shallowest core. And perfectly fits with the stratification of the lake at during those months (Fig. 3.2).

The trend observed for the 1963/64 deposits is similar as the one described for the 1948/49 clay caps. First of all, lahars reached the lake in May of 1963 and in March of 1964, so as in 1948/49 the lake went through two periods of thermal stratification and secondly, the entry points of the lahars were also at the South of the lake. But, unlike the event of 1948/49, when 2 large lahars reached the lake, in 1963/64 lahars were smaller. This difference in magnitude between the

lahars is recorded in the thickness of the lahar clay cap in the cores influenced by an underflow (VI14 and VILLSC05). The thicknesses at the latter locations are much larger for the 1948/49, compared to the 1963/64 event (Fig. 5.8 and Fig 5.9). The reason why the core VI11 (Fig. 5.3) has a very thin lahar clay cap deposit, about 0.15 cm, was interpreted in the same way as for the event in 1948/49 in the previous paragraph (i.e. its sheltered location). On the other hand, the thickness in the shallow cores ranges from 0.2 to 0.35 cm, with a trend of increasing the thickness with the depth. Hence, the sedimentation was carried out by an interflow located between 60 and 110 m deep, because there is a change from VI7 to VI9, and the thickness in VILLSC02 (~80 m) is still much more than 0, so a large part of the interflow must occur above that point.

To interpret the results obtained in the events of 1904, 1909 and 1920, the first thing to consider is that there are no reports of lahars reaching the shore of the lakes during these events. This feature is very important because the interpretations are not as consistent as the previous ones since the inflow points of the lahars are not known. In general the thickness values resulting from these events range from 0.1 to 0.3 cm. The events of 1904 and 1909 show that the shallower cores that are closer to the outflow of the lake, are those with thicker clay cap lahar deposits. The explanation is that the material was transported and accumulated at the westernmost part of the lake. This is interpreted as the sedimentation occurred through an interflow heavily influenced by the currents of the lake. An overflow is not an option since, like it was said before, in VILLAR1 (the shallowest core; Fig. 4.1; Tab. 4.1; appendix B.1) there are no lahar deposits. In 1920 the interpretation is a slightly different. Unlike the other two episodes, of which no reports about the season in which they occurred exist, the 1920 event was reported during the austral spring (September and October). This means that the lake would have a very primary or very weak stratification (Fig. 3.2). Considering this feature and the increase of 0.1 cm of the thickness of the lahar clay cap deposit comparing to the deposits at the same location during the previous events, the sedimentation process in 1920 could be by a weak underflow, but with enough energy to settle in the deeper areas of the main basin, and by interflow which transported and accumulated the material at the westernmost part of the lake, as in older events, highly influenced by the current.

The most recent event (1991) is the one for which less information is available, as in previous studies had not been taken into consideration, so perhaps it was not even a lahar and the clay caps identified correspond an enhanced amount of material transported by the rivers. Thus, its results were considered less reliable.

6.2 Long cores

6.2.1 Application of the different age models to the correlation of the lahars

The results obtained after analysing the sedimentary record of the lakes Villarrica and Calafquén has been interpreted based on two age models from previous studies. The age model of the Lake Villarrica is based on the one calculated by Heirman (2011), and in Lake Calafquén by Moernaut (2010) and Viel (2012).

Before discussing the results, obtained by applying those age models to the values showed in chapter 5.2 of this thesis, it is important to take into account that the age models are based on three different types of data: (from more to less reliable) Historical data, ^{14}C samples of macroscopic organic matter and bulk organic matter (Fig. 4.2; see chapter 4.1 of this thesis). This means that the age models are not perfect. But as it was mentioned before, some tephra layers, already correlated by Fontijn, K. (see chapter 5.2 of this thesis), were used as key levels for the correlation. Based on correlation of tephra marker layers between the two lakes (and age models), an estimation of the errors of the age models can be achieved. At the two marker horizons the age model VIL1 is younger with a maximum offset of less than 300 years (Table 6.1). Since the offset between the two age models reach up to several hundreds of years, lahar numbers and thicknesses have been cumulated per 500 years. In this way the results from the two lakes are comparable.

Lake	**Villarrica**			**Calafquén**		
Name of the event	**Label in correlation**	**Depth (cm)**	**Estimated age (cal yr BP)**	**Label in correlation**	**Depth (cm)**	**Estimated age(cal yr BP)**
Quetrupillán	VT10	294	2545	CT10	274	2835
Ranco	VT9	752	4840	CT11	495	4970

Table 6.1 Estimated age of the samples from the master cores of lakes Villarrica and Calafquén of two historical eruptive events based on the age models from Heirman (2013) and Moernaut (2010) and Viel (2012), respectively. "Label in correlation" corresponds to the name of the layer in the correlation.

In general, the evolution of the lahar deposits in both lakes follow a similar trend (Fig. 6.7). However, from 4.5 to 3 ka there is a clear discrepancy between number and thickness of the lahar deposits in both lakes.

During the first 6.5 ka two periods with a higher event frequency occur (i.e. 10 to 7.5 ka and 7 to 5.5 ka) that are separated by punctual fall around 7-7.5 ka. During the youngest period the amount of lahars is about 50% higher than during the first period. From 5.5 to 4.5 ka the lahar frequency was similar to that between 10 and 7.5 ka. These results perfectly fit with the results obtained in each lake without having considered the age (Fig. 5.22b; Fig. 5.24b).

Apart from the already correlated tephra layers (Table 6.1), at 3.7 ka (cal yr BP) the Pucón eruption occurred and changed the morphology of the Villarrica Volcano (chapter 3.2; Clavero and Moreno, 2004; Fig. 6.7). The eruption resulted in a new caldera, and that the Pucón Ignimbrite (resulting from the Pucón eruption) is mainly occurring in the northern part of the Volcano (towards Lake Villarrica) (Silva Parejas et al., 2010). The very thick lahars in Lake Villarrica around 4 ka are therefore considered to be a product of the Pucón eruption and might represent the Pucón Ignimbrite. In the projection (Fig. 6.7) these thick deposits seem a lot older than 3.7 ka, but it should be taken into account that a deposit at 3.9 ka is also projected at 4.15. After the Pucón eruption, just after that (3.6 ka), there occurs a trough in lahar frequency in both Villarrica and Calafquén. This could be explained by the Pucón eruption releasing all the pressure in the magma Chamber of the volcano, resulting in a period of relative quiescence. Around 3.1 ka many lahars occur in Lake Villarrica, but Lake Calafquén experimented a decrease of the number of the lahars. However, after about 700 years the trends changed with a decrease in lahar frequency in Lake Villarrica and an increase in Lake Calafquén. Hence, from 3 to 0 ka there was a normalization with relatively a lot lahars in both lakes Villarrica and Calafquén, with similar proportions as before 4.5 ka between the two lakes. This could be explained by a modified morphology of Villarrica Volcano by the Pucón eruption, which formed the caldera, but creating an open gate for lava flows and lahars to Lake Villarrica and closing all pathways to Lake Calafquén. But after 700 hundred years (approximately) the new cone was built and the lahar pathways to Lake Calfquén were reopened. This also interpretation is supported by the Pucón Ignimbrite, which is deposited on the Villarrica side of the volcano, which is also the reason for the very thick lahars linked to Pucón in Villarrica (4.1 ka) (Clavero and Moreno, 2004).

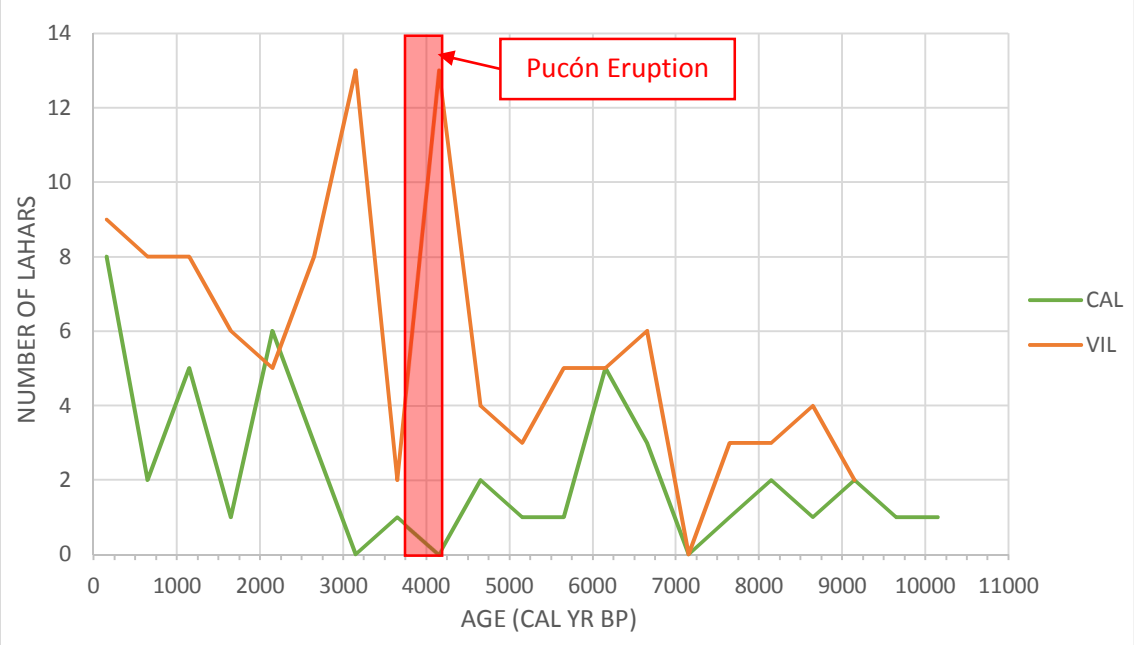

Figure 6.7 Evolution of the number of the lahars during the Holocene in the lakes Villarrica and Calafquén.

Considering that Pucón eruption had a great influence on the evolution of the lahars registered in the lakes record, it can be appreciated that in Lake Villarrica the cumulative thickness does not seem to be directly influenced by the eruption (Fig. 6.8). Although the trend is to increase the amount of lahars the magnitude seems to be ranging in the same values as for the events

before Pucón eruption. At around 4.25 ka a huge amount of material was cumulate due to the new caldera was built after Pucón eruption and all the lahars were focussed to Lake Villarrica. The thick lahars were probably the direct deposit from the ignimbrite.

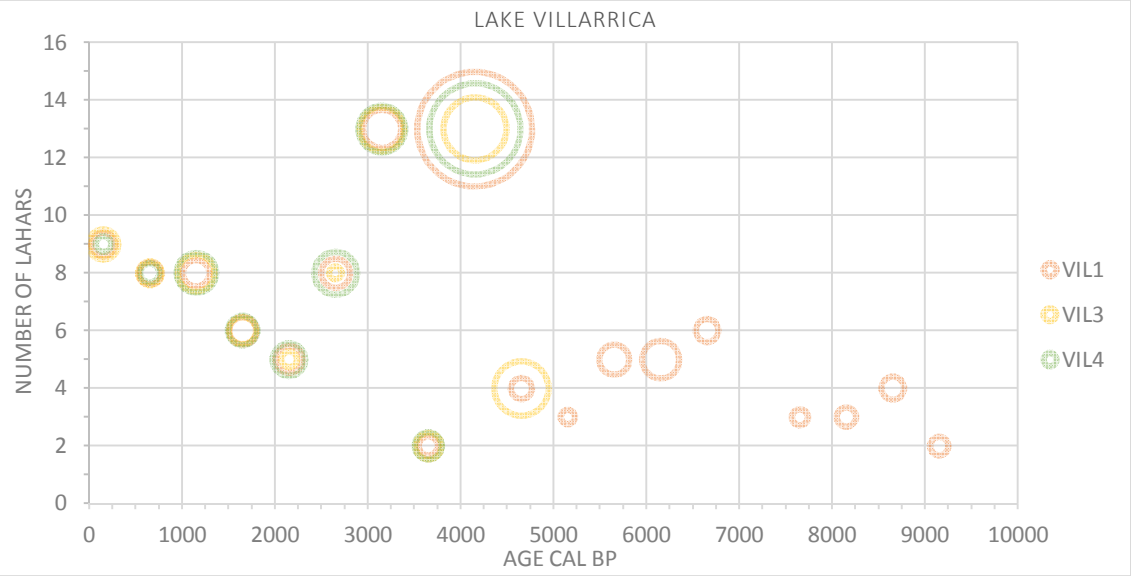

Figure 6.8 Relationship between the cumulative thicknesses, represented by the size of the colored circles, the number of the correlated lahars each 50 cm, and the age in Cal yr BP based on the master core (VIL1) in Lake Villarrica. The sum of the thicknesses was calculated gathering lahars in intervals of 500 years. The result is set at the average distance of each interval.

On the other hand, the cumulative thickness registered in Lake Calafquén shows that from the last 3000 years the thickness of single lahars stays very similar. The cumulative thickness increases but mainly because the number of lahars increases, not the magnitude of each lahar (Fig. 5.22a). Since the lahar pathways to Lake Calafquén were reopened after Pucón eruption, (after approximately 3 ka) it seems like lahars to Villarrica and Calafquén are back in balance, similar to before 4.5 ka.

Something else to take into account is of that CAL2 is located in a more protected area of the lake Calafquén, further away from the lahar inflows than VIL1 in Lake Villarrica.

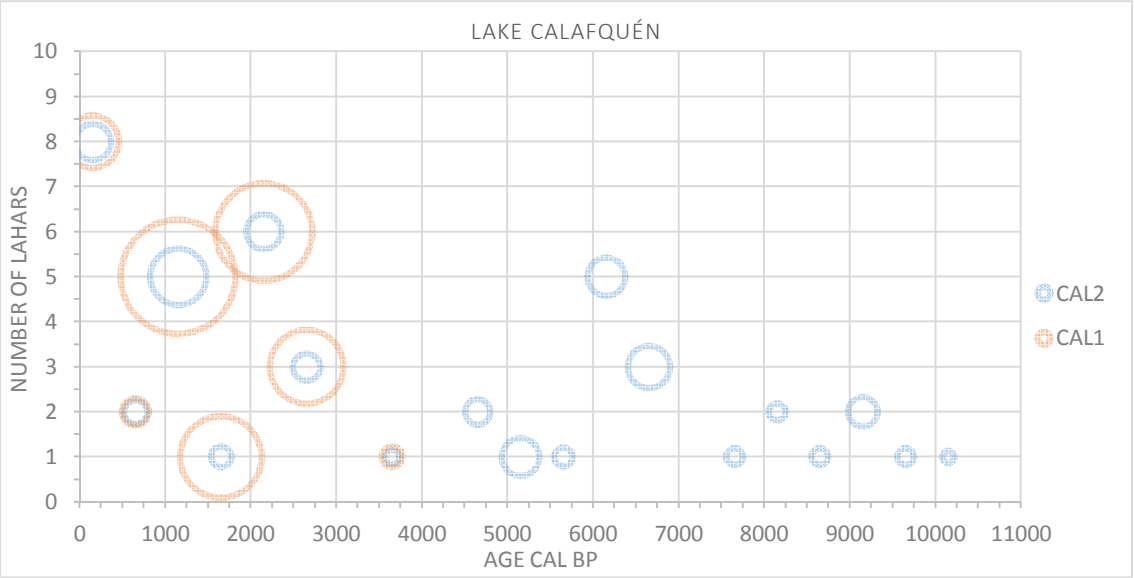

Figure 6.9 Relationship between the cumulative thicknesses, represented by the size of the colored circles, the number of the correlated lahars each 50 cm, and the age in Cal yr BP based on the master core (CAL2) and the age model in Lake Calafquén. The sum of the thicknesses was calculated gathering lahars in intervals of 500 years. The result is set at the average distance of each interval.

6.2.2 Relation between the precipitation model and the evolution of the lahars during the Holocene

One of the factors that control the generation of a lahar is the amount of water on the slopes of the volcano, either as snow, ice cover or rain. Therefore it is important to relate the evolution of the lahars to the evolution of the precipitation along the Holocene.

Plotting the evolution of the lahars along the Holocene by the sum of the curves registered at both lakes, and comparing it with the evolution of the precipitation during the same period of time in Central Chile, it can be appreciated that both curves co-vary during the Holocene (Fig. 6.10 and Fig. 6.11). The first 4000 years show low values, intermediate values occur from 6 to 3 ka (cal yr BP) and high values the last 3000 years.

Considering the results it could be asserted that there is now more snow/ice on Villarrica Volcano that then in the start of the Holocene. Obviously there is a direct influence between the amount of water available (as snow or ice cover) and the production of lahars. One of the evidences that precipitation might have a strong influence is that there are tephras (mostly from Villarrica; Fontijn, K.; appendix B.1) occurring quite regularly throughout the cores, showing that the number of eruptions is probably quite constant.

But it must be considered that the main trigger of a lahar is an eruption, so the amount of water it is not the only factor of the increase of the number of lahars. The general trend might be climate, but for example the trough before the Pucón eruption (Fig. 6.7) might mean that there was really less eruptive activity; during which pressure built up, followed by a very explosive (Pucón) eruption (Clavero and Moreno, 2004). Similarly the trough after the Pucón eruption and

the following discrepancy in lahar frequency between the two lakes is most probably a result of this eruption.

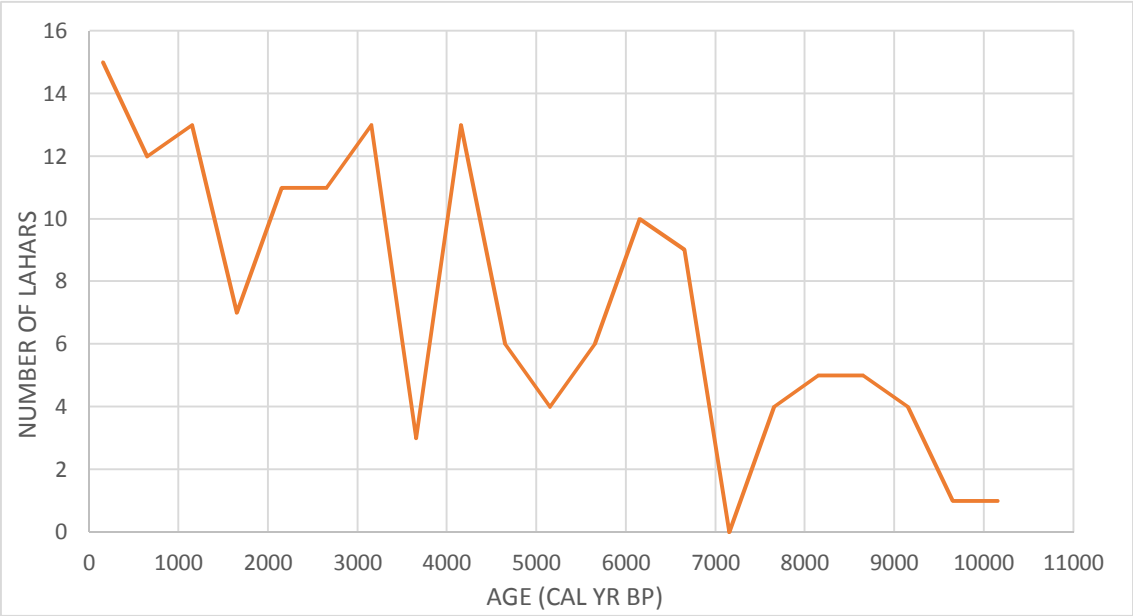

Figure 6.10 Evolution of the lahars during the Holocene in the lakes Villarrica and Calafquén sumarized.

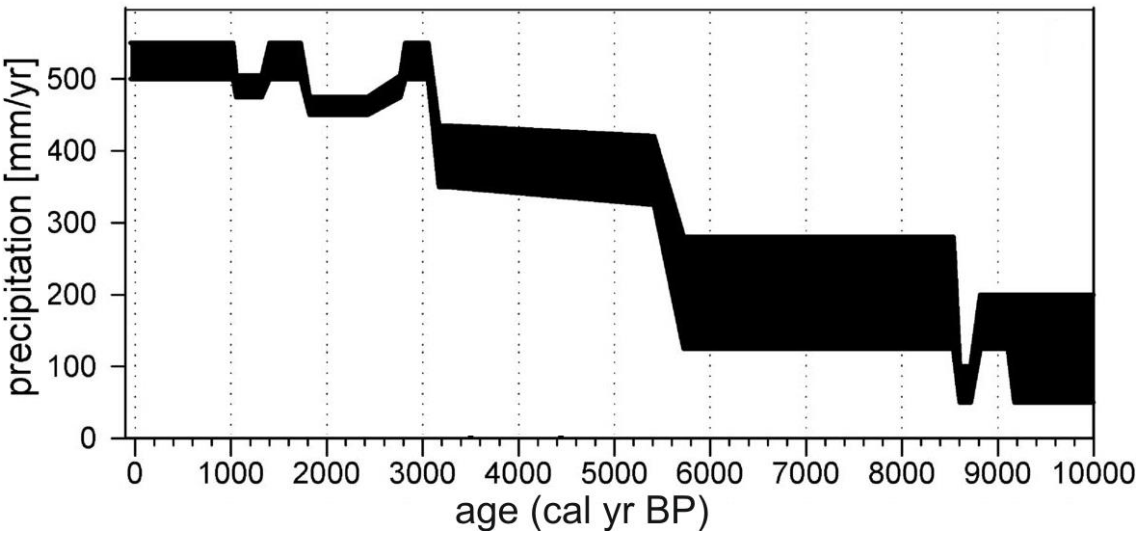

Figure 6.11 Holocene precipitation estimates based on a water balance model for Laguna Aculeo in south-central Chile (33°50'S) (Figure modified from Jenny, 2002).

Chapter 7: Conclusions and future research

7.1 Conclusions

This thesis consist on a study of the lahar deposits from Villarrica Volcano in several sediment cores from the lakes –Villarrica and Calafquén– beside the volcano. Based on previous research, suite some information about the events and the geological and eruptive history of the volcano and the lakes was available. After analysing the main characteristics of the lahar deposits in the cores, some common trends of depositional behaviour in the lakes and the reasons of the frequency and magnitude of the events during the Holocene were observed and comment in the following paragraphs.

The general hypotheses posed at the beginning of this study can be classified mainly into two: How lahars deposited in lakes and what is the lahar history throughout the Holocene.

During the first part of this study, after working with the short cores, it can be conclude that the use of CT-scan images was basic and very useful to measure the thickness of the lahar clay-caps. A first conclusion reached is that, in general, the deposition of lahars in both lakes, Villarrica and Calafquén, depends on the combination of many factors. The main feature of the sedimentation of the lahars in the lakes is that it is produced by two types of flows: underflow and interflow. The reason that an underflow or an interflow (and the depth at which it flows) is determined mainly by the degree of stratification of the lake water. According to the results, it can be said that during the austral summer (from late November to early May) the degree of stratification is enough that, depending on the density and temperature at what the lahar reaches the lake, is distributed through one or both of those two flow types. On the other hand, it can be concluded that there is no clear evidence of material deposited by overflows. Hence, it can be conclude that there was no laharic material transported by overflows.

The second conclusion reached is that the morphological characteristics of the lake and the point at which the lahar reaches the lake determine the distribution of the material on the lake basin. However, the influence of each of the morphological characteristics depends on the flow by which the lahars are being deposited:

(i) In the case that the material is transported through an underflow, the first thing that stands out is that the behaviour of the flow is always the same: once the lahar enters the lake, the underflow descends following the bathymetry to the deepest parts of the lake. Material is deposited on the areas where the underflow pass through until reaching the maximum depth, and then when it reaches the maximum depth is homogeneously distributed. Only in cases in which the slope is too soft may result in a rise of the material due to the energy own energy of the flow. Considering this premise, the most influential factor for a deposition processes by underflow is the distance travelled by the flow from the point where the lahar enters the lake. Another example to confirm this is that in all the cases in which there are evidences of material deposited by an underflow, the cores located nearby or in front of the lahar inflows are the thickest.

(ii) On the other hand, if the material is transported through an interflow, the depth to which the flow circulates is the factor that determines the distribution of the material in the lake. The interflow flows at a certain depth covering the whole area of the lake, and the material settles equally for all the points below the bottom of the flow. Except for the areas in which the basin is at the same range of depths than where the interflow flows, then deeper means thicker. For example in Lake Villarrica, the thickest deposits occur sometimes in the western area of the lake, because the interflow transported everything to the west, where it then settles.

In the second part of the thesis it can be concluded that, in general, from the start to the present of the Holocene (10-0 ka) there has been a progressive increase in the number of lahars in both lakes, but not in the magnitude. Due to the concordance with the curve of average precipitation during the Holocene in the study area, it can be concluded that the number of lahars is mainly determined by the climate –more water, either in the form of snow or ice cover, results in more lahars–. But, apparently it has no influence on the magnitude of lahars. Then, it can be concluded that the eruptions of the volcano is the factor that controls the magnitude of lahars.

The fact that around 3-4 ka large amounts of laharic material were recorded in Lake Villarrica and virtually nothing in Lake Calafquén is concluded that was due to the Pucón eruption (3.7-4 ka) changed the morphology of the volcano, creating a new caldera with a different morphology that made that all the pathways towards Lake Calafquén were blocked and then, after a quiescence of some centuries all the material went towards Lake Villarrica. With the next major eruption (3 ka) and after several centuries of eruptions (approximately 700 years) the caldera was filled up by the new growing cone and the pathways to Lake Calafquén opened again.

With the data studied in this thesis, it cannot be clearly conclude why there was a volcanic quiescence during some centuries around 7 ka.

7.2 Future research

Especially with the long cores it would be very interesting to measure only the clay cap, since considering the thicknesses of the entire event the results are sometimes a little bit exaggerated since the brown part is sometimes very thick. It would also be interesting to improve the age model by more ^{14}C dates on macro-organic matter and have more tephra correlations between the lakes. And finally, it would complete the study trying to correlate the lahars also between the lakes.

On the other hand, with the short cores the study could be also extended, but not too much. For example, it would be interesting to make a grain-size analysis to get an idea of which grain sizes are transported by the interflow. Extra cores in the shallower areas to map in more detail the top of the interflow would be also interesting.

References

Angermann, D., Klotz, J. and Reigber, C.; 1999. Space-geodetic estimation of the Nazca-south America euler vector. Earth and Planetary Science Letters, 171, 329-334 pp.

Bertrand, S.; 2005. Sédimentation lacustre postérieure au dernier maximum glaciaire dans les lacs Icalma et Puyehue (Chili meridional): reconstitution de la variabilité climatique et des évènements sismo-tectoniques. PhD Thesis, Université de Liège, 266 pp.

Bertrand, S. and Fagel, N.; 2008. Nature, origin, transport and deposition of andosol parent material in south-central Chile (34°-42°S). Catena, 73, 10-22 pp.

Bertrand, S., Daga, R., Bedert, R. and Fontijn, K.; 2014. Deposition of the 2011 Puyehue-Cordón Caulle tephra (Chile, 40°S) in lake sediments: Implications for tephrochronology and volcanology. Abstract presented at the Tephra 2014 workshop « Maximizing the potential of tephra for multidisciplinary science », Portland, Oregon, USA, 3-7 August 2014.

Brayshaw, A.C.; 1984. Characteristics and origin of cluster bedforms in coarse-grained alluvial channels. In: Sedimentology of Gravels and Conglomerates (Ed. by E.H. Koster and R.J. Steel). 77-85 pp. Mem. Can. Soc. Petrol. Geol., 5, Calgary.

Campos, H., Steffen, W., Román, C., Zúñiga, L. and Agüero, G.; 1983. Limnological studies in Lake Villarrica: Morphometric, physical, chemical, planktonical factors and primary productivity. Archiv für Hydrobiologie Supplement, 65, 371-406 pp.

Campos, H.; 1984. Limnological study of Araucanian lakes (Chile). Verhandlungen des Internationalen Vereinigung fur Limnologie, 22, 1319-1327 pp.

Cifuentes, I.L.; 1989. The 1960 Chilean earthquakes. Journal of Geophysical Research-Solid Earth and Planets, 94, 665-680 pp.

Clark, P.U., Dyke, A.S., Shakun, J.D., Carlson, A.E., Clark, J., Wohlfarth, B., Mitrovica, J.X., Hostetler, S.W. and McCabe, A.M.; 2009. The Last Glacial Maximum (LGM). Science 325, 710.

Clavero, J. and Moreno, H.; 2004. Evolution of Villarrica Volcano. Boletín del Servicio Nacional de Geología y Minería, Gobiernode Chile, 61, 27.

Cnudde, V., Cnudde, J.P., Dupuis, C. and Jacobs, P.J.S.; 2004. X-ray micro tomography used for the localisation of water repellents & consolidants inside natural building stones. Materials Characterization, 53, 259-271 pp.

Cohen, A.S.; 2003. Paleolimnology. The History and Evolution of Lake Systems. Oxford University Press, Oxford, 500 pp.

Glasser, N.F., Jansson, K.N., Harrison, S. and Kleman, J.; 2008. The glacial geomorphology and Pleistocene history of South America between 38°S and 56°S. Quaternary Science Reviews, 27 (3-4): 365-390 pp.

González-Ferrán, O.; 1994. Volcanes de Chile. Instituto geográfico militar, Santiago, 642 pp.

González, R.C. and Woods, R.E.; 2002. Digital Image Processing. Prentice Hall (2nd ed). Library of Congress Cataloging-in-Pubblication Data, 188 pp.

Dearing, J.A.; 1999. Environmental magnetic susceptibility using the Bartington MS2 system. ChiPublishing, Kenilworth, UK. 54 pp.

DeMets, C., Gordon, R.G., Argus, D.F. and Stein, S.; 1994. Effect of recent revisions to the geomagnetic reversal time scale on estimates of current plate motions. Geophysical Research Letters, 21, 2191-2194 pp.

Heirman, K., Van Daele, M. and Moernaut, J.; 2008. Lago Villarrica and the Siete Lagos: Región de la Araucania and the Región de los Ríos, Chile. Expedition report. Renard Centre of Marine Geology, University of Ghent, Ghent. Belgium. 42 pp.

Heirman, K.; 2011. "A Wind of Change": Changes in Position and Intesity of the Southern Hemisphere Westerlies during Oxygen Isotope Stages 3, 2 and 1. Unpublished PhD Thesis, Ghent University, Ghent, 227 pp.

Heusser, C.; 2003. Ice age Southern Andes – A chronicle of paleoecological events. Elsevier, Amsterdam.

Hogg, A.G., Hua, Q., Blackwell, P.G., Niu, M., Buck, C.E., Guilderson, T.P., Heaton, T.J., Palmer, J.G., Reimer, R.W., Turney, C.S.M. and Zimmerman, S.R.H.; 2013. SHCal13 Southern Hemisphere calibration, 0-50 000 Years cal BP. Radiocarbon, 55 (4)**.**

Jenny, B., Wilhelm, D. and Valero-Garcés, B.L.; 2002. The Southern Westerlies in Central Chile: Holocene precipitation estimates based on a water balance model for Laguna Aculeo (33°50'S). Climate Dynamics (2003) 20: 269-280 pp.

Jordan, T.E., Burns, W.M., Veiga, R., Pangaro, F., Copeland, P., Kelley, S. and Mpodozis, C.; 2001. Extension and basin formation in the southern Andes caused by increased convergence rate: A mid-Cenozoic trigger for the Andes. Tectonics. 20(3): 308-324 pp.

Kay, S.M., Ramos, V.A., Mpodozis, C. and Sruoga, P.; 1989. Late Paleozoic to Jurassic silicic magmatism at the Gondwana margin: Analogy to the Middle Proterozoic in North America. Geology 17(4): 324-328 pp.

Laugenie, C.; 1982. La region des lacs, Chili meridional. Université de Bordeaux III, Bordeaux, France, 822 pp.

Lowe, D.J.; 2011. Tephrochronology and its application: A review. Quaternary Geochronology. 6(2): 107-153 pp.

Maizels, J.K.; 1989. Sedimentology, paleoflow dynamics and flood history of jökulhlaup deposits: paleohydrology of Holocene sediment sequences in southern Iceland sandur in deposits. J. sedim. Petrol., 59, 204-223.

Maijor, J.J. and Newhall, C.G.; 1989. Snow and ice perturbation during historical eruptions and the formation of lahars and floods. Bull. Volcanol., 52, 1-27.

Moernaut, J., Van Daele, M. and Heirman, K.; 2009. Región de la Araucanía, Región de los Ríos, Región de los Lagos and Región de Magellanes. Expedition report. Renard Centre of Marine Geology, University of Ghent, Ghent. Belgium. 39 pp.

Moernaut, J.; 2010. Sublacustrine landslide processes and their paleoseismological significance: Revealing the recurrence rate of giant earthquakes in South-Central Chile. PhD, Ghent University, Ghent, 274 pp.

Moernaut, J., Van Daele, M., Stark, N., Wiemer, G., De Rycker, K. and Kempf, P.; 2011. Expedition report Chile 2011-2012. Leg 1: Geotechnical study on Lake Villarrica. Expedition report. Renard Centre of Marine Geology, University of Ghent, Ghent. Belgium. 11 pp.

Moreno, M., Melnick, D., Rosenau, M., Baez, J., Klotz J., Oncken, O., Tassara, A., Chen, J., Bataille, K., Bevis, M., Socquet, A., Bolte, J., Vigny, C., Brooks, B., Ryder, I., Grund, V., Smalley, B., Carrizo, D., Bartsch, M. and Hase, H.; 2012. Toward understanding tectonic control on the Mw 8.8 2010 Maule Chile earthquake. Earth and Planetary Science Letters, 321-322, 152-165.

Mulder, T. and Alexander, J.; 2001. The physical character of subaqueous sedimentary density flows and their deposits. Sedimentology, 48, 269-299 pp.

Orton, G.J.; 1996. Volcanic environments. In: Sedimentary environments – Processes, facies and stratigraphy (Reading, H.G.; editor). Blackwell Science, London, 485-567 pp.

Pankhurst, R.J. and Hervé, F.; 2007. Introduction and overview. In: The Geology of Chile (Moreno, T. and Gibbons, W.; editors). The Geological Society, London, p. 1.

Petit-Breuilh, M.E.; 2004. La Historia Eruptiva De Los Volcanes Hispanoamericanos (Siglos XVI al XX): El Modelo Chileno. Servicio de publicaciones exmo. Cabildo insular de Lanzarote, 435 pp.

Pierson, T.C. and Scott, K.M.; 1985. Downstream dilution of a lahar: transition from debris flow to hyperconcentrated streamflow. Water Resour, Res., 21, 1511-1524 pp.

Pierson, T.C., Janda, R.J., Umbal, J.V. and Daag, A.S.; 1992. Immediate and long-term hazards from lahars and excess sedimentation in rivers draining Mt Pinatubo, Philippines. U.S. Geol. Surv. Water-resour. Investig. Rep., 92-4039, 1-35 pp.

Rodolfo, K.S.; 1989. Origin and early evolution of lahar channel at Mabinit, Mayon Volcano, Philippines. Bull. Geol. Soc. Am., 101, 414-426.

Rodolfo, K.S. and Arguden, A.T.; 1991. Rain-lahar generation and sedimentary delivery systems at Mayon volcano. In: Sedimentation in Volcanic Settings (Ed. by R.V. Fisher and G.A. Smith), pp. 71-88. Spec. Publ. Soc. Econ. Paleont. Miner., 45, Tulsa.

Scott K.M.; 1988. Origin, behaviour, and sedimentology of lahars and lahar-runout flows in the Toutle-Clowlitz River system. Prof. Pap. US geol. Surv., 1447-A, 1-74 pp.

Siebert, L., Simkin, T. and Kimberly, P.; 2010. Volcanoes of the World – Third Edition. University of California Press, Berkeley and Los Angeles, California, 551 pp.

Silva Parejas, C., Druitt, T.H., Robin, C., Moreno, H. and Naranjo, J.A.; 2010. The Holocene Pucón eruption of Volcán Villarrica, Chile: deposit architecture and eruption chronology. Bull. Volcanol. 16 pp.

Smith, G.A. and Lowe, D.R.; 1991. Lahars: volcano-hydrologic events and deposition in the debris flow-hyperconcentrated flow continuum. In: Sedimentation in Volcanic Settings (Ed. by R.V. Fisher and G.A. Smith), pp. 59-70. Spec. Publ. Soc. Econ. Paleontol. Miner., 45, Tulsa.

Stern, C.R.; 2004. Active Andean volcanism: its geologic and tectonic setting. Revista Geológica de Chile, 31, 161-208.

Stern, C.R., Moreno, H., López-Escobar, L., Clavero, J.E., Lara, L.E., Naranjo, J.A., Parada, M.A and Skewes, M.A.; 2007. Chilean Volcanoes. In: The Geology of Chile (Eds T. Moreno and W. Gibbons), 147-178 pp. The Geological Society of London, London.

St-Onge, G. and Long, B.F.; 2009. CAT-scan analysis of sedimentary sequences: An ultrahigh-resolution paleoclimatic tool. Engineering Geology 103, 127-133 pp.

Sturm, M. and Matter, A.; 1978. Turbidites and varves in Lake Brienz (Switzerland): deposition of clastic detritus by density currents. Spec. Publs int. Ass. Sediment. In: Modern and ancient lake sediments (Matter, A. & Tucker, M. E., eds). Blackwell Scientific Publications, Oxford, 147-168.

Talbot, M.R. and Allen, P.A.; 1996. Lakes. Sedimentary environments: Processes, facies and stratigraphy (Reading, H.G., ed). Blackwell Science, Oxford, Third edition, 83-124.

Thompson, R. and Oldfield, F.; 1986. Environmental Magnetism. Allen and Unwin publishers. Quaternary Science Reviews, Volume 6, Issue 1, p. 71-72, 227 pp.

Van Daele, M.; 2013. Recent history of natural hazards in Chile: Imprints of earthquakes and volcanic events in lacustrine and marine sediments. PhD, Ghent University, Ghent, 195 pp.

Van Daele, M., Moernaut, J., Silversmit, G., Schmidt, S., Fontijn, K., Heirman, H., Vandoorne, M., De Clercq, M., Van Acker, J., Wolff, C., Pino, M., Urrutia, R., Roberts, S.J., Vincze, L. and De Batist, M.; 2014. The 600 yr eruptive history of Villarrica Volcano (Chile) revealed by annually laminated lake sediments. Geological Society of America Bulletin, 18 pp.

Vandoorne, W., Van Daele, M., Moernaut, J., De Rycker, K.; 2011. The sedimentological imprint of the 27th February 2010 Chilean megathrust earthquake. Leg 1: The 2010 zone. Expedition report. Renard Centre of Marine Geology, University of Ghent, Ghent. Belgium. 32 pp.

Viel, M.; 2012. Lacustrine sedimentary records of Lago Calafquén, Chilean Lake District. South-central Chile. PhD, Ghent University, Ghent, 68 pp.

Walker, G.P.L.; 1981. Plinian eruptions and their products. Bull. Vulcanol. 44, 223-240.

Wells S.G. and Harvey, A.M.; 1987. Sedimentological and geomorphic variations in storm-generated alluvial fans, Howgill Fells, northwest England. Bull. Geol. Soc. Am., 95, 182-198.

Wetzel, R.G.; 1983. Limnology (Second edition). Saunders College Publishing, Philadelphia, 858 pp.

Zolitschka, B., Mingram, J., van der Gaast, S., Jansen, F.J.H. and Naumann, R.; 2001. Sediment logging techniques. In: Tracking Environmental Change Using Lake Sediments. Volume 1: Basin Analysis, Coring, and Chronological Techniques (Eds W.M. Last and J.P. Smol), 1, 137-153 pp. Kluwer Academic Publishers, Dordrecht, The Netherlands.